Copyright Warning & Restrictions

The copyright law of the United States (Title 17, United States Code) governs the making of photocopies or other reproductions of copyrighted material.

Under certain conditions specified in the law, libraries and archives are authorized to furnish a photocopy or other reproduction. One of these specified conditions is that the photocopy or reproduction is not to be "used for any purpose other than private study, scholarship, or research." If a, user makes a request for, or later uses, a photocopy or reproduction for purposes in excess of "fair use" that user may be liable for copyright infringement,

This institution reserves the right to refuse to accept a copying order if, in its judgment, fulfillment of the order would involve violation of copyright law.

Please Note: The author retains the copyright while the New Jersey Institute of Technology reserves the right to distribute this thesis or dissertation

Printing note: If you do not wish to print this page, then select "Pages from: first page # to: last page #" on the print dialog screen

A STUDY OF HEAT TRANSFER AND INLET FLOW BEHAVIOR IN MOLTEN POLYMER SYSTEMS

BY

MIN HO CHOI

A THESIS

PRESENTED IN PARTIAL FULFILLMENT OF

THE REQUIREMENTS FOR THE DEGREE

OF

MASTER OF SCIENCE IN CHEMICAL ENGINEERING

AT

NEWARK COLLEGE OF ENGINEERING

May, 1971

Newark, New Jersey

APPROVAL OF THESIS

A STUDY OF HEAT TRANSFER AND

INLET FLOW BEHAVIOR IN MOLTEN POLYMER SYSTEMS

BY

MIN HO CHOI

FOR

DEPARTMENT OF CHEMICAL ENGINEERING

NEWARK COLLEGE OF ENGINEERING

BY

FACULTY COMMITTEE

APPROVED: _____

_____

_____

NEWARK, NEW JERSEY

MAY, 1971

ABSTRACT

A Study of Heat Transfer and

Inlet Flow Behavior in Molten Polymer Systems

Two separate studies have been done in the present work: one to study the entrance effects in flow in molten polymer systems and the other to investigate the heat transfer to thermally softened flowing polymer.

The equipment for the entrance effect was designed to study the isothermal flow behavior of a polymer melt in the entrance region. The main object of this investigation was to find the entrance length for the melt to relax and to separate the pressure drop into viscous and elastic effect. Due to the failure in developing a proper pressure measuring device the experiment was not conclusive.

In addition to the entrance flow study the heat transfer to thermally softened flowing polymer was studied. A depression in temperature in the central region of the tube and a peak in temperature near the wall when heating the flowing polymer was observed. When cooling the polymer melt the effect of viscous dissipation was greatly reduced due to the alteration of the velocity profile heat transfer to the cold wall.

In general aspects the results of heat transfer study were in good agreement with the previous theoretical and experimental works.

ACKNOWLEDGEMENT

The author wishes to express his deepest appreciation to Dr. R. G. Griskey for his suggestion of this topic, the financial support and the timely guidance to make this investigation finished.

The author also wants to express his gratitude to Dr. N. Siskovic for his advice and guidance in building up the equipment and the experimental work.

Many helps of the people in the school machine shop are appreciated, where the equipment was constructed.

The author would like to thank his fellow graduate students for their advice and help during this investigation.

TABLE OF CONTENTS

I. INTRODUCTION 1

II. BACGROUND 2

Classification of Fluids 2

Flow of Fluids in the Circular Conduits 7

Entrance Effects 10

General Entrance Effects 10

Entrance Effects in the Inertial Range 11

Newtonian Fluids 13

Non-Newtonian Fluids 18

Viscoelastic Fluids 26

Entrance Effects in the Creeping Range 31

Newtonian Fluids 31

Non-Newtonian Fluids 35

Viscoelastic Polymeric Fluids 36

Flow Pattern 36

Actual Analysis 37

Heat Transfer to Flowing Molten or Thermally Softened Polymers 45

Fluid Flow and Heat Transfer 45

Graetz-Nusselt Problem 46

Effect of Temperature on Fluid Properties 50

Compressibility 51

Non-isothermal non-Newtonian Flow 52

Viscous Heat Dissipation 53

Heat Transfer to the Polymeric Fluids 54

III. EXPERIMENTAL 62
Plan of the Experimentation 62
Development of Equipment 63
General 63
Entrance Region Test Section 65
Test Section 65
Pressure Measuring System 73
Heat Transfer Test Section 75
Experimental Procedure 80
Entrance Region Tests 80
Calibration of Pressure Measuring Systems 81
Actual Test Procedure 85
Heat Transfer Tests 86
Materials and Equipment 88
Materials 88
Equipment 89
IV. RESULTS AND DISCUSSION 98
Entrance Region Studies 98
Results 98
Discussion 98
Heat Transfer Studies 112
Heating of Flowing Thermally Softened Polymer Systems 112
Results 112
Discussion 121
Colling of Flowing Thermally Softened Polymer Systems 127
Results 127

Discussion 129

Recommendations 138

V. CONCLUSION 139

VI. SUMMARY 141

VII. BIBLIOGRAPHY 142

APPENDIX A Notation 148

APPENDIX B Sample Calculation 154

APPENDIX C Data and Results..... 158

Original Data of Point Temperatures for Polymethylmethacrylate 158

Reduced Temperature for Molten Polymethylmethacrylate 223

LIST OF TABLES

Table		Page
I.	Position of Pressure Holes in the Entrance Region.....	71
II.	Position of Pressure Holes in the Exit Region	72
III.	Pressure Measurement of the First Run	99
IV.	Temperature Measurement of the First Run.....	100
V.	Pressure Measurement of the Second Run	101
VI.	Temperature Measurement of the Second Run	102
VII.	Span and 1 mv-Equivalent Pressure	109
VIII.	Pressure Equivalent to $1^{\circ}F$	109
IX.	A Typical Raw Point Temperature Data(Heating).....	120
X.	A Typical Raw Point Temperature Data(Cooling)	129
XI.	Original Data of Point Temperatures for Polymethylmethacrylate	158
XII.	Reduced Temperature for Molten Polymethyl methacrylate.	223

LIST OF FIGURES

Figure		Page
1.	Flow Curves of Various Fluids	6
2.	Entrance Length and Couette Correction Factor	6
3.	Pressure Drop in the Entrance Region	12
4.	Test Section for Entrance Effect(Smaller Pipe).....	67
5.	Test Section for Entrance Effect(Chamber)	68
6.	Position of Pressure and Temperature Tap Holes	69
7.	Entrance and Exit Section	70
8.	A Schematic Transducer Calibration System	83
9.	A Typical Calibration Curve	84
10.	Equipment and Pipe Layout	64
11.	Heat Exchanger Section(for Heat Transfer)	76
12.	A Schematic Diagram of Heat Transfer Apparatus	77
13.	Multi-Probe-Profile Ring	79
14.	Coordinate Systems Used in Analysis of Converging Flows	27
15-16	Calibration Curves of Transducers before the Run	103-104
17-20	Calibration Curves of Transducers after the Run	105-108
21.	A Typical Thermal Sensitivity Shift	110
22-28	Experimental Dimensionless Temperature Profiles at Different Heat Transfer Lengths and Various Flow Rates (Heating)	113-119
29-30	Comparison of Experimental and Calculated Temperature Profiles.....	125-126
31.	Comparison of Theoretical and Experimental Point Temperature at z/L = 1 with wall Temperature as Parameters	128

32-37 Experimental Dimensionless Temperature Profiles at Different Heat Transfer Lengths and Various Flow Rates(Cooling) 130-135

38. Theoretical Steady State Velocity Distribution at a Reduced Axial Length z/L = 1 137

I. INTRODUCTION

During the past thirty years the polymer industry has experienced a tremendous rate of growth. This growth unfortunately has not been accompanied by a corresponding growth in the area of polymer engineering.

In particular, those aspects relating to processing of polymers have been badly neglected. Examples are the behavior of flowing molten or thermally softened polymer systems with respect to such factors as heat transfer and flow contractions or expansions.

The present investigation was undertaken to overcome this lack of understanding. The study was first directed to developing an apparatus for investigating contraction and expansion effects in flowing molten polymer systems and second to consider heat transfer to thermally softened flowing polymer systems.

II. BACKGROUND

A. Classification of Fluids [10,37,61]

Fluids can be classified into the two main categories of Newtonian and non-Newtonian according to their behavior at constant temperature under imposed shearing forces. The flow curves are shown in Fig. 1.

Newtonian Fluids.

Newtonian fluids are those which exhibit a direct proportionality between shear stress and shear rate in the laminar flow region. This is usually stated

$$\tau = \mu \dot{\gamma} \qquad (1)$$

where τ is shear stress, μ is the viscosity of the fluid and $\dot{\gamma}$ is rate of shear. Newtonian behavior has been found to be common to the following systems:

(a) all gases

(b) all liquids or solutions of low molecular weight (i.e., nonpolymeric) materials.

The common denominator of these Newtonian fluids is that the dissipation of viscous energy in them is due to the collision of reasonably small molecular species.

Non-Newtonian Fluids

By definition the term "non-Newtonian" encompasses all

materials which do not obey the direct proportionality between shear stress and shear rate depicted by Eq. 1 and their behavior is commonly observed in the following kinds of systems.

(a) First, and most important, solutions or melts of high molecular weight polymeric materials are non-Newtonian except when unusually dilute.

(b) Suspensions of solids in liquids become increasingly non-Newtonian with increasing solids concentration and are particularly non-Newtonian if the solid tends to swell, slovate, or otherwise associate with the liquid phase.

These non-Newtonian fluids are again classified into three broad categories in a classical sense and the relationship between shear stress and rate of shear is not linear and may also depend on both the duration of the shear and the extent of the deformation produced.

1. Time Independent Fluids

Fluids with properties independent of time or duration of shear.

The following three materials fall into this category.

(1) Bingham Plastic

This is the simplest of all non-Newtonian fluids in the sense that the relationship between shear stress and shear rate differs from that of a Newtonian fluid only by the fact that the linear relationship does not pass through the origin. The equation of the flow curve is

$$\tau - \tau_0 = \eta \dot{\gamma} \qquad (2)$$

where η is the plastic viscosity or coefficient of rigidity and τ_0 is the yield stress. When the shear stress exceeds τ_0, the flow behavior is somewhat like a Newtonian fluid.

(2) Pseudo-plastic Fluids

On arithmatic coordinates these materials displays the concave-downward flow-curve relationship shown in Fig. 1. On logarithmic coordinates it exhibit flow curves the slope of which is between zero and unity. In most cases the flow curve may be well defined by the equation,

$$\tau = K\dot{\gamma}^n \qquad (3)$$

where n is flow behavior index and K is consistency index.

(3) Dilatant Fluids

Dilatant fluids display a rheological behavior opposite to that of pseudoplastics in that the apparent viscosity increases with increasing shear rate. Examples of dilatant fluids are such as starch, pottassium silicate and gum arabic in water.

2. Time Dependent Non-Newtonian Fluids

More complex fluids for which the relationship between shear stress and shear rate depends upon the duration of shear.

These time-of-shear dependent non-Newtonians may be divided into two groups, depending on whether the shear stress increases or decreases with time of shear at a constant shearing rate. The former are termed rheopectic and the latter thixotropic fluids. Rheopexy has been observed in certain sols and in bentonitic clay suspensions. Thixotropy is common to paints, ketchup and other

foods and to some polymeric solutions. Thixotropy is thus of much greater practical importance than rheopectic behavior.

3. Viscoelastic Fluids

A viscoelastic material is one which posses both elastic and viscous properties, i.e. although the material might be viscous, it exhibits a certain elasticity of shape.

Suppose the simple case where we assume Newton's law for the viscous component and Hook's law for the elastic component, which is the case proposed by Maxwell.

For the Newtonian fluid:

$$\tau = \mu \dot{\gamma} \tag{1}$$

For the Hookian elastic body:

$$\tau = G\gamma \tag{4}$$

where τ = shear stress

μ = Newtonian viscosity

G = Shear modulus

γ = shear strain

From Equations 4 and 1 one can writes the total rate of shear as

$$\dot{\gamma} = \frac{\tau}{\mu} + \frac{\dot{\tau}}{G} \tag{5}$$

or

$$\tau + \lambda\dot{\tau} = \mu\dot{\gamma} \tag{6}$$

where $\lambda = \frac{\mu}{G}$

The parameter λ has dimensions of time and it is the time constant of the exponential decay of stress at a constant strain, i.e. if the motion is stopped the stress will relax as $\exp(-t/\lambda)$.

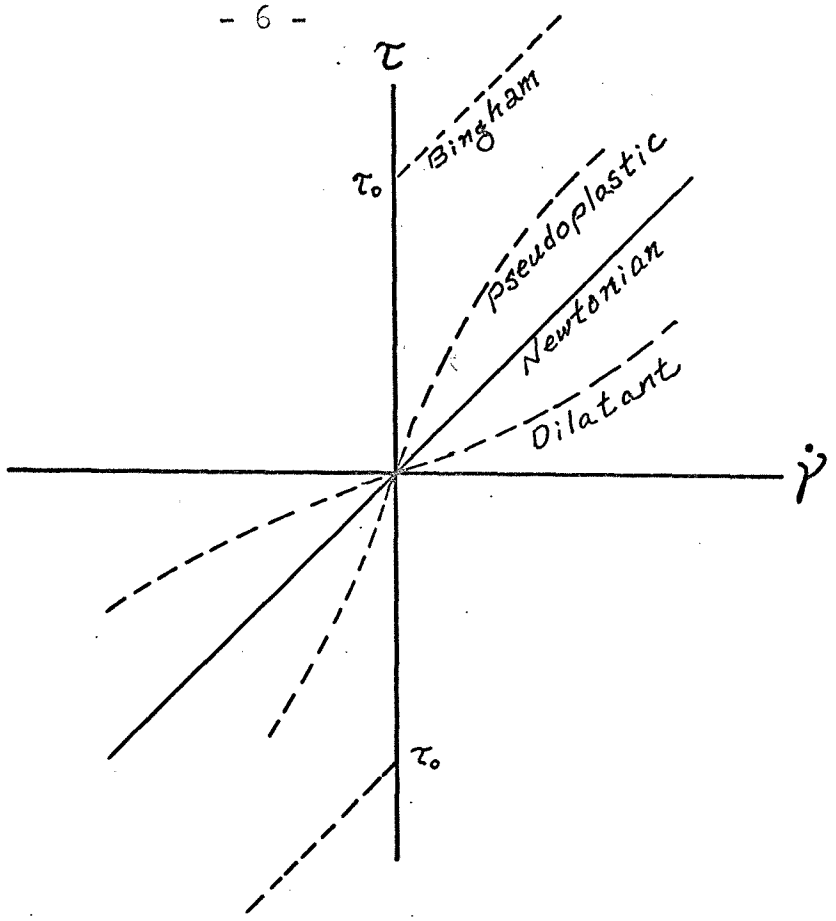

FIGURE 1. Flow Curves of Various Fluids

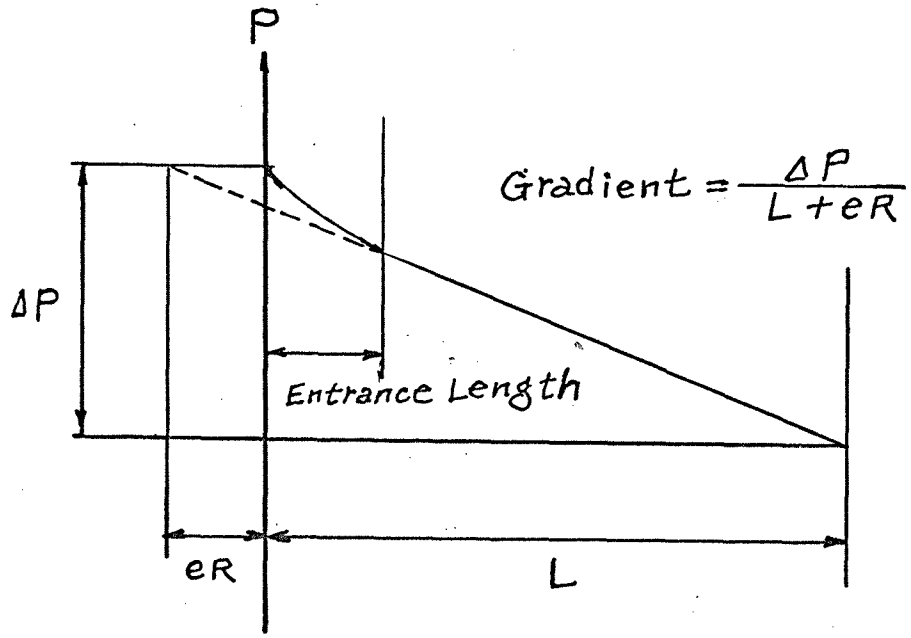

FIGURE 2. Entrance Length and Couette Correction Factor

Consequently λ is known as the relaxation time.

B. Flow of Fluids in the Circular Conduits [10,37,41,61]

Consider a laminar steady state flow through a circular tube of radius R. The volume flow rate Q is related to the axial velocity $v_z(r)$ by

$$Q = \int_0^R 2\pi r\, V_z(r)\, dr = \pi R^2 V \tag{7}$$

where V denotes the mass average velocity. An integration by parts gives

$$Q = \pi r^2 V_z \Big|_0^R - \int_0^R \pi r^2 \frac{dV_z}{dr} dr \tag{8}$$

Assume no slip at the tube wall, i.e., $v_z = 0$ at r = R, then

$$Q = -\int_0^R \pi r^2 \frac{dV_z}{dr} dr \tag{9}$$

for this simple shear flow the only non-zero component of the rate of deformation tensor is $\frac{dV_z}{dr} = \Delta_{12}$

Now let the shear rate-shear stress relationship be written in the functional notation

$$-\Delta_{12} = f(\tau_{12}) \quad \text{or} \quad \dot{\gamma} = f(\tau) \tag{10}$$

The balance of forces on a cylindrical element of fluid of radius r and length L gives

$$2\pi r L \tau = \pi R^2 \Delta P \tag{11}$$

$$\tau = \frac{r \Delta P}{2L} \tag{12}$$

and for the shear stress at the wall, τ_w , we have

$$\tau_w = \frac{R \Delta P}{2 L} \tag{13}$$

Therefore

$$\tau = \tau_w \frac{r}{R} \tag{14}$$

and We can get the followings from Eq. 14,

$$d\tau = \tau_w \frac{dr}{R} \tag{15}$$

$$\gamma^2 = \frac{\tau^2}{\tau_w^2} R^2 \tag{16}$$

Combining Equations 9,10,15, and 16, one finds

$$\frac{4Q}{\pi R^3} = \phi(\tau_w) = \frac{4}{\tau_w^3} \int_0^{\tau_w} \tau^2 f(\tau)\, d\tau \tag{17}$$

where $\phi(\tau_w)$ is defined by this equation. Taking $\frac{d\phi}{d\tau_w}$ and using Leibniz' rule one gets

$$\frac{d\phi}{d\tau_w} = -\frac{3\phi}{\tau_w} + \frac{4}{\tau_w} f(\tau_w) \tag{18}$$

or

$$\dot{\gamma}_w = f(\tau_w) = \frac{3}{4}\phi + \frac{1}{4}\tau_w \frac{d\phi}{d\tau_w} \tag{19}$$

Equation 19 is known as the Weissenberg-Rabinowitch-Mooney equation.

(a) Newtonian Fluid

For a Newtonian fluid in laminar flow we have

$$\tau = \mu \dot{\gamma} \tag{1}$$

$$f(\tau) = \frac{\tau}{\mu} \tag{20}$$

Substituting in Equation 17, one gets

$$\frac{Q}{\pi R^3} = \frac{1}{\mu \tau_w^3} \int_0^{\tau_w} \tau^3 \, d\tau \tag{21}$$

which on integration gives

$$Q = \frac{\pi R^3 \tau_w}{4 \mu} \tag{22}$$

Combining Equations 13 and 22 we get the Poiseuille equation as

$$Q = \frac{\pi R^4 \Delta P}{8 \mu L} \tag{23}$$

From Equation(20)we have

$$\dot{\gamma}_w = f(\tau_w) = \frac{\tau_w}{\mu} \tag{24}$$

Substituting Equation(22) into (24) one can write

$$\dot{\gamma}_w = \frac{4Q}{\pi R^3} \tag{25}$$

(b) Power Law Fluids

For a power law fluid we have

$$\tau = K \dot{\gamma}^n \tag{3}$$

$$f(\tau) = \left(\frac{\tau}{k}\right)^{\frac{1}{n}} \tag{26}$$

Hence from Equations(26) and (17) one finds

$$\frac{Q}{\pi R^3} = \frac{1}{K^{\frac{1}{n}} \tau_w^3} \int_0^{\tau_w} \tau^{2+\frac{1}{n}} \, d\tau \tag{27}$$

and after integrating and substituting for $\tau_w$we get

$$Q = \frac{n \pi R^3}{3n+1} \left(\frac{R \Delta P}{2 L K}\right)^{\frac{1}{n}} \tag{28}$$

and

$$\dot{\gamma}_w = f(\tau_w) = \left(\frac{\tau_w}{K}\right)^{\frac{1}{n}} \tag{29}$$

Equations(29) and (28) gives

$$\dot{\gamma}_w = \frac{3n+1}{n} \frac{Q}{\pi R^3} \tag{30}$$

which is the shear rate at the wall.

C. Entrance Effects

1. General Entrance Effects.

When a fluid is allowed to flow through a sharp-edged entrance or sudden contraction the velocity profile changes from a reservior into a tube of smaller cross section.

One can consider the entrance effects in two aspects: One is the case when the flow is in the range of very low Reynolds number and the other in the range of comparatively higher Reynolds number but still in the range of laminar flow. Bogue et al.[11] described these two flow ranges (based on the pressure drop data of Astarita and Greco [1,2]) as the INERTIAL RANGE(where Reynolds number is greater than about 100) and CREEPING RANGE(where Reynolds number is unity or less). There is also an INTERMEDIATE RANGE which was considered by Chu[18].

Change of velocity profiles in the entrance region implies that there is a pressure gradient or a pressure drop in the axial direction. Pressure drop in the entrance geometries may be considered in terms of three mechanisms: inertial, viscous and

elastic [11]. In the case of polymeric melts inertial effects are usually negligible because of the very slow flow and, hence, the viscous and elastic terms constitute the major entrance pressure drop.[11,35]

One can find both the entrance length and entrance pressure drop by plotting the pressure drop versus L/R ratio and extrapolating to the zero L/R value.[37] The intercept shows the pressure drop at the entrance and the distance from the entrance to the point where the straight line deviates is designated as entrance length. The entrance pressure drop and the entrance length are shown in Fig. 2 and 3. Note that the constancy of the pressure gradient is a necessary but not sufficient condition.[30]

In the flow of very low Reynolds number, most of the pressure drops occur in the reservior near the entrance into the smaller pipe.[4,5,11,48,57] As the velocity of the fluid increases the entrance effects move inside the entrance of the tube. It loses one inertial "velocity head" of pressure ($\rho V^2/2g_c$, where ρ is the density and V is the mean velocity in the tube) as it accelerates from essentially zero velocity to the mean velocity in the tube. [11,34,19,12]

2. Entrance Effects in the Inertial Range

In this range the inertial and viscous effects predominate as a result, pressure drop can be split into two portions, namely, the drop in the chamber and that in the smaller pipe.(Fig. 3)

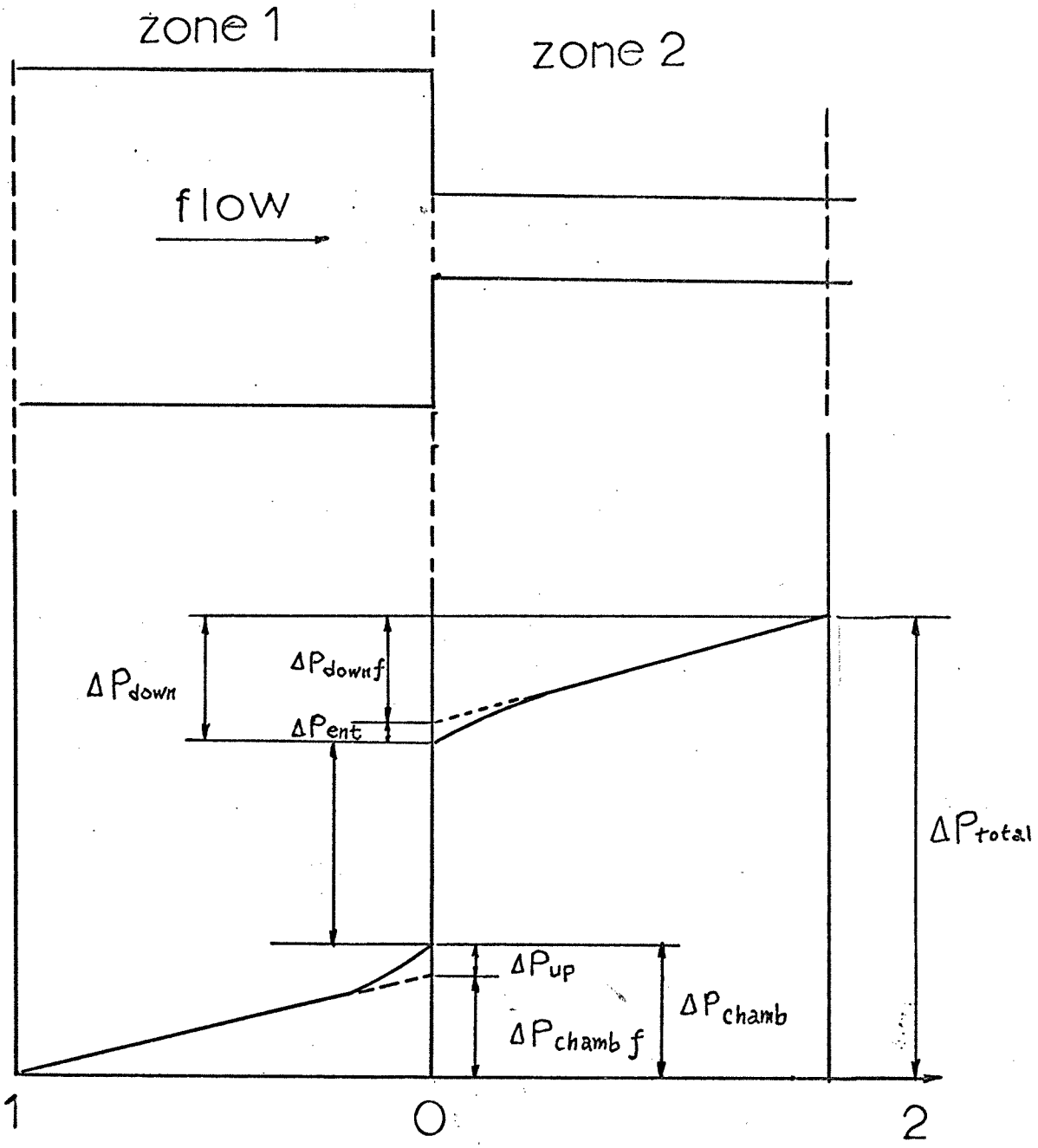

FIGURE 3. Pressure Drop in the Entrance Region

Subscript f denotes fully developed profile.

The reservior pressure drop is small.[34]

There have been many studies for both Newtonian and Non-Newtonian fluids.

a. Newtonian Fluids

As noted above there have been both experimental[1,46,32,58] and theoritical studies [13,15,27,33,46,17,47] for Newtonian fluids.

The entrance effect for Newtonian fluid can be explained by a mechanical energy balance for horizontal circular tube.[47]

In section 1 and 2 in Fig. 3 the velocity is fully developed and section 0 is the entry plane. Referring to this one can write the following equation by mechanical energy balance.

$$\Delta P_{tot} = \Delta P_{12} = \frac{\rho V_2^2}{2\alpha_2 g_c} - \frac{\rho V_1^2}{2\alpha_1 g_c} + \rho F_{12} \qquad (31)$$

$$\rho F_{12} = \Delta P_{chamb\,f} + \Delta P_{ent} + \Delta P_{down\,f} + \Delta P_{up}$$

Where the subscript f denotes the fully developed flow.

$V_1 \approx 0$, assuming infinite contraction ratio, and $\alpha_2 = \frac{1}{2}$ for parabolic velocity profile.

Dividing Equation(31) by $\frac{\rho V^2}{2g_c}$ one gets

$$\frac{\Delta P_{tot}}{\rho V^2/2g_c} = \frac{\Delta P_{down\,f}}{\rho V^2/2g_c} + 2 + \frac{\Delta P_{ent} + \Delta P_{chamb\,f} + \Delta P_{up}}{\rho V^2/2g_c} \qquad (32)$$

From the deginition of Reynold's number and the friction factor for the fully developed flow in the circular tube[10] one can write

$$f = \frac{D \Delta P g_c}{4L} \frac{1}{\frac{1}{2} \rho V^2} = \frac{16}{N_{Re}} \tag{33}$$

or

$$\frac{\Delta P}{\rho V^2/2g_c} = \frac{32\, L/R}{N_{Re}} \tag{34}$$

so that Equation(32) becomes

$$\frac{\Delta P_{tot}}{\rho V^2/2g_c} = \frac{32\, L/R}{N_{Re}} + C_a \tag{35}$$

Where Ca is $2 + \dfrac{\Delta P_{ent} + \Delta P_{chamb} + \Delta P_{up}}{\rho V^2/2g_c}$

Mechanical energy balance in Zone 2 is

$$\Delta P_{02} = \frac{\rho V_2^2}{2\alpha_2 g_c} - \frac{\rho V_0^2}{2\alpha_0 g_c} + \rho F_{02} \tag{36}$$

$\alpha_0 = 1$ for flat velocity and $V_0 = V_2$

and $\rho F_{02} = \Delta P_{down\,f} + \Delta P_{ent}$

In this case ΔP_{ent} is the entrance pressure drop in the smaller pipe only.

Dividing Equation(36) by $\dfrac{\rho V^2}{2g_c}$ gives

$$\frac{\Delta P_{02}}{\rho V^2/2g_c} = \frac{\Delta P_{down\,f}}{\rho V^2/2g_c} + 1 + \frac{\Delta P_{ent}}{\rho V^2/2g_c} \tag{37}$$

or

$$\frac{\Delta P_{02}}{\rho V^2/2g_c} = \frac{32\, L/R}{N_{Re}} + C_b$$

from Equations(35) and (37) one can see the kinetic energy change is one velocity head and cross sectional area change

causes one velocity head.

The entrance length L_e for newtonian fluid is given[31]

$$Le = 0.0575\ D\ N_{Re} \tag{38}$$

The numerical factor depends on the criterion of the per cent of fully developed flow in the entrance region.

Atkinson & Goldstein[27] presented a simplified form of Schiller's equation[33] in the entrance region. Schiller[46] assumed the parabolic velocity profile as

$$\frac{V_x}{U} = 2\frac{y}{\delta} - \frac{y^2}{\delta^2} \tag{39}$$

where $y = R - r$, δ is the boundary layer thickness.

Then defining $\psi = \frac{U}{V} - 1$, U as the core velocity,

$$\frac{x}{R\frac{2RV}{\mu}} = \frac{x/R}{N_{Re}}$$

$$= \frac{1}{8}\left\{\frac{58}{15}\psi - \frac{22}{5}\log(1+\psi) - \frac{17}{15}\sqrt{(4+2\psi-2\psi^2)}\right.$$

$$- \frac{16}{5}\left(\frac{4-2\psi}{1+\psi}\right)^{\frac{1}{2}} - \frac{37\sqrt{2}}{10}\sin^{-1}\frac{2\psi-1}{3} + \frac{26}{3}$$

$$\left. - \frac{37\sqrt{2}}{10}\sin^{-1}\frac{1}{3}\right\} \tag{40}$$

For fully developed flow

$$U = V_{max.} \text{ and since } V_{max.} = 2V,\ \psi = 1$$

Then from Equation(40)

$$x = 0.0575\ R\ N_{Re} \tag{41}$$

$$P_o - P = 1.5\ \rho V^2 \tag{42}$$

So one can write in the entrance region

$$\frac{P_o - P}{\rho V^2/2g_c} = 1.16 + \frac{32\pi}{R N_{Re}} \qquad (43)$$

or

$$\frac{\Delta P_{tot}}{\rho V^2/2g_c} = 2.16 + \frac{32\pi/R}{N_{Re}} \qquad (44)$$

C_a of Schiller's experiment was reported as C_a = 2.115, 2.35, 2.36, 2.45

To find an accurate solution of equation of motion in the entrance region the stream function was represented by a power series for axial positions close to the inlet. This solution was joined with one obtained by the method of Boussinesq to detail the velocity profiles over nearly the entire entrance section.

Campbell and Slattery[15] extended Schiller's method taking into account the energy loss due to viscous dissipation in a macroscopic energy balance rather than by applying Bernoulli's equation. Application to the center core determined pressure as a function of axial position such as

$$\Delta\left(\tfrac{1}{2}\rho S V^3\right) + W\int_{P_1}^{P_2}\frac{dP}{\rho} + E_v = 0 \qquad (45)$$

where

$$E_v = -\int_0^z\int_0^{2\pi}\int_0^R (\tau : \Delta V)\, r\,dr\,d\theta\,dz \qquad (46)$$

represents viscous dissipation.

They presented C_b value of 1.090. Recently La Nieve [34] reported a C_a of 2.53 for 94.9% ethylene glycol-water solution which is Newtonian. The experiment was carried out in the range of Reynolds number from 500 to 1500. The fluid flowed from 6" pipe to 0.547" pipe so the contraction ratio was 12:1 which could be compared with those for ∞: 1 contractions. The upstream pipe was 6-ft long and the downstream section was 5ft in length. The study attempted to measure the pressure drop in the chamber and in the entrance region of small pipe. The nearest tap hole was 0.2" apart from the entry plane, but vena contraction effect reduced the use of this tap. The experimental results were plotted as $\frac{P_o - P}{\rho V^2/2g_c}$ vs $\frac{x/R}{N_{Re}}$

The $C_b + 1$ value was determined by a pressure tap located on the entry plane at a radial distance of $\frac{1}{2}$" from the center line. The reported values for C_a are 2.525, 2.53, 2.56, 2.53 and for $C_b + 1$ 2.55 and 2.50. The differences between C_a and $C_b + 1$ are about 0.03, which would be the pressure drop in the chamber. The experimental value is higher than that predicted by theory and the vena contracta was not noted with Reynolds number below 400. The study noted that this indicated a radial flow at the entrance and that the plug flow assumption is not correct above this flow rate.

Christiansen and Lemmon[17] solved the equation of motion in the entrance region for an isothermal, laminar, Newtonian fluid by finite difference numerical method.

The governing equation was Equation (62) and it was solved with the assumptions

1. Axial molecular transport of momentum is negligible.
2. The pressure is a function of z and is independent of r.
3. The velocity at the tube entrance is uniform.

The entrance region of the tube was considered to comprise N concentric annuli, a radial distance h across, cut by planes perpendicular to the axis into annular segments a distance k long. And the governing equation was written for each of the N + 1 cylindrical boundaries of a set of N annular concentric segments k long and solved by a modified Gauss-Seidel method. It was noted that with the axial diffusion term the numerical method was operable, which indicated that axial diffusion of momentum is negligible at N_{Re} as low as 200. It was also noted that the inclusion of the radial convection of momentum in the numerical solution significantly increased the pressure loss.

b. Non-Newtonian fluids

A number of experimental[34,20] and theoritical[19,12,49,50] studies existed for non Newtonian fluids. One can derive a relationship simillar to Equation(34) for Non-Newtonian fluids: From Equation(19) and (17)

$$\dot{\gamma}_w = \frac{3}{4}\frac{4Q}{\pi R^3} + \frac{1}{4}\left(\frac{D\Delta P}{4L}\right)\frac{d\left(\frac{4Q}{\pi R^3}\right)}{d\left(\frac{D\Delta P}{4L}\right)} \qquad (47)$$

Substituting $\frac{4Q}{\pi R^3} = \frac{8V}{D}$ into Equation.(47) one gets

$$\left(-\frac{dV_z}{dr}\right)_w = \frac{3}{4}\left(\frac{8V}{D}\right) + \left(\frac{8V}{D}\right) \frac{d\left[\frac{1}{4}\left(\frac{8V}{D}\right)\right]/\left(\frac{8V}{D}\right)}{d\left[\frac{D\Delta P}{4L}\right]/\left[\frac{D\Delta P}{4L}\right]}$$

$$= \frac{8V}{D}\left[\frac{3}{4} + \frac{1}{4}\frac{d\ln\left(\frac{8V}{D}\right)}{d\ln\left(\frac{D\Delta P}{4L}\right)}\right] \qquad (48)$$

Rearranging Equations(48) gives

$$\left(-\frac{dV_z}{dr}\right) = \frac{8V}{D}\left[\frac{3}{4} + \frac{1}{4n'}\right] = \frac{3n'+1}{4n'}\frac{8V}{D} \qquad (49)$$

where

$$n' = \frac{d\ln(D\Delta P/4L)}{d\ln(8V/D)} \qquad (50)$$

Equation(50) can be written as

$$\tau_w = K'\left(\frac{8V}{D}\right)^{n'} \qquad (51)$$

where K' and n' are constants.

Combining Equations(49) and(51) one can write

$$\tau_w = K'\left(\frac{4n'}{3n'+1}\right)^{n'}\left(-\frac{dV_z}{dr}\right)_w^{n'} \qquad (52)$$

Comparing Equations(1) and(52) one gets

$$n = n'$$

$$K = K'\left(\frac{4n'}{3n'+1}\right)^{n'} \qquad (53)$$

From Equation(33)

$$f = \frac{D\Delta P/4L}{8V^2/2g_c} = \frac{16}{N_{Re}}$$

Substituting Equation(51) into(33) gives

$$f = \frac{K'\left(\frac{8V}{D}\right)^{n'}}{\rho V^2/2g_c} = \frac{16}{\frac{D^{n'}V^{2-n'}\rho}{g_c K' 8^{n'-1}}} \qquad (54)$$

Comparing Equation(33) and(34) one can define a generalized Reynolds number

$$N_{Re}'' = \frac{D^{n'}V^{2-n'}\rho}{g_c K' 8^{n'-1}} \qquad (55)$$

For power law fluid from Equations(55) and (53)

$$N_{Re}' = \frac{D^{n}V^{2-n}\rho}{g_c K\left(\frac{3n+1}{4n}\right)^{n} 8^{n-1}} \qquad (56)$$

So one can write an equation for power law fluids simillar to Equation(34).

Then

$$f = \frac{16}{N_{Re}'} = \frac{D\Delta P/4L}{\rho V^2/2g_c} \qquad (57)$$

$$\frac{\Delta P}{\rho V^2/2g_c} = \frac{32\,L/R}{N_{Re}'}$$

Then as in the Newtonian case Equation(57) can be written for the entrance region as

$$\frac{\Delta P}{\rho V^2/2g_c} = \frac{32\,L/R}{N_{Re}'} + C_a \qquad (58)$$

In the case of Non-Newtonian fluids area change still causes a pressure drop of one velocity head. However,the kinetic energy change in the down stream is not one velocity head as

in the Newtonian case. The kinetic energy conection factor is determined in the following manner. For power law fluids the velocity profile in the fully developed region is given as [37]

$$V_z = V \frac{3n+1}{n+1}\left[1 - \left(\frac{r}{R}\right)^{\frac{n+1}{n}}\right] \tag{59}$$

The total kinetic energy at that cross section is

$$\pi R^2 V \rho \frac{V^2}{2\alpha g_c} = \int_A \rho V_z \, dA \, \frac{V_z^2}{2 g_c}$$

$$= \frac{\pi \rho}{g_c} \int_0^R V_z^3 \, r \, dr \tag{60}$$

Substituting Equation(59) into Equation(60) and solving one gets

$$\alpha = \frac{\left(\frac{n+1}{3n+1}\right)^3}{2\left[\frac{1}{2} - \frac{3n}{3n+1} + \frac{3n}{4n+2} - \frac{n}{5n+3}\right]} \tag{61}$$

for

$$n = 1 \quad \alpha = \frac{1}{2} \quad , \quad n = \frac{1}{2} \quad \alpha = 0.617$$

This means that the kinetic energy correction is always less than one velocity head for pseudoplastic fluid and greater than one for dilatant materials.

Bogue[12] presented a solution of equation of motion in the entrance region for the power law fluids which concerned only the entrance region in the smaller pipe. A plug like velocity profile was assumed at the entrance. Furthermore, the core of the moving fluid was assumed to be plug like until the profile developed. A cubic equation was used to represent the boundary layer velocity profile. The basic equation was the z component

in the general equation of motion

$$v_y \frac{\partial v_z}{\partial r} + v_z \frac{\partial v_z}{\partial z} = - \frac{g_c}{\rho} \frac{dP}{dz} - \frac{g_c}{\rho} \frac{1}{r} \frac{\partial (r \tau_{rz})}{\partial r} \qquad (62)$$

Equation(1) was substituted for τ_{rz}

Using the von Karman integral method and by rearranging an ordinary differential equation was obtained which was solved to give

$$\frac{x/R}{N_{Re'}} = \frac{\left(\frac{3n+1}{n}\right)^n}{8} \int_0^{\delta^+} f(\delta^+) d\delta^+ \qquad (63)$$

where $$\delta^+ = \frac{\delta}{R}$$

Included in Equation(63) is the assumption of cubic equation for the velocity profile in the entrance region as

$$\frac{v_z}{U} = a\left(\frac{y}{\delta}\right) + (3 - 2a)\left(\frac{y}{\delta}\right)^2 + (a-2)\left(\frac{y}{\delta}\right)^3 \qquad (64)$$

a was taken equal to $\frac{n+1}{n}$

This is actually a generalization of Schiller's method.[46]

Solving Equation(63) numerically gives entrance length at $\delta^+ = 1$, entry pressure drop, and correction factor C_b. For the Newtonian case $C_b = 1.16$ and the entry length is $\left[\frac{x/R}{N_{Re}}\right]_{ent} = 0.0575$

This result is one half on the conventional value which is based on 99% of fully developed flow.

Collins and Schowalter[19] also studied the situation by applying the boundary layer technique in the region both near

the entry and near the fully developed profile. The flow was described in terms of a perturbation to the fully developed velocity profile.

The basic equation was the same as Equation(62) and the technique used was simillar to that of Atkinson and Goldstein.[27] A power series for stream function was defined as

$$\psi = -R^2 U_0 \sum_{i=1} \alpha^i f_i(\eta) \tag{65}$$

where

$$\eta = \frac{(1 - \frac{r^2}{R^2})}{2\alpha}$$

$$\alpha = \left[\frac{2\chi}{\alpha N_{Re}}\right]^{\frac{1}{n+1}} \tag{66}$$

Outside the boundary layer the velocity was expressed as

$$V_z(z) = U\left[1 + \sum_{i=1} \alpha^i K_i\right] \tag{67}$$

Where K_i is another constant.

Putting Equations(65) and(67) together with $v_z = \frac{1}{r}\frac{\partial \psi}{\partial r}$, $v_y = -\frac{1}{r}\frac{\partial \psi}{\partial z}$ An infinite set of ordinary differential equations was obtained by equating coefficients of like powers of α

Solving these equations gives f_1, f_2, f_3 etc.

Then it can be written that

$$V_z = \frac{1}{r}\frac{\partial \psi}{\partial r} = U \sum_{i=1} \alpha^{i-1} f_i'(\eta)$$

$$\approx U \sum_{i=1}^{i=4} f_i' \alpha^{i-1} \tag{68}$$

For the solution approaching fully developed flow the flow was described in terms of a perturbation to the fully developed velocity profile such as

$$v_z = U\left(\frac{1+3n}{1+n}\right)\left[1-\left(\frac{r}{R}\right)^{\frac{n+1}{n}}\right] - U^* \qquad (69)$$

This perturbation velocity was obtained by solving the equation of motion with Equation(69).

Equation(68) was considered valid only as long as the absolute value of each successive term in that equation decreased and at this point the solution was combined with the perturbation velocity. Their result shows for the Newtonian $\frac{x_D/R}{N_{Re}} = 0.122$

The C_b was found to be 1.33 for 99% development. It was also shown that the entry length actually increases as the flow index decreases from 1 to about 0.1.

Experimental values of the excess pressure drop in the entrance region can be found in Dodge's[20] and La Nieve's.[34]

Dodge[20] carried an experiment using Carboxymethycellulose and Carbopol solution with different weight percent in water so the flow behavior index of each solution were different. The contraction ratio was 1:2.56 as the fluid flowed from a $1\frac{1}{2}$" pipe to 1" pipe. The pressure drop was measured only in the small pipe. The contraction loss was found to be 0.88 velocity head regardless of flow behavior index and the experimental data was

found to be in good agreement with both Bogue's and Collins' and Schowalter's theoretical studies.

La Nieve[34] who used Carbopol-Water gels, reported overall contraction losses for the Reynolds number range from 100 to 1500 as follows:

n	C_a
0.62	2.30
0.47	2.27
0.42	2.20

This result is a little higher value than predicted by the theory of Bogue and Collins and Schowalter. This was explained by a possible upstream effect. Furthermore, it was reported that

$$C_{up} = 0.044 \quad \text{for } n = 0.475 \text{ and } N_{Re} > 1000$$

and

$$C_{up} = 0.12 \quad \text{for } n = 0.425 \text{ and } N_{Re} < 100$$

This is greater than the 0.03 value for the Newtonian fluid with $Re > 1000$.

Astarita and Greco[1] introduced an equation which encompasses the entrance pressure drop for both before and after the contraction as following

$$\Delta P = \left(M + \frac{M'}{N_{Re}}\right) \frac{\rho V^2}{2} \qquad (70)$$

where M and M' are constants and M value showes the pressure drop after the contraction and M' before the contraction.

A smillar equation can be derived from Equations(87) and (35) referring to Fig. 3.

$$\Delta P_{ent} = \frac{3\eta Q}{2R^3} + \frac{M\rho V^2}{2} \tag{71}$$

$$\frac{\Delta P_{ent}}{\rho V^2/2} = \frac{3\eta Q}{R^3 \rho V^2} + M$$

$$= \frac{3\eta V \pi R^2}{R^3 \rho r^2} + M = \frac{3\eta\pi}{R\rho V} + M$$

$$= \frac{6\pi}{N_{Re}} + M \tag{72}$$

The M and M' value are higher than predicted previously.[12,19,34,44,57]

A critical Reynolds number of 146 was proposed. This was obtained by plotting the experimental data as $\frac{2\Delta P}{\rho V^2}$ vs N_{Re} on log-log paper. The correlation can be summarized as

$$N_{Re} < 146, \qquad \Delta P = \frac{795}{N_{Re}} \frac{\rho V^2}{2}$$

$$N_{Re} > 146, \qquad \Delta P = 5.48 \frac{\rho V^2}{2}$$

This means when the flow is in the range of $N_{Re} < 146$, the kinetic energy correction does not apply in the entrance region of the smaller pipe.

c. Viscoelastic Fluids

Recently Metzner, Uebler and Chan Man Fong[40] tried to express the pressure and the stress field by means of a diagonal deformation rate tensor in converging flows of viscoelastic

materials. In their experiment the fluid flowed from a large duct of 18" square into a small tube of 1.48" I.D. The materials used were 70% Globe brand white corn syrup in water(Newtonian fluid) and a 0.5% separan AP 30 (viscoelastic fluid). The flow of the fluid was made visible by small air bubbles which traced out the streamlines.

Some difference in the flow patterns were found between viscoelastic polymeric solution and the Newtonian fluid. For the viscoelastic polymeric solution fluid in the chamber converged only in a very slender conical section. Outside this conical section a secondary flow was seen which was not visible in the Newtonian fluid flow.

One more difference observed was that an the increasingly intense haze developed in the converging viscoelastic fluid as the flow rate increased.

A spherical coordinate was adopted to express the velocity field in the converging conical region. Its origin was located downstream within the small duct at a point determined by extending the converging streamlines to intersection shown in Fig. 14.

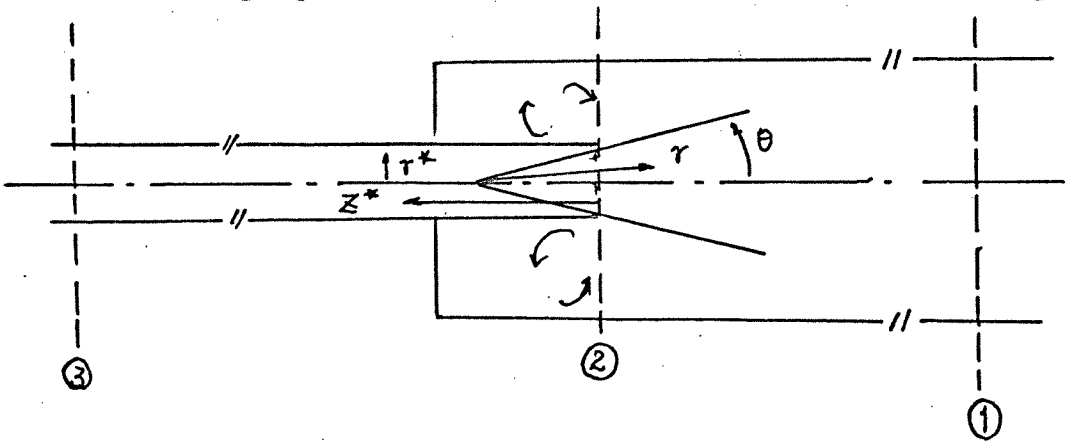

FIG. 14 Coordinate systems used in analysis.

The visual observation suggested that the upstream flow in the reservior were radially directed toward the origin of this spherical coordinate system. Then the continuity equation in the conical section is

$$Ur^2 = f(\theta) \tag{73}$$

This equation was proved to be valid by plotting $\frac{u}{V}$ VS $\frac{r}{R}$ on logarithmic coordinates. The result implied that the fluid is subject only to stretching or elongational modes of deformation and that shearing deformations were negligibly small.

The velocity field was then expressed as

$$u_r = u = \frac{W}{r^2} \quad \text{where } W = f(\theta) \propto Q \tag{74}$$

$$u_\theta = u_\phi = 0$$

Spherical coordinates were used to explain the velocity field of Equation(74). A cylindrical metric r^*, θ^*, z^* with its origin on the axis of the tube at its upstream and was applied for the prediction of macroscopic momentum and pressure drop.

Letting A_1, A_2 and A_A denote the cross sectional areas of the upstream duct, the down stream tube(of radius R) and the annular region of secondary flow outside the conical section a momentum balance between control surfaces 1 and 2 in Fig. 14 was obtained.

$$P_1 - P_{A2}\frac{A_A}{A_1} = \rho V^2 \frac{A_2}{A_1} - (T_{11})_2 \frac{A_2}{A_1} \tag{75}$$

In this equation V denotes the mean velocity in the smaller tube and $(T11)_2$ is the total normal stress in the radial direction in the converging flow field.

In the Θ direction the total normal stress can be written as

$$(T_{22})_2 = (-P)_2 + (\tau_{22})_2 \tag{76}$$

and

$$(T_{22})_2 = -P_{A2} + \cancel{(\tau_{22})}^{\,0}_{A2} \tag{77}$$

Combining Equations(76) and (77) gives

$$-(P)_2 = -P_{A2} - (\tau_{22})_2 \tag{78}$$

Then one can write

$$\begin{aligned}(T_{11})_2 &= -(P)_2 + (\tau_{11})_2 \\ &= -P_{A2} + (\tau_{11} - \tau_{22})_2\end{aligned} \tag{79}$$

With these results Equation (75) can be written as

$$P_1 - P_{A2} = \rho V^2 \frac{A_2}{A_1} - (\tau_{11} - \tau_{22})_2 \frac{A_2}{A_1}$$

Simillar derivation was made between sections 2 and 3 as

$$P_{A2} - P_3 = \rho V^2 \left(\frac{n}{n+1}\right) + (\tau_{11} - \tau_{22})_2 - \left[\frac{2}{R^2}\int_0^R (P_3 + T_{11})\, r\, dr\right]_3 + \frac{2L}{R}(\tau_{12})_w \tag{80}$$

Where L is the axial distance between sections 2 and 3. The entrance pressure drop is written as

$$\Delta P_{ent} = P_{A2} - P_3 - \frac{2L}{R}(\tau_{12})_w$$
$$= \rho V^2\left(\frac{n}{n+1}\right) + (\tau_{11} - \tau_{22})_2$$
$$- \left[\frac{2}{R^2}\int_0^R (P_3 + \tau_{11})\, r\, dr\right]_3 \qquad (81)$$

The integrated term is neglected because it is small in quantity compared to the other terms and $\frac{n}{2n+1}$ is replaced with ϕ because $\rho V^2 \frac{n}{n+1}$ is not correct practically.

For Newtonian fluids ϕ was calculated as 1.33 by Collins and Schowalter.[19] At Reynolds numbers greater than about 500 the occurrence of vena contracta effects appears so that in general ϕ must be evaluated experimentally.

So one can write

$$\Delta P_{ent} = \phi \rho V^2 + (\tau_{11} - \tau_{22})_2 \qquad (82)$$

Using a convected Maxwell model as a constitutive equation and the deformation rate tensor in the converging entrance region the following relation.

$$(\tau_{11} - \tau_{22})_2 = \alpha_1 \tau_w \qquad (83)$$

was derived.

Where α_1 is a large and positive constant.

By definition the isotropic pressure is

$$P = -\frac{1}{3} T_{11} \tag{84}$$

Combining Equations(84),(76) and (78) gives

$$(P)_2 = -\frac{1}{3}(T_{11} + T_{22} + T_{33})_2$$

$$= -\frac{1}{3}(-P_{A2} + (\tau_{11} - \tau_{22})_2 - P_{A2} - P_{A2})_2$$

$$= P_{A2} - \frac{\tau_{11} - \tau_{22}}{3} \tag{85}$$

and from Equations(85) and(83)

$$P_2 = P_{A2} - \frac{\alpha_1 \tau_w}{3} \tag{86}$$

End effect measurement may be used to evaluate α_1 from Equations(81) and(82). Hence, the isotropic pressure was obtained at the inlet plane to the small duct as a decrement below P_{A2}, the gage pressure measured at this axial position.

3. Entrance Effects in the Creeping Range.

a. Newtonian Fluids

Sampson[45] theoretically derived the pressure drop of a Newtonian through an orifice in 1891. In 1949 Roscoe[44] derived an expression for the rate of slow viscous flow of Newtonian

fluids through an elliptic aperture in a thin wall in analogy to an electrical potential field

$$Q = \frac{2S^2}{3\pi\mu s}\Delta P \tag{87}$$

S : Area of the aperture

s : Perimeter of the aperture

P : Pressure difference between two sides

For a circular aperture of radius R, Equation (87) becomes

$$\Delta P = \frac{3\mu Q}{R^3} \tag{88}$$

Later Weissburg[57] calculated by a variational method an upper bound for the pressure drop near the ends of a long tube. The rate of energy dissipation W, is written

$$W = \frac{1}{2} Q \Delta P = \mu \int \omega^2 dV + 2\mu \int (\bar{u}\cdot\bar{\nabla})\bar{u}\cdot\bar{n}\, dS \tag{89}$$

Where, ΔP is the pressure drop between the two ends of the tube and the last two terms are volume and surface integrals over the region and its boundary, ω is the vorticity and is the unit outward normal to the surface element dS. From the vector identity and the symmetric velocity field one can show the surface integral vanishes.

From the minimum-energy theorem of Helmholtz and Equation(89) an equation of unequality which gives the upper bound of the entry pressure drop as

$$\frac{1}{2} Q \Delta P_e < \mu \int \langle \omega^2 \rangle \, dV_e \tag{90}$$

is derived. Here, $\Delta P_e = \Delta P - \Delta P_{tube}$

Applying an axially symmetric stream function ψ and oblate spherical coordinates x,t,ϕ makes Equation(90)

$$\Delta P_e < \frac{4\pi\mu}{Q} \int_0^1 \int_0^\infty \frac{1}{t^2 + a^2 x^2} \left[\left(\frac{t^2 + a^2}{1 - x^2} \right)^{\frac{1}{2}} \frac{\partial^2 \langle \psi \rangle}{\partial t^2} + \left(\frac{1 - x^2}{t^2 + a^2} \right)^{\frac{1}{2}} \frac{\partial^2 \langle \psi \rangle}{\partial x^2} \right]^2 dt \, dx \tag{91}$$

The trial stream function used was

$$\langle \psi \rangle = \frac{Q}{2\pi} \left[x^3 + f(t)(x^4 - x^3) \right] \tag{92}$$

where $f(t)$ is any function chosen so that $\bar{u}$ satisfies the required boundary conditions. Various forms of $f(t)$ were tried in Equation(92) and the resulting double integral in Equation(91) was computed numerically. The upper bound presented was

$$\Delta P_e < 3.47 \, \mu Q / R^3 \tag{93}$$

For the orifice case the result obtained by Sampson,[45]

$$\psi_o = \frac{1}{2} Q x^3 / \pi$$

was put into Equation(91) and this yielded

$$\Delta P = 3 \mu Q / R^3 \tag{88}$$

in confirmation of a previous calculation of Roscoe.

Recently J. S. Chong, E. B. Christiansen and A. D. Baer[16] attempted to solve the Navier-Stokes equation of orifice flow by assuming a velocity profile at the orifice. The assumed profile was

$$F\left(\frac{r}{R}\right) = k\left[1 - \left(\frac{r}{R}\right)^2\right]^n$$

For n = 0, the velocity profile at the orifice is flat and the calculated average pressure drop for this case is

$$\Delta\bar{P} = 3.31\,\frac{\eta Q}{R^3}$$

For n = 1/2 and k = $30/2\pi R^3$

$$\Delta P = \eta\,\frac{3Q}{\pi R^3}\begin{cases}\frac{\pi}{2}, & 0 \le r < R \\ \sin^{-1}\left(\frac{R}{r}\right) - \frac{1}{\left[\left(\frac{r}{R}\right)^2 - 1\right]^{\frac{1}{2}}}, & r > a\end{cases}$$

The pressure drop for this case coincides with that of Rosco for $r < R$.

For parabolic velocity profile (n = 1 and k = $\frac{2Q}{\pi R^2}$)

A series of experiments with different orifice diameters was also considered. The diameter ratio of the vessel to orifices ranged from 8.75 to 23.60. One side of the orifices was tapered and the orifices were mounted at the bottom of the vessel with the tapered edge facing inside.

The work was done at room temperature using a standard-viscosity OB Oil and a Dow-Corning #200 fluid as testing materials.

The data was plotted ΔP vs $\frac{Q}{R^3}$.

The resultant data was correlated with the equation.

$$\Delta P = C_o \eta \frac{Q}{R^3}$$

The results indicated that the velocity profile would lie between a flat profile and that proportional to the square root of a fully developed parabolic profile.

b. Non-Newtonian Fluids

Tomita[48] has treated the problem for a power law fluid in an approximate manner. The Couette correction factor ε defined in the following equation has been calculated

$$L_c = L + \varepsilon D \tag{94}$$

where L_e is corrected fictitious length, L and D are the tube length and diameter respectively.

Two separate regions were considered. One far from the entrance where the streamline is in the radial direction. The other region was close to the mouth of smaller pipe with assumed flow lines. With an assumed stream function an equation was derived to represent the energy dissipated per unit time. The final result is

$$\Delta P_{ent} = 12^{\frac{\ell+1}{2\ell}} \mu_{psu}^{\frac{1}{\ell}} \frac{Q^{\frac{1}{\ell}}}{R^{\frac{3}{\ell}} \pi^{\frac{1}{\ell}}} \left\{ \frac{2}{3} mA + \frac{2}{m+4} B \right\}$$

(95)

where $\frac{1}{\ell} = n$

μ_{PSU} is the pseudo viscosity defined in a generalized Reynolds number as

$$Re^* = \frac{\rho D^{\frac{1}{\ell}} V^{2-\frac{1}{\ell}}}{\mu_{PSU}^{\frac{1}{\ell}}} \qquad (96)$$

A and B are numerical series containing ℓ.

The Couette correction factor for the Newtonian case was found to be 0.444.

Tomita's result do not reduce exactly to Equation (88) for the Newtonian case. Bogue et al.[11] modified the result in which the multiplying coefficient has been empirically reduced by the factor 1.5. This final result is

$$\Delta P_{ent} = \frac{1.18K}{n^{0.7}} \left[\left(\frac{4Q}{\pi R^3} \right) \left(\frac{3n+1}{4n} \right) \right]^n \qquad (97)$$

where n and k are defined by the power law equation.

c. Viscoelastic Polymeric Fluids

1. Flow Pattern

Metzner et al.[40] studied the viscoelastic polymeric fluid case. In the Newtonian case of very low Reynolds number the fluid converged into a small duct through a full 180° solid angle. At larger Reynolds numbers small vortices formed in the corner of upstream chamber. The flow patterns of non-Newtonian and

viscoelastic fluid were found to be simillar to those of Newtonian fluid.[11]

A number of flow visualization studies of polymer melts have been made in connection with melt fracture. A typical one can be found in the experiment by Bagley and Birks.[5] They showed in their experiment that the flow of branched polyethylene(low density polyethylene) produced a funnel-shaped pattern near the entrance leaving stagnant regions or circulating eddies in the corners. In contrast linear polyethylene(high density polyethylene) does not leave these corner regions.

Maxwell and Galt[25] carried a visual study of polymer melt in a tube of $\frac{1}{4}$" in diameter and a $\frac{1}{2} \times \frac{1}{8}$ rectangular conduit by a tracer technique. They descrived three regions of distinct type of flow: boundary annulus, shear annulus and plug flow region.

Bogue et al.[11] studied the flow pattern of the polymeric solutions by a birefringent. They reported unusual features. One was the tendency of the stresses to concentrate near the centerline rather than near the corner, strongly suggestive of the channeling behavior described earlier. The second feature was the occurrence of a stress discontinuity just before and right after the entrance plane. No explanation of this features was presented.

2. Actual Analysis

In 1958 philippoff and Gaskins[43] showed that the elastic

potential energy of the emerging liquid in a capillary experiments led to a new kind of correction. In essence, the end correction was increased by 1/2 the recoverable shear s_R. In the capillary the elastic energy is imparted to the liquid at the entrance of the capillary and is carried out of the capillary by the flowing liquid.

$$P_T Q = P_c Q + m\rho V^2 Q + E \qquad (98)$$

where P_T : total pressure drop

P_c : the pressure held in equilibrium inside the capillary

$m\rho V^2$: kinetic energy correction term

E : elastic energy transported out at the capillary

Dividing by Q we obtain

$$P_T = P_c + m\rho V^2 + E/Q \qquad (99)$$

Philippoff and Gaskins designated the term E/Q as the mean elastic energy or the axial normal force P_{11}, the normal stress acting as a pull or tension in the direction of flow. They derived in their earlier work that this elastic energy per unit volume is the product of the shearing stress and the recoverable shear s, called "normal stress", P_{11}, which is a constant for each rate of shear.

$$P_{11} = \tau s \qquad (100)$$

Assuming that P_c is a constant over the capillary area and that $(P_{11})_R$ is the normal force at the rim of the capillary, then Equation(35) becomes

$$P_T = P_c + m\rho V^2 + (P_{11})_R \tag{101}$$

Any real geometrical end correction would increase the active length of the capillary by $\delta L = nR$. n is termed the "Couette Correction". Then from Equation(13) one can write

$$P_c = \frac{2(L+\delta L)}{R}\tau_{cR} = \frac{2(L+nR)}{R}\tau_{cR} \tag{102}$$

where τ_{cR} is the shear stress at the capillary wall and the "total or apparent shear stress" τ_T becomes

$$P_T = \frac{2L}{R}\tau_T \tag{103}$$

Furthermore at the radius R

$$(P_{11})_R = \tau_{cR} S_R \tag{104}$$

we can rearrange Equation(101) to obtain

$$\tau_{TR} = \tau_{cR}\left[1 + \frac{R}{L}\left(n + \frac{S_R}{2}\right)\right] + \frac{R}{2L} m\rho V^2 \tag{105}$$

Similarly, for $r = R$, Equation(101) can be written as

$$P_T = \tau_{cR}\left[\frac{2L}{R} + 2n + S_R\right] + m\rho V^2 \tag{106}$$

From their experimental result it was seen that Equation(106) had been correct within the whole possible range of capillary lengths from 0 to ∞ .

In 1961 Bagley[4] tried to separate the elastic and viscous effects in polymer flow. He stated that for a certain polymer if Hook's law in shear is obeyed one can write the following expressions from Equations(4) and (106).

$$\tau = G s_R \tag{107}$$

$$\tau_{cR} = \tau_w = \frac{PR}{2(L+eR)} \tag{108}$$

where

$$e = n + s_R/2 \tag{109}$$

Combining Equations (107) and (109) gives

$$e = \frac{1}{2G}\tau_w + n \tag{110}$$

Plots e versus τ_w have been found to be linear for some polyethylenes[3]. From these linear plots the shear modulus G, the Couette correction n, and the recoverable shear strain s_R at any stress can be found.

Bogue and Lanieve[35] tried to correlate entrance pressure drop with the primary normal stress difference in an experiment using polymer solutions and capillary tubes. By dimensional analysis with equation of motion, a general integral constitutive theory and a general power series they derived the following

form of equation for the entrance pressure drop.

$$\Delta P_{end} = \alpha_2 \tau_{ch} \lambda_{ch}^{b_2} \dot{\gamma}^{b_2} + \alpha_3 \tau_{ch} \lambda_{ch}^{b_3} \dot{\gamma}^{b_3} \qquad (111)$$

where α_i , b_i are constants and τ_{ch} , λ_{ch} are characteristic shear stress and time. The first term is for viscous effect and the second term is for elastic effect.

The entrance pressure loss was extracted conventionally from P_{tot} versus L/R. They approximated the viscous portions of the pressure drop with Weissberg's and Tomita's viscous analysis and the difference between the measured total and estimated viscous end effects losses was assumed to be the loss due to elasticity..

These entrance pressure drops versus shear rate were plotted together with the normal stress difference $T_{11}-T_{22}$ which was measured with rheogoniometer. It was noted the normal stress difference has a linear relationship with shear rate on log-log paper.. So it could be assumed there exist a linear relation between the entrance pressure drop and the primary normal stress difference as

$$\Delta P_E = \alpha_3 (T_{11} - T_{22}) \qquad (112)$$

From Equations(111) and (112) one can write

$$T_{11} - T_{22} = k' \dot{\gamma}^{2m} \qquad (113)$$

where k' and m are constants.

It was stated that throughout the flow field of interest or the converging flow before the entrance, there is actually a spectrum of shear rates, all lower than the characterizing tube shear rate. The elastic entrance pressure drop might then be visualized as a sum of incremental pressure losses over this flow field, each with its characteristic shear rate between zero and the tube shear rate.

Since the normal stress difference is specified explicitly by the shear rate, each of the increments of the elastic entrance pressure loss has its own characteristic normal stress difference. This normal stress difference describes the property of the fluid that causes the elastic entrance pressure loss.

Recently Bogue et al.[11] summarized the previous work concerning the entrance pressure drop. They stated that although the recoverable strain concept in PGB method does not rest on a sound mathematical basis it is qualitatively appealing in the sense that one can take a viscoelastic theory and obtain a comparable result.

From Equations(107),(108), and (109) the entrance pressure drop can be described as

$$\frac{\Delta P_{ent}}{\tau_w} = 2n + \frac{\tau_w}{G} \qquad (114)$$

For the power law fluid Equation(114) becomes

$$\Delta P_{ent} = 2n K \dot{\gamma}_w^n + \left(\frac{K^2}{G}\right) \dot{\gamma}_w^{2m} \qquad (115)$$

where m = n and $\dot{\gamma}_w$ is defined in Equation(30). Comparing Equations (113) and (115) one can see $K^2/G = k'$ for the case m = n if one neglects the viscous term.

Han, Charles and Philippoff[30] carried an experiment in which the axial pressure distribution of polymer melt in a circular tube was measured. The shear rate range was from 100 sec^{-1} to 500 sec^{-1} and L/D ratio 4. The result showed the entrance length, based on the constancy of the radial normal stress at the wall was less than one equivalent diameter of the tube.

The experiment was extended later on[31] and the entrance effect was described in relation with exit pressure and die swell ratio. The entrance length based on the constancy of the exit pressure and die swell ratio of the polymer melt under investigation was about twenty equivalent tube diameter.

It was described that as the fluid moves through the entrance region it is subject to greater relative strains and shear rates than in the capillary itself. Therefore in this region the fluid builds up normal stress which is greater than those consistent with fully developed flow within the capillary. So these stresses must relax prior to the attainment of fully developed flow.

The exit pressure and die swell ratio versus L/D at a certain shear rate and interpreted that the constant slope showed the constancy of the elastic property and the exit pressure is related to the primary normal stress difference

as follows:

$$(T_{zz} - T_{rr})_{R,L} = - T_{rr}(R,L) \tag{116}$$

The exit pressure $P_{R,L}$ was defined as

$$P_{R,L} = - T_{rr}(R,L) \tag{117}$$

Then Equation (116) can be written as

$$(T_{zz} - T_{rr})_{R,L} = P_{R,L} \tag{118}$$

It was also shown a certain relationship between the exit pressure and shear rate.

D. Heat Transfer to Flowing Molten or Thermally Softened Polymers.

The study of heat transfer to molten flowing polymers is one of the basic research needs for polymer processing operations such as extrusion, injection molding, calendering and melt spinning.

Many difficulties have been encountered in such studies because the polymer has elastic non-Newtonian properties and a high apparent viscosity.

The purpose of this investigation is to study the heat transfer to molten polymer flowing in a circular tube by measuring the radial temperature profile at different axial position and by correlating the data in the form of dimensionless parameters.

1. Fluid Flow and Heat Transfer

There can be several cases in studying heat transfer to flowing fluid in a conduit. The most frequently considered cases are constant heat flux and constant wall temperature .

In order to study the heat transfer phenomena the velocity profile behavior should be known since the velocity of the fluid affects the rate of convective heat transfer and the temperature profile. The physical properties of a fluid are a function of temperature and pressure and hence any change in temperature or pressure causes a corresponding change in velocity and temperature profile.

The flow behavior in a circular conduit under isothermal condition has been described previously.

Generally the temperature profile of a fluid under non-isothermal flow can be obtained by solving the energy equation with proper isothermal velocity profile and boundary conditions.

a. Graetz-Nusselt Problem

The basic and simple problem to be considered is the classical Graetz-Nusselt problem in which the fluid of a constant temperature with the same wall temperature is suddenly subjected to enter a tube whose wall temperature is another constant temperature. By shell energy balance with the assumptions of constant physical property, steady state and heat conduction to the radial direction only, one can write the energy equation as

$$\rho C_p V_z \frac{\partial T}{\partial z} = \frac{k}{r}\left[\frac{\partial}{\partial r}\left(r\frac{\partial T}{\partial r}\right)\right] \qquad (124)$$

ρ = density of the liquid, lb_m/ft^3

C_p = Specific heat

V_z = velocity of the fluid in the axial direction.

$\frac{\partial T}{\partial z}$ = the rate of change of temperature in the axial direction, $^oF/ft$

k = thermal cinductivity of the fluid, Btu/ft ^oF

r = the radial distance from the center of the tube, ft.

$\frac{\partial T}{\partial r}$ =the radial temperature gradient ^{o}f/ft

$\frac{\partial}{\partial r}(r\frac{\partial T}{\partial r})$= the rate of change of the radial distance times the temperature gradient with radial distance, ^{o}F/ft

In 1885 Graetz[28] solved this equation for two different velocity profiles, i.e., the flat and the parabolic velocity profiles over the entire cross section. His solution for plug flow was of the form of a Bessel function:

$$\frac{t - t_w}{t_1 - t_w} = \sum_{j=1}^{\infty} \frac{2J_o(\eta_j \frac{r}{R})}{J_1(\eta_j)} \exp\left(-\eta_j^2 \frac{\pi K L}{W C_p}\right) \tag{125}$$

where

t = temperature of the fluid at any point, ^{o}F.

tw = the wall temperature, ^{o}F

t_1 = the initial mixing cup temperature of the fluid, ^{o}F

η_j = j^{th} root of J_o

J_o = Bessel function of zeroth order

J_1 = Bessel function of first order

L = the axial distance of heat transfer, ft

W = mass flow rate, lb_m/hr

For the parabolic velocity profile he got

$$\frac{t - t_w}{t_1 - t_w} = \sum_{j=1}^{\infty} \frac{-2\phi_j(\frac{r}{R})}{\eta_j (\frac{\partial \phi}{\partial \eta_j})_{\frac{r}{R}=1}} \exp\left(-\eta_j^2 \frac{\pi K L}{W C_p}\right) \tag{126}$$

$\phi_j(\frac{r}{R})$ = Series solution of the following differential equation.

$$\phi_j'' + \frac{R}{r}\phi_j' + \eta_j^2\left[1 - \left(\frac{r}{R}\right)^2\right]\phi_j = 0 \qquad (127)$$

The mixing cup temperature for this case is given by

$$\frac{t_2 - t_w}{t_1 - t_w} = 8P_2\left(\frac{\pi KL}{WC_p}\right) \qquad (128)$$

Since both of these solutions have the variables expressed in the form of the dimensionless expression $\frac{WC_p}{KL}$, this expression has become to be known as the Graetz number (Gz). Defining an average heat transfer coefficient h_a as

$$q = h_a A\left[\frac{(t_w - t_1) + (t_w - t_2)}{2}\right] \qquad (129)$$

where

q = rate of convective heat transfer, Btu/hr

A = area of heat transfer surface, ft^2

Then the Graetz solutions can be expressed in terms of Graetz and Nusselt numbers:

For plug flow

(130)

$$N_u = \frac{h_a D}{K} = \frac{2G_z}{\pi}\left[\frac{1 - 0.692\,e^{\left(-\frac{5.78}{\pi}G_z\right)}}{1 + 0.692\,e^{\left(-\frac{5.78}{\pi}G_z\right)}}\right]$$

For parabolic velocity profile

$$Nu = \frac{h_a D}{K} = \frac{2 Gz}{\pi} \quad \frac{1 - 8 P_2 \left(\frac{\pi}{Gz}\right)}{1 + 8 P_2 \left(\frac{\pi}{Gz}\right)} \tag{131}$$

Vaughn [55] presented an asymtotic expression for Equation(118) for plug flow with the assumption of small temperature difference between the fluid and the tube wall. The result showed

$$Nu = \frac{8}{\pi} + \frac{4}{\pi} Gz^{\frac{1}{2}} \tag{132}$$

Later Drew, Hogan and McAdams[21] have shown for parabolic flow as

$$Nu = 1.75 \; Gz^{\frac{1}{3}} \tag{133}$$

Lyche and Bird[36] solved the Graetz-Nusselt problem for the case power-law fluid. The governing equation was Equation (118) and the solution was in the form such as

$$\theta(\xi', \xi) = \sum_{i=1}^{\infty} (-1)^{i+1} B_i \psi_i(\xi) \phi_i(\xi') \tag{134}$$

where

$$\theta = \frac{T - T_w}{T_1 - T_w}$$

$$\xi' = \frac{r}{R}$$

$$\xi = \left(\frac{K}{\rho C_p V_{max} R^2} \right) z$$

The $\phi_i(\xi')$ are the eigen functions obtained from the solution of

$$\frac{1}{\xi'} \frac{d}{d\xi'} \left(\xi' \frac{d\phi_i}{d\xi'} \right) + C_i \left(1 - \xi'^{n+1} \right) \phi_i = 0 \tag{135}$$

the C_i being the eigen values.

The $\psi_i(\xi)$ are

$$\psi_i(\xi) = e^{-C_i \xi} \tag{136}$$

and the B_i are determined from

$$B_i = \frac{\int_0^1 \phi_i (1-\xi'^{n+1}) \xi' d\xi'}{\int_0^1 \phi_i^2 (1-\xi'^{n+1}) \xi' d\xi'} \tag{137}$$

Here the n is the reciprocal value of the n in Equation(1).

b. Effect of Temperature on Fluid Properties

Temperature is an important factor affecting the physical and rheological properties of polymeric materials. For example Newtonian viscosity is dependent on temperature and this can be expressed as follows:

$$\mu = A \exp\left(\frac{\Delta H}{R_g T}\right) \tag{138}$$

where

ΔH= the energy of activation for flow, ft lb_f/lb mole

A= an empirical constant depending on the nature of the fluid, lb_f-sec/ft^2

The non-Newtonian viscosity η is a function of temperature and shear rate or shear stress.

McKelvey[37] presented an equation to express the temperature dependence of non-Newtonian viscosity holding shear rate, or shear stress constant.

$$\eta = A \exp(\Delta H_\tau / R_g T)_\tau$$

or

$$\eta = A \exp(\Delta H_{\dot\gamma} / R_g T)_{\dot\gamma} \tag{139}$$

Gee and Lyon used the following linear relationships to calculate the thermal diffusivity and specifie heat in their study of non isothermal flow.

$$\alpha = \alpha_0 / [1 + a(T - 273)]$$

$$C_p = (C_p)_0 [1 + b(T - 273)] \tag{140}$$

c. Compressibility

In most polymer processing high pressure is needed for the polymer to flow. In a circular conduit the high pressure gradient causes the polymer melt to expand in the down stream and therefore cooling effect arises at the center of the tube. In the energy equation compressible energy effects are expressed in the term

$$E_p = T\left(\frac{\partial P}{\partial T}\right)_\rho \left(\frac{\partial v_z}{\partial z}\right) \tag{141}$$

Where E_p = energy consumed due to the expansion, lb_f/ft^2-sec.

By definition

$$\epsilon = -\frac{1}{\rho}\left(\frac{d\rho}{dT}\right)_P , \qquad \text{Coefficient of thermal expansion, } {}^oF^{-1}$$

$$\beta = \frac{1}{\rho}\left(\frac{d\rho}{dP}\right)_T , \qquad \text{Compressibility, } ft^2/lb_f$$

From the above definitions one can write

$$\left(\frac{\partial P}{\partial T}\right)_\rho = \frac{\epsilon}{\beta} , \qquad lb_f/ft^2\ {}^oF \qquad (142)$$

Foster, Waldman and Griskey [24] used the Spencer and Gilmore equation of state to determine the compressibility of the high density polyethylene.

2. Nonisothermal non-Newtonian Flow

There are some difficulties to study the nonisothermal flow of viscous non-Newtonian fluids, i.e., the viscosity of the fluids changes with temperature and, therefore, heat transfer affects the velocity distribution. Frictional heat generated during flow and cooling due to expansion must be included in

many cases and variations of thermal diffusivity and heat capacity with temperature must be considered.

a. Viscous Heat Dissipation

When the fluid flows, the friction between the layers of the fluid causes mechanical energy to be converted into heat, which is called viscous heat dissipation. In most cases effect can be neglected, but if high velocity gradients or high viscosities are encountered, viscous heat dissipation would be consderable. In general the flow of polymer is in this catyory.

Brinkman[14] solved the problem of viscous heat dissipation for the first time for laminar flow of a Newtonian fluid through capillaries. Toor[53,54] and Bird[9] have extended Brinkman's work to include Non-Newtonian flow.

The amount of viscous heat dissipation for the axial steady flow of a fluid can be expressed as

$$\phi_v = \tau_j^i v_j^i = \eta \left(\frac{d v_z}{d r}\right)^2 \tag{143}$$

The Brinkman number is defined for Newtonian fluids as

$$B_r = \frac{\mu V^2}{\kappa (T_w - T_0)} \tag{144}$$

for non-Newtonian fluids

$$B_r' = \frac{K(V)^{n+1}}{\kappa R^{n-1}(T_w - T_0)} \tag{145}$$

The Brinkman number is a measure of the extent to which viscous heating is important as compared to the heat transfer from the tube wall to the center of the tube.

b. Heat Transfer to the polymeric Fluids

When molten plastics are extruded through conduit at high shear stresses a temperature distribution may result from the heat produced by viscous dissipation. Many theoretical and experimental work have been done on this subject.

Bayer and Dahl[7] carried an experiment to measure the temperature profile of polystyrene in an injection molding machine. The mass average temperature was calculated from the temperature profile measurement by weighing the temperature at each point with the amount of polymer flowing past the point. They found that the mass average temperature was within three percent of the temperature measured at 0.6 of the radius from the center of the polymer stream. Schott and Kaghan[51] measured the radial temperature profile of a low density polyethylene flowing through a one inch I. D. circular donduit three inches long.

The radial distance of the thermocouple tip inside the die channel was measured with a travelling microscope to within ± 0.001 inches. They found the ratio r/R at which the temperature

was equal to the calculated average temperature was found to be between 0.65 and 0.70, regardless of whether the melt at the center was warmer or cooler than the melt near the wall.

Bird[9] has theoretically studied the case, where the polymer melt through a tube with an isothermal wall. From the equation of the energy he developed an expression including viscous heat dissipation term as

$$\mu\left(\frac{\partial v_z}{\partial r}\right)^2 + \kappa \frac{1}{r}\frac{\partial}{\partial r}\left(r\frac{\partial T}{\partial r}\right) = \rho v_z C_p \left(\frac{\partial T}{\partial z}\right) \qquad (146)$$

The velocity distribution for a power law fluid can be stated as

$$v_z = \frac{R}{\alpha+2}\left(\frac{\tau'}{\mu'}\right)\left(\frac{\tau_w}{\tau'}\right)^{\alpha+2}\left[1-\left(\frac{r}{R}\right)^{\alpha+2}\right] \qquad (147)$$

The following form of power law model was used in this derivation

$$\frac{1}{\mu} = \frac{1}{\mu'}\left(\frac{\tau_w}{\tau'}\right)^{\alpha}\left(\frac{r}{R}\right)^{\alpha} \qquad (148)$$

where

τ' = shear stress

μ' = the viscosity at shear stress, τ'

α = a measure of the deviation from Newtonian behavior.

The expression for the heat produced by viscous dissipation is given as

$$\mu\left(\frac{dv_z}{dr}\right)^2 = \frac{(\tau')^2}{\mu'}\left(\frac{\tau_w}{\tau'}\right)^{\alpha+2}\left(\frac{r}{R}\right)^{\alpha+2} \qquad (149)$$

Defining the following dimensionless group Bird solved Equation(140) for two cases, one is for the case of isothermal tube wall and the other is for the case of insulated wall.

Isothermal wall:

$$\theta = \frac{1}{4}(1-\xi'^{\alpha+4}) - \sum_{i=1}^{\infty} B_i \phi_i(\xi') \exp(-e_i \zeta) \tag{150}$$

Insulated wall:

$$\theta = \frac{(\alpha+4)^2}{8(\alpha+2)}\left[\xi'^2 - \frac{2\xi'^{\alpha+4}}{\alpha+4} + 4\zeta\right] - \sum_{i=1}^{\infty} B_i \phi_i(\xi') \exp(-e_i \zeta) \tag{151}$$

For $\zeta = 0$, the constants, B_i, can be evaluated for isothermal wall:

$$B_j = \frac{1}{4} \frac{\int_0^1 (1-\xi'^{\alpha+4})(1-\xi'^{\alpha+2}) \xi \phi_j \, d\xi'}{\int_0^1 (1-\xi'^{\alpha+2}) \xi' \phi_j^2 \, d\xi'} \tag{152}$$

and for insulated wall

$$B_j = \frac{(\alpha+4)^2}{8(\alpha+2)} \frac{\int_0^1 (\xi^2 - \frac{2\xi'^{\alpha+4}}{\alpha+4})(1-\xi'^{\alpha+2}) \xi' \phi_j \, d\xi'}{\int_0^1 (1-\xi'^{\alpha+2}) \xi' \phi_j^2 \, d\xi'} \tag{153}$$

where

$$\xi' = \frac{r}{R}$$

$$\zeta = \frac{Z(\alpha+2)\, K \mathcal{U}'}{C_p R^3 \tau_w (\tau_w/\tau')^{\alpha}}$$

$$\theta = \frac{T(\alpha+4)^2 K \mathcal{U}'}{4 R^2 \tau_w^2 (\tau_w/\tau')} \qquad (154)$$

Toor[53,54] made the same assumtions as Bird but assuming compressible fluid. He used a power law rheological equation of the form:

$$\frac{dV_z}{dr} = -F \tau^{m-1} \qquad (155)$$

where F = rheological constant $\left(\frac{ft^2}{lb}\right)^{m-1}$/hr

m = rheological constant, dimensionless

and $F = K^{1-m}$

$m = \frac{1}{n} + 1$

Toor modified the equation of motion:

$$-\left(\frac{\Delta P}{\Delta Z}\right) = \frac{1}{r} \frac{\partial (r \tau_{rz})}{\partial r} \qquad (156)$$

and obtained

$$V_z = \frac{m+2}{m} V_{max} (1 - \xi'^{m}) \qquad (157)$$

where (158)

$$\xi' = \frac{r}{R}$$

and

$$V_{max} = \frac{F R^m}{m+2} \left(-\frac{dP}{2dz} \right)^{m-1} \quad ft/hr \tag{158}$$

He modified the energy equation as

$$V_z C_p \frac{\partial T}{\partial z} = T \frac{\epsilon}{\beta} \left(\frac{\partial V_z}{\partial z} \right) + \frac{k}{r} \frac{\partial}{\partial r} \left[r \frac{\partial T}{\partial r} \right] + \frac{m+2}{2} W' s'^m \tag{159}$$

where $W' = - V_{max} \frac{dP}{dz}$, $lbf/ft^2 . hr$

Combining Equations (152) and (153) he obtained

$$\left(\frac{m+2}{m} \right) V_{max} (1 - s^m) \frac{\partial T}{\partial z}$$

$$= \frac{\kappa}{\rho C_p r} \frac{\partial}{\partial r} \left[r \frac{\partial T}{\partial r} \right] + \frac{m+2}{m} \frac{W'}{\rho C_p} \left[\frac{m}{2} s'^m - \epsilon' (1 - s'^m) \right] \tag{160}$$

Gee and Lyon[26] extended the heat transfer problem to non-isothermal non-Newtonian fluid including the factors of the variations of and thermal diffusivity with temperature, the heat generated by friction and cooling resulting from expansion. They considered only one material, Acrilic Resin, Polymethyl Methacrylate (Lucite 140).

They used an rheological equation as

$$\frac{1}{\eta} = \frac{1}{\eta_0} (1 + \kappa \tau^n) \tag{161}$$

where

E is the activation energy

R is the gas constant

A is the Newtonian Viscosity extrapolated to $0^{\circ}K$, poises.

The resultant energy equation is

$$\frac{v_z}{L_o}\frac{\partial T}{\partial z} + \frac{\partial T}{\partial \theta} = \frac{\alpha}{R_o^2}\left(\frac{\partial^2 T}{\partial y^2} + \frac{1}{y}\frac{\partial T}{\partial y}\right) + \frac{\eta}{\rho C_p R_o^2}\left(\frac{\partial v}{\partial y}\right)^2 + \frac{v}{L_o}\left(\frac{\bar{T}_{flow} \times \acute{\epsilon}}{\rho C_p}\right)\frac{\partial P}{\partial z} \qquad (162)$$

where

$y = \frac{r}{R}$

$\bar{T}_{flow}$ = average flow temperature

L_o = length of tube

E = coefficient of expansion at $\bar{T}_{flow}$

and for the temperature dependent physical property they used Equation(140). The equation was solved using a Gauss-Seidel iterative type method. For the case where the wall temperature is approximately equal to the initial fluid temperature the position of the maximum temperature, resulting from frictional heat generation shifts slightly toward the center of the tube for increasing distances down the tube. The average flow temperature lay between $\frac{r}{R}$ of 0.62 and 0.66. This value is in agreement with the measured value of 0.6 reported by Bayer and Dahl. Of interest in the result was the prediction that the wall

temperature must be reduced below its initial value by 60°F for the center core to feel the wall temperature. The assumptions were justified by the good agreement between the calculated flow rate and the measured one.

Griskey and Wiehe[29] attempted to extend the Graetz-Nusselt problem to the case of polymer melt. Polyethylene and polypropylene were used in their experiment. The polymer extruded by one inch Killion screw extruder was delivered to a mixing orifice to get uniform temperature and then sent into a heat transfer section of Schedule 80 $\frac{3}{8}$" pipe the wall temperature of which was maintained constant.

The measured polymer melts temperature were less than those predicted from theoretical calculations and the Graetz-Nusselt data measured for polyethylene melts agrees fairly well with theoretical curves.

Forsyth and Murphy[22,23] obtained temperature profiles of molten flowing polymers through an isothermal wall heat exchanger. A one inch screw extruder melted the polymer and pumped it to a metering pump, which delivered the melt to the heat exchanger at a steady state. The heat exchanger was 3.7 ft long of 0.370 in. I. D. At the heat exchanger exit, a thermocouple was inserted $\frac{3}{4}$ in. into the polymer side of the heat exchanger, parallel to the tube axis. The radial position of the thermocouple tip was measured to within 0.002 in. by a set of micrometer gages. The thermocouple was 0.0355" in O. D.

They noticed a maximum temperature is observed in the temperature profile for cooling polymer melts at low Graetz numbers at a radial position between 0.70 and 0.80. It was concluded the temperature dependent power law model with viscous heating effects is a more accurate method of predicting temperature profile calculations for cooling of polymer melts. The result showed large viscous heating effects, particularly for cooling.

Recently Saltuk[51] developed a similar experiment as Wiehe's to measure the temperature profile of polyethylene flowing in 1" schedule 80 stainless tube. An oil circulating system was used rather than electrical heating to get the uniform wall temperature. The equipment is the same one used in this investigation and the details has been described in the experimental section.

The melt temperature were measured at seven different radial position(including wall temperature) and five different axial position of 0.527, 3.560, 6.600, 9.560 and 12.600 ft from the inlet temperature thermocouple.

The plot of reduced temperature and reduced radius showed significant viscous heating effect between Graetz No. of 7.5 to 595.0.

III. EXPERIMENTAL

A. Plan of the Experimentation

There was previous experimental work[34,40,20] concerning the entrance region flow in a pipe for the Newtonian and Non-Newtonian fluids. In additon, some studies were directed to capillary flow for polymer melts.[30,31,39,6] The apparatus for this work is quite different from the previous studies both in size and complexity.

The equipment was designed to study the isothermal flow behavior of a polymer melt in the entrance region. The apparutus was used to separate the pressure drop into viscous and elastic effects. This was to be done by measuring the pressure drop in a larger pipe of chamber and then the pressure drop developed during a contraction and finally the pressure drop in a smaller pipe following the contraction..

Another facet of the study was to try to find the entrance length for the the melt to relax. This relaxation is due to the excessive normal stress developing just before the mouth of the entrance.

In additon to the entrance flow study, attention was directed to the transfer of heat to a thermally softened flowing polymer (polymethyl methacrylate). The device used for this work is also described herewith.

B. Development of Equipment

1. General

Two separate experimental devices were required for the present work: one to study the entrance effects in flow in molten polymer systems and the other to investigate the transfer of heat to thermally softened flowing polymer systems. Although two devices were needed some components were common to both. These will be described below.

In any study relating to a flowing polymer system (whether molten or thermally softened) a rugged precise, pumping apparatus is needed. The method used in the present work was to combine a 2" diameter screw extruder with a gear pump-vari-drive combination. The polymer flowed from the extruder to the gear pump which served as a metering pump for the extruder outputs. The gear pump not only allowed exact metering of the polymer flow but also smoothed out possible flow fluctuations originating in the extruder. The vari-drive made it possible to precisely set the speed at which the gear pump was driven. One additional aspect(important for the heat transfer study) was that the polymer temperature profile was flat at the gear pump exit.

Another common segment was a heat unit for the test sections following the gear pump. The components of the system were reservoir tank, rotary pump and two sets of heating coils in two containers. (See Figure 10.)

FIG. 10 EQUIPMENT AND PIPE LAYOUT

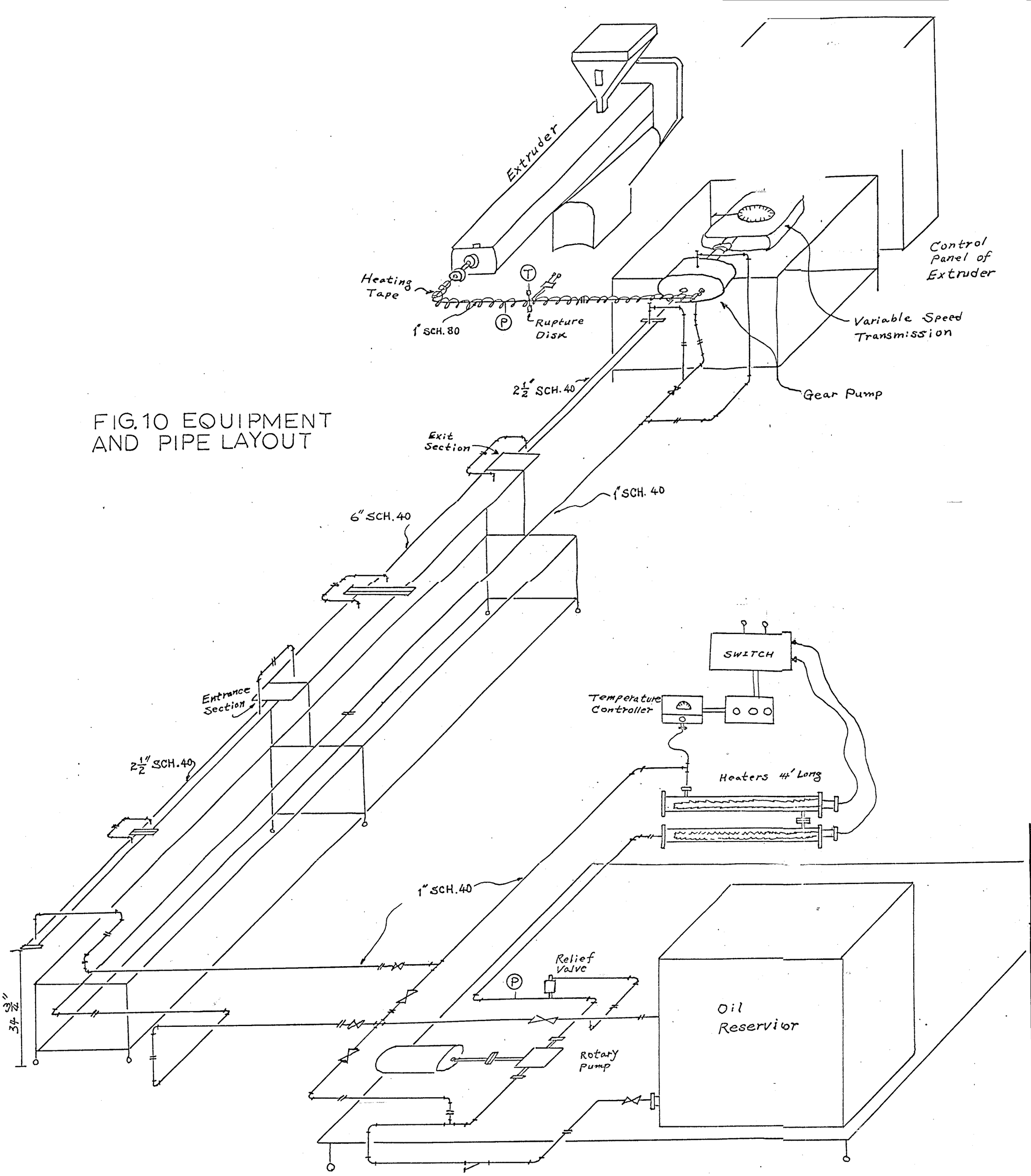

The oil was drawn from the reservoir by a rotary pump and passing through the heater supplied to the double pipe heat exchanger (test section) and gear pump housing. It then returned to the pump to form a closed circulation system.

The heating unit was designed to compensate for the heat loss from the equipment to the surroundings.[42] Heat loss from gear pump, test section and heating unit itself was approximately calculated as 5 Kwh at the operating temperature of 200°C. Two 6 Kw heating coil were selected to supply the amount of heat required(considering a safety factor).

Mobiltherm 600 was used as the oil in the heating unit. Oil temperature was set and controlled by Partlow Industrial temperature controllers. This type of controller has a metal bulb filled with mercury. The metal bulb is immersed in the heater. Temperature is controlled by the expansion of mercury through a capillary tube to a spring and plunger loaded diaphragm. The entire system was insulated with asbestos and insulation cement.

2. Entrance Region Test Section

a. Test Section

The entrance region test section was designed in the following manner. A length of pipe (1" schedule 80) led from the gear pump to an enlarged section. The enlarged section

which was 4" schedule 80 pipe led in turn to another length of 1" schedule 80 pipe. The result (see Figure10) was an expansion from the 1" to the 4" pipe and then a contraction from the 4" pipe to the 1" pipe. The entire test section was jacketed and heated in the manner described previously.

The particular pipe diameters used were selected so that the polymer shear rates would be in a range which could be obtained with the Weissenberg Rheogoniometer (Model R18). In addition, careful attention was also given to the design of the axial lengths for the 1" diameter entrance and exit sections as well as the 4" diameter enlarged section. These were all checked by estimates made from earlier work on polymer melt.[39,6] Details are shown in Figures 4, 5 and 10.

A total of 28 pressure tap holes were used. These are shown schematically in Figure 6 together with the placement of wall temperature taps (9 in number). Tables I and II also list the positions of the various taps. The pipe entrance and exit regions had five different pressure tap holes symmetrically at various axial and radial positions. (See Figure 7). The placement of the pressure taps was partially based on the earlier work of La Nieve[34] and a desire to maximize information concerning entrance and exit flow behavior for molten polymer systems.

Pressures were measured with transducers manufactured by the I.T.I. Corporation (4631 Scotts Valley Drive, Santa Cruz, Calif. 95060). These devices, developed originally for

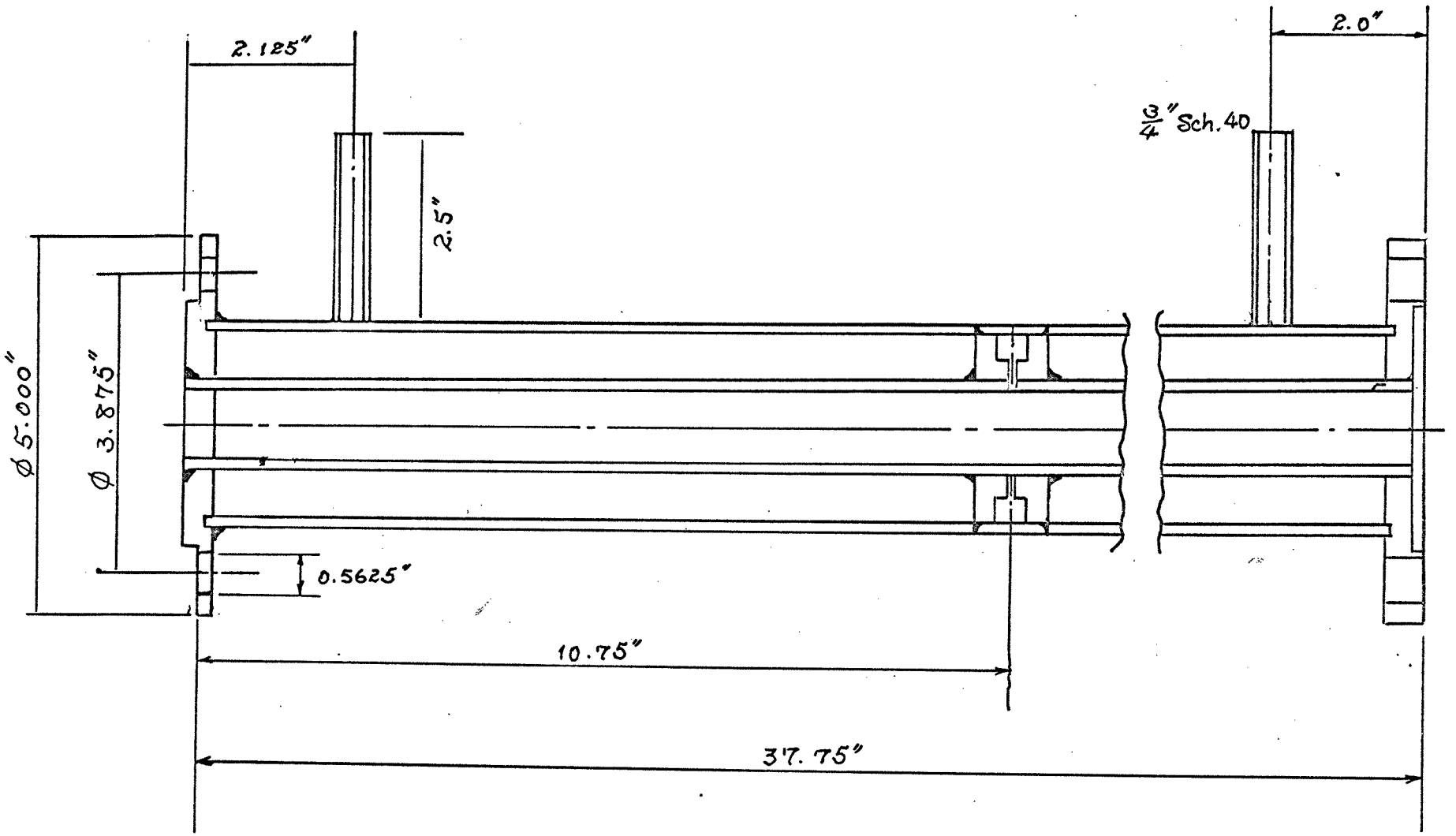

FIG. 4 1" SCH. 80 JACKETED BY $2\frac{1}{2}$" SCH. 40
SCALE = 1 : 2

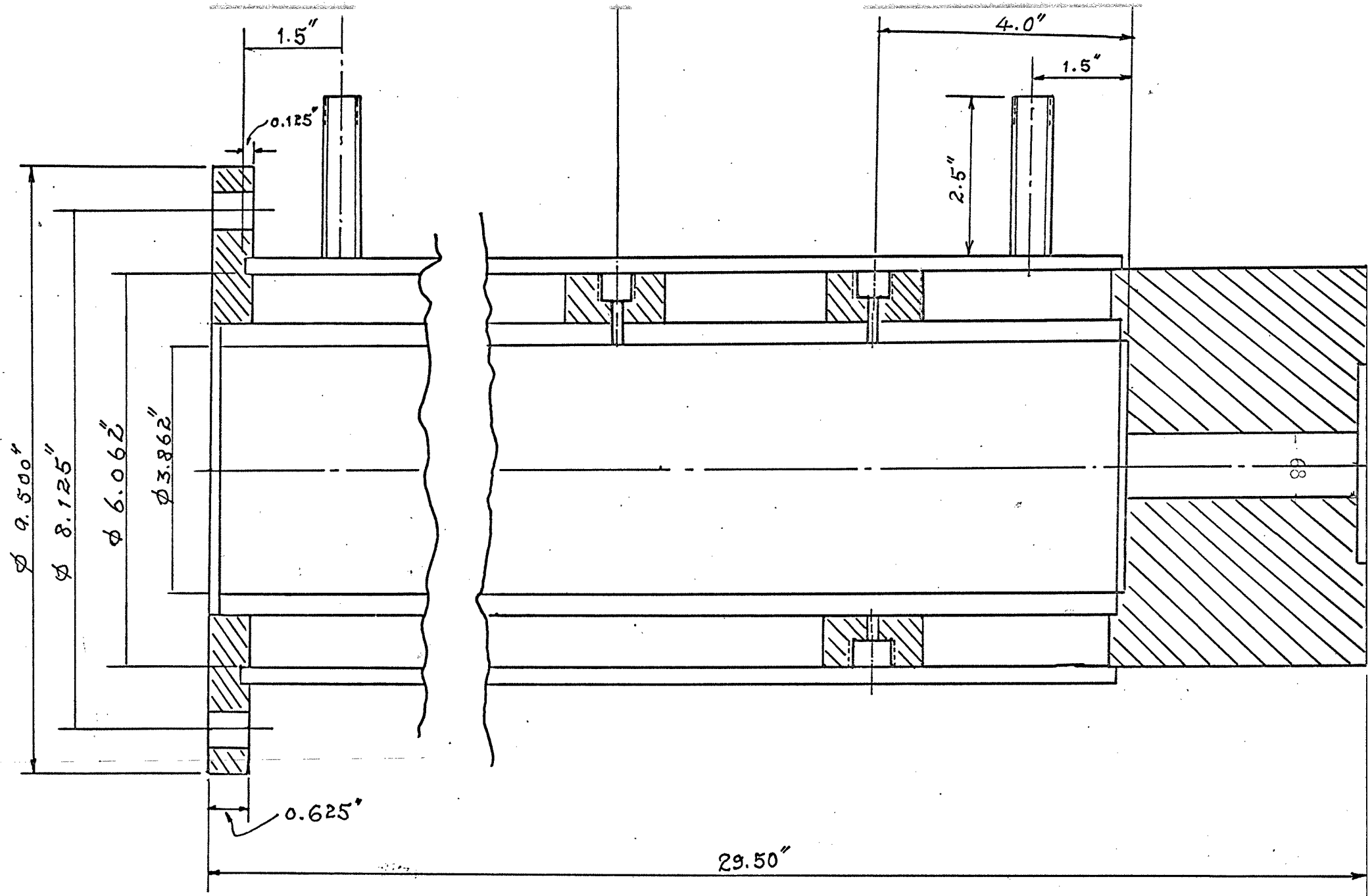

FIG. 5 4" SCH. 80 JACKETED BY 6" SCH. 40

SCALE = 1:2

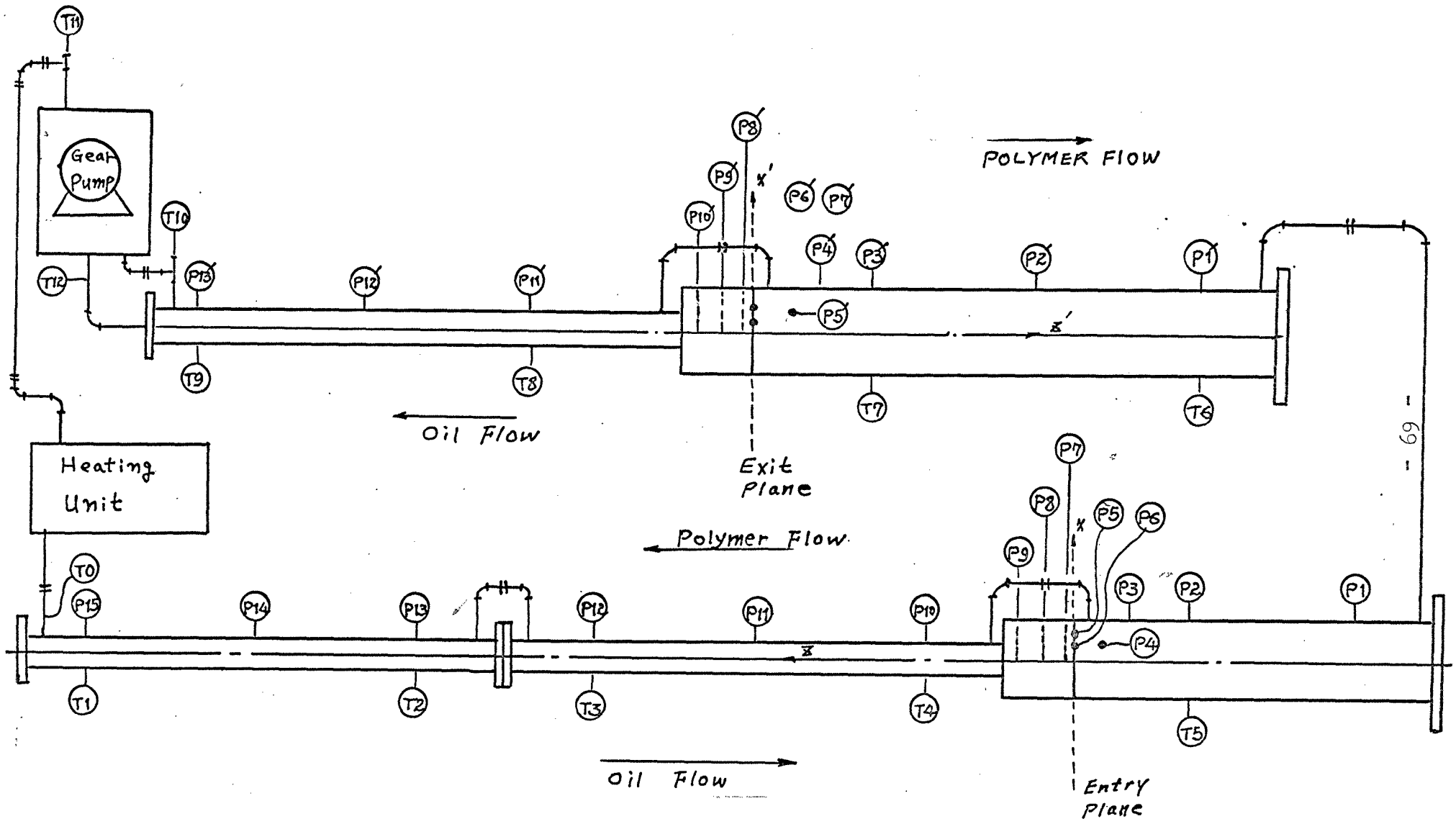

FIG: 6 POSITION OF PRESSURE AND TEMPERATURE TAP HOLES

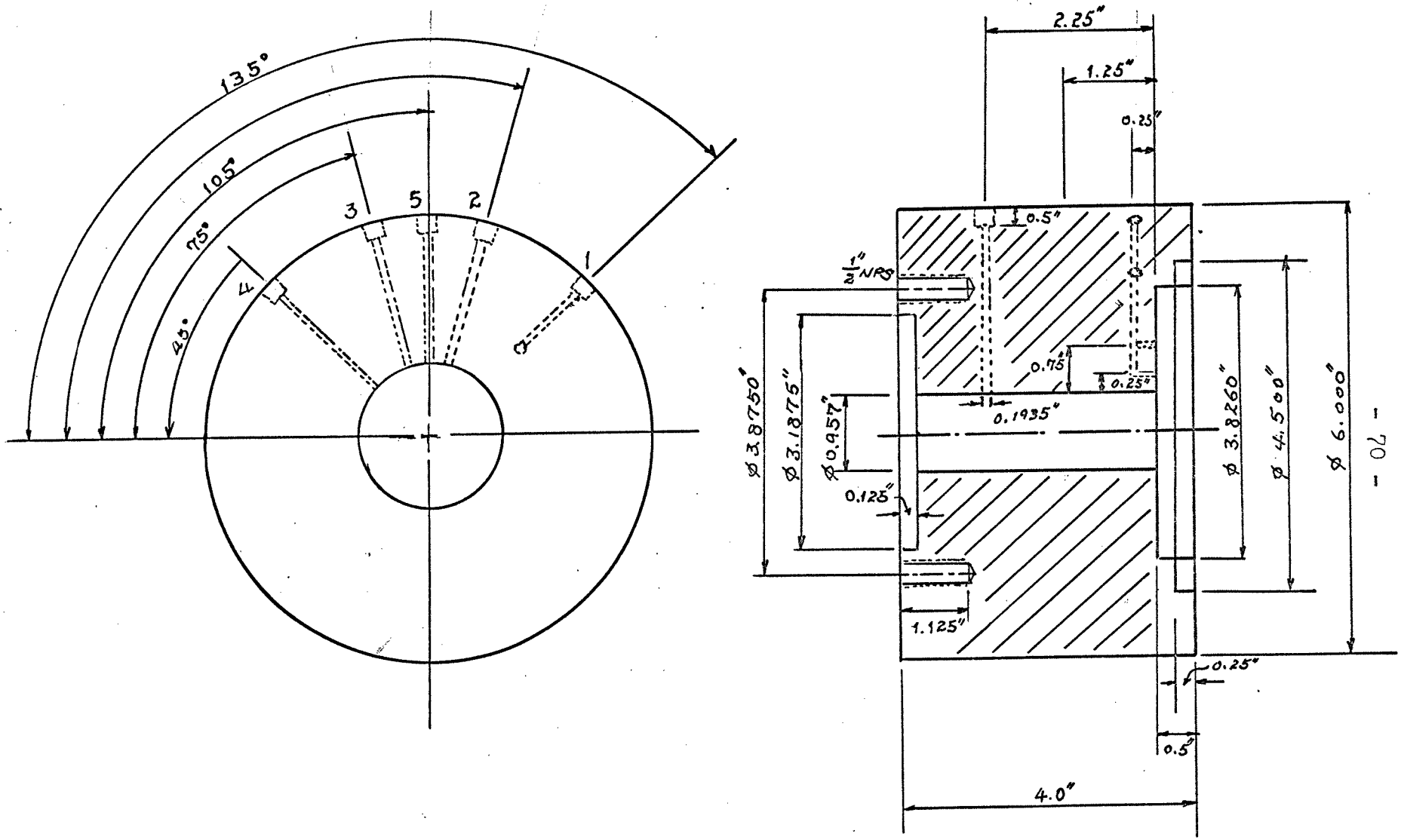

FIG. 7 ENTRANCE AND EXIT SECTION

SCALE = 1 : 2

TABLE I POSITION OF PRESSURE HOLES IN THE ENTRANCE REGION

TAP NO.	X(in)	Z(in)
P1	1.931	-20.000
P2 (T5)	1.931	-8.000
P3	1.931	-4.000
P4	45° deviation from X axis as shown in Fig. 6	-2.000
P5	1.2285	0.000
P6	0.7285	0.000
P7	0.4785	0.250
P8	0.4785	1.250
P9	0.4785	2.250
P10(T4)	0.4785	10.750
P11	0.4785	22.750
P12(T3)	0.4785	34.750
P13(T2)	0.4785	48.000
P14	0.4785	61.000
P15(T1)	0.4785	73.000

TABLE II POSITION OF PRESSURE HOLES IN THE EXIT REGION

TAP NO.	X'(in.)	Z'(in.)
P1'	1.931	32.000
P2'	1.931	20.000
P3' (T7)	1.931	8.000
P4'	1.931	4.000
P5'	45^{o} deviation from X axis as shown in Fig. 6	2.000
P6'	1.2285	0.000
P7'	0.7285	0.000
P8'	0.4785	-0.250
P9'	0.4785	-1.250
P10'	0.4785	-2.250
P11' (T8)	0.4785	-14.000
P12'	0.4785	-26.000
P13' (T9)	0.4785	-38.000

oceanographic studies, had a wide range of pressure capability. The behavior under varied temperature conditions was not as well known. However, the vendor(Louis Johnson) indicated that prior experience with temperature was favorabel. Very favorable aspects of the transducers were their relatively low cost and infinite resolution.

System temperatures were measured with iron constantan thermocouples placed as per Figure 6. In addition, each pressure transducer unit was itself equipped with a alumel-chromel thermocouple.

b. Pressure Measuring System

The pressure transducer used was similar to the memory core of a computer (Size: 0.070" outside diameter, 0.02" high; weight: 0.015 grans). The device is a ferrimagnetic transducer made of Nickel ferrite which exhibits a property called magnetostriction. The transducer converts the parameters of pressure or force or weight to usable voltage levels. The sensor was equipped with primary and secondary windings similar to a transformer. When the sensor was embedded into a medium and then electrically exerted, pressure forces would act hydrostatically in it. These forces caused the volume to decrease infinitesimally. The result which was a change in the magnetic flux content together with a change in flux content.

The latter caused a change in output voltage since

$$E = N \frac{d\phi}{dt}$$

where E = output voltage

N = numbers of turns

$d\phi/dt$ = change in flux with respect to the switching time of the core

The output voltage was a maximum at zero pressure and decreases with increasing pressure. An auxiliary system supplied the electric current and depicted the output voltage. The auxiliary consisted of two fundamental circuits. One was an oscillator driver and the other the sense electronics. The circuits in the auxiliary operated from ± 15 VDC supplied by DC dual power supply. The oscillator operated as a current source and supplied a 1 amp., 2.5 sec pulse to the primary winding of the core. The voltage pulse from the sensor secondary winding was fed to the sense electronics and the peak detect or circuit accepted the voltage pulse. This was presented at the output as a DC voltage equal to that of the pulse peak. There were three amplifiers in the auxiliary pulse generator: the buffer amplifier, an inverter amplifier and the high gain amplifier. The inverter amplifier simply inverted the output so the reader gave zero output voltage at zero pressure. The high gain amplifier and associated gain adjust provided amplification of the sensitivity between unity and 100.

The orifinal transducers as provided needed some provision

to prevent the leakage of the molten polymer melt through the device under the high pressures of the study. This was done as follows: First, the four extension wire of the core were carefully separated by four teflon tubes of small diameter and placed with the core in a stainless steel tube. A commercial epoxy resin was used as a seal between the teflon tubes and the stainless steel.

3. Heat Transfer Test Section

The test section was smooth stainless tubing (0.957" inside diameter). This type of tubing not only assured streamline flow but also eliminated any possibility of interior wall roughness. The test section was jacketed and heated with oil. The heat exchanger units were preceisely regulated so that the wall temperature of the test section was kept essentially constant. A drawing of a heat exchanger section is given in Figure 11 while a schematic of the hot oil circulating unit is given in Figure 10. It should be noted that the gear pump unit was also heated by oil flowing through a jacket.

Temperature profile measuring devices were set at various axial lenghts in the test section. The first of these at a distance 0.525 feet from the gear pump exit and the others at 3.525, 6.525, 9.525 and 12.525 feet, respectively, from the same exit. (See Figure 12.)

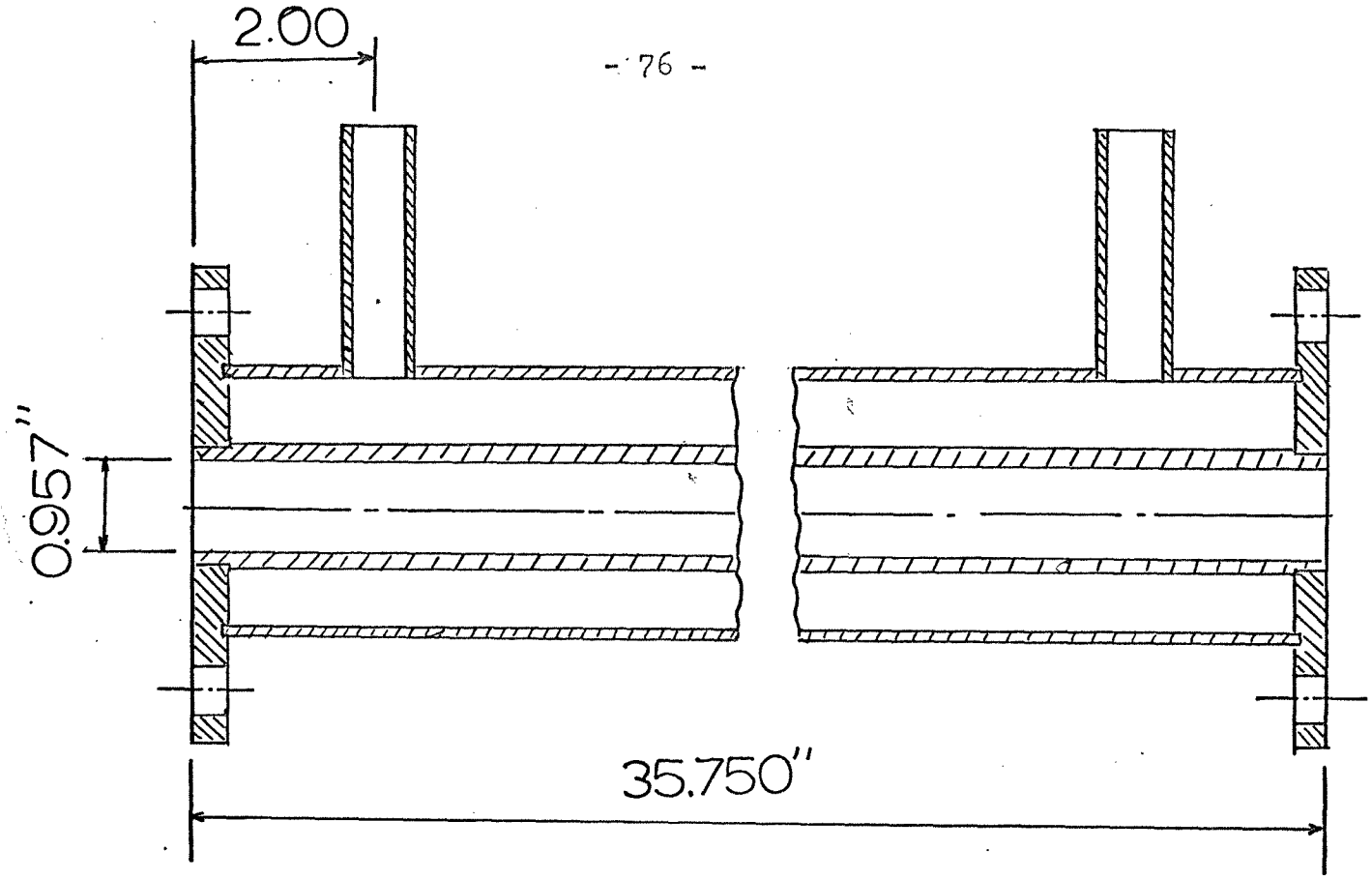

SCALE = 1 : 2

FIGURE 11. Heat Exchanger Section

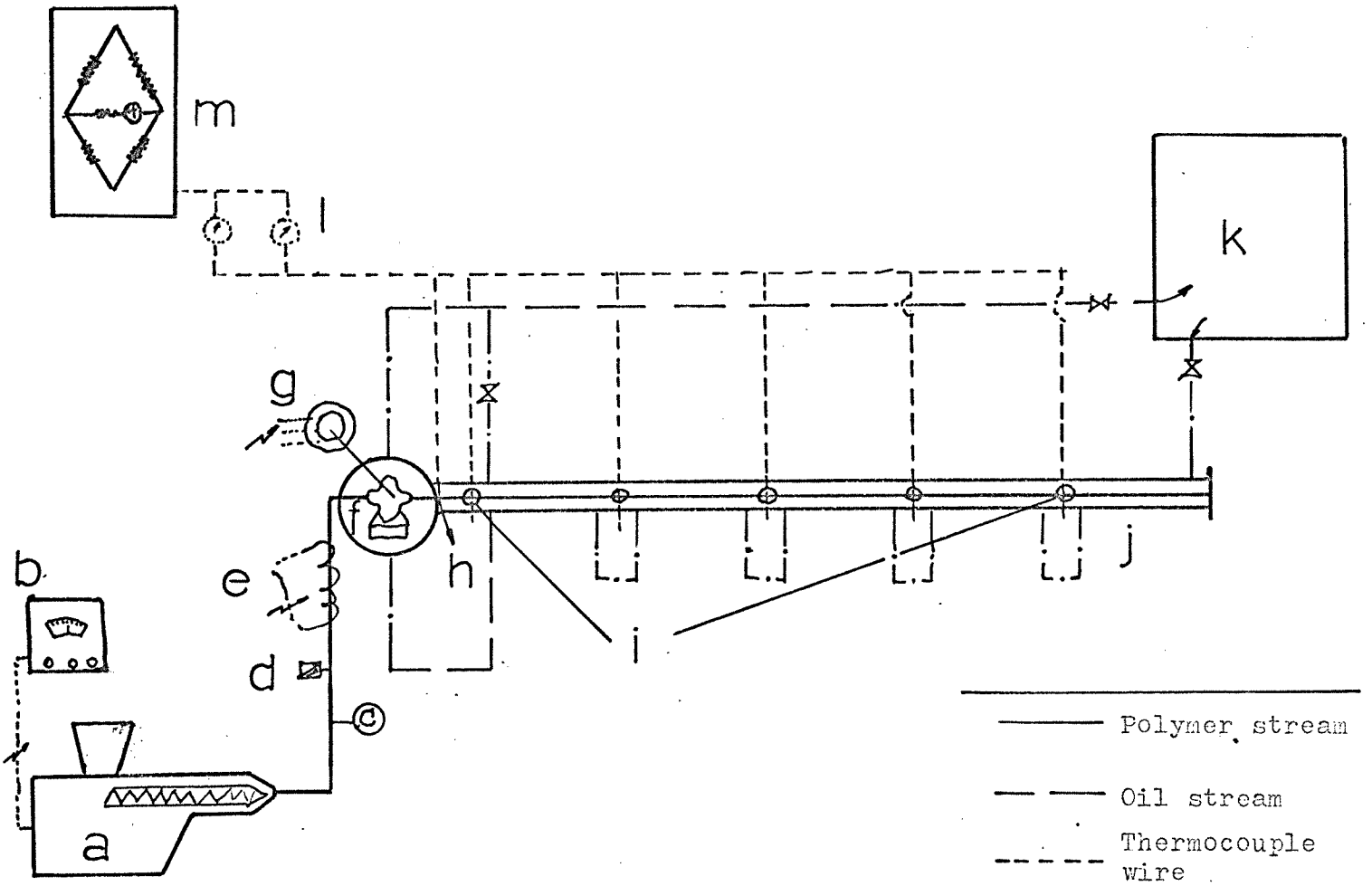

a - extruder
b - control panel
c - pressure gage
d - safety rupture disc
e - heating tape
f - metering pump in oil jacket
g - vari-drive
h - average inlet temperature Thermocouple
i - multi-probe-profile ring at different heat transfer lengths
j - a heat exchanger section
k - hot-oil-circulating unit
l - multi-point Thermocouple switches
m - potentiometer facility

FIGURE 12. A Schematic Diagram of Heat Transfer Apparatus

The temperature profile measuring device is shown in Figure 13. Thermocouples were parallel to the flowing polymer and pointed upstream. This configuration was used because it gave excellent dynamic response, thermal precision and mechanical stability. In addition, flow disturbances and viscous heating at the thermocouple itself were minimized. A total of six thermocouples were used in each measuring device.

The thermocouples were iron-constantan enclosed first in hypodermic tubing and then in a stainless steel sheath. Teflon packing was used as an insulation between the hypodermic tubing and the stainless steel sheath. This type of thermocouple insured against the possibility of errors due to heat conduction.

The outside diameter of each probe was 0.0625 inches. This meant that the given thermocouple surface "seen" by the flowing polymer was only 0.5 per cent of the total tube cross sectional area. This figure was considerably less than that in the other studies of temperature measurement in molten flowing polymer systems.

All of the probes were set at different reduced radial points (0.00, 0.186, 0.373, 0.560, 0.746 and 0.931). The pattern of the probes when viewed from the position of the flowing polymer was spiral-like. Such a pattern meant that there was minimal interference of any probe with its neighbors. In addition, it should be noted that the spiral pattern was changed at each axial length position.

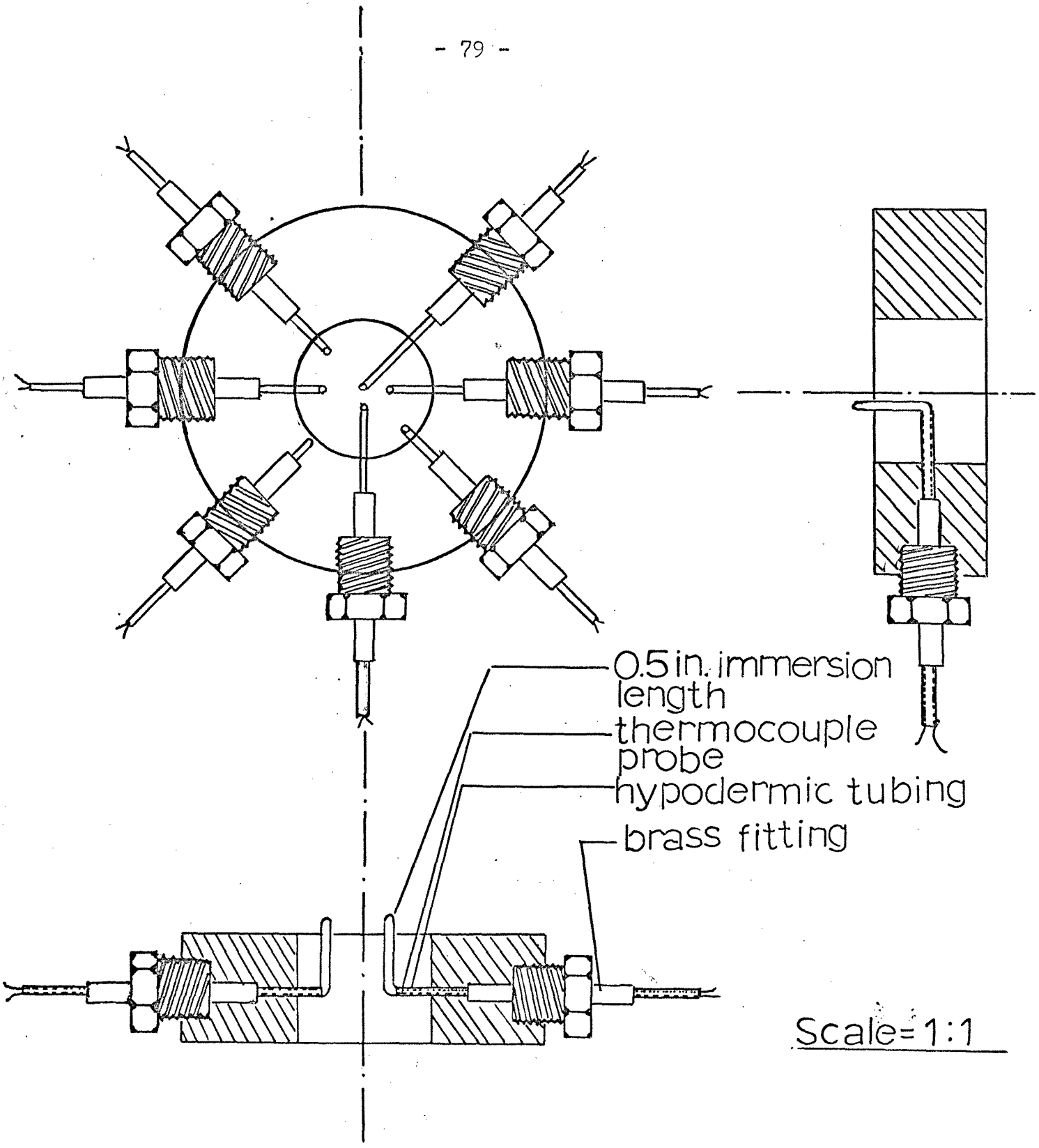

FIG. 13 Multi-Probe-Profile Ring

Each probe extended 0.5" into the flowing melt. This immersion length was determined by both mechanical stability and the need to avoid heat conduction errors.

The combination of the small diameter of each probe, the spiral like pattern for the probes and the pattern alteration at each axial length all helped to minimize both flow disruptions and viscous heating at the probe. This can be more clearly understood by considering the situation in more detail.

First, polymer flow is directed to a very small cylinder (each probe). The resultant boundary layer at the probe is consequently very small with essentially no flow disruption. Furthermore, the separation of the probes by the spiral like pattern assures that any disruption (although minimal) does not become synergistic. Finally, the alteration of the spiral pattern at each axial length means that any transmission of flow disruptions from axial length to axial length will be eliminated.

In a similar way the small probe diameter minimizes viscous heating at each probe surface. Next, the spiral like pattern prevents any cumulative effect of probe viscous heating. The axial length separations further insure that no probe viscous heating effect will be transmitted to the next axial length.

C. Experimental Procedure

1. Entrance Region Tests

a. Calibration of Pressure Measuring Systems

A special metal chamber was made to calibrate the transducer (Figure 8). The chamber had provisions for an oil pressure inlet, a thermocouple, one transducer, and a screw for purging the air in the chamber. The chamber was submerged in a silicon oil heat bath to keep temperature constant. A dead weight tester was used to supply the necessary pressure.

It was found, however, that oil leaked into the transducer because the epoxy resin did not adhere well enough to the teflon and stainless steel tubing. The teflon tubing was etched with teflon etching agent and the stainless tube with aqua regia to provide better adhesion. However, there was still leakage. In fact, the extension wire and the soldered junction between the extension wires broke because of the thermal expansion of the materials and improper protection of the wire. Another try was made to seal the gap by using an epoxy melt, but again it failed. Finally, a ceramic tube with six tiny holes was used in place of the teflon tube. This procedure yielded somewhat better results.

Two types of transducers were calibrated. One had a core that was prestressed with epoxy resin to give high sensitivity. This was to be used for low pressure measurements (0-500 psi). The other which had no epoxy resin in the core was to be used for the measurement of higher pressures (0-2000 psi).

Output voltage in both cases was measured by nulling the voltage with a Harrison D. C. Power Supply at D. C. output terminals.

The following is the actual calibration procedures. First, the hot oil bath was heated up to the desired temperature, one of 160°C, 190°C and 220°C. All the instrument were turned on for about 30 minutes to be stabilized. D. C. Dual Power Supply was connected to the auxiliary read-out (System 2000) during the calibration. The calibration started from zero pressure. When the cable from the transducer was hooked up to the auxiliary read out the reading of the auxiliary read-out was fixed at a certain point between 0-100 by controlling the referrence adjust.

After disconnecting the cable a.D..C. voltage was applied to the auxiliary read out through the pulse output. By adjusting the applied voltage the needle of the auxiliary read-out was brought up to the same point fixed previously. The applied voltage was read for the zero pressure from D. C. Digital Power Supply.

In the same way the equivalent output-voltage for 250 psi was recorded and all the way up to 2000psi by 250 psi increment. The temperature was checked for each pressure measurement.

Considerable difficulty was encountered in calibrating the transducers. The needle of the auxiliary read-out drifted continuously. A check of the various system combinations showed that the problem seems to lie in the cable linking the sensor

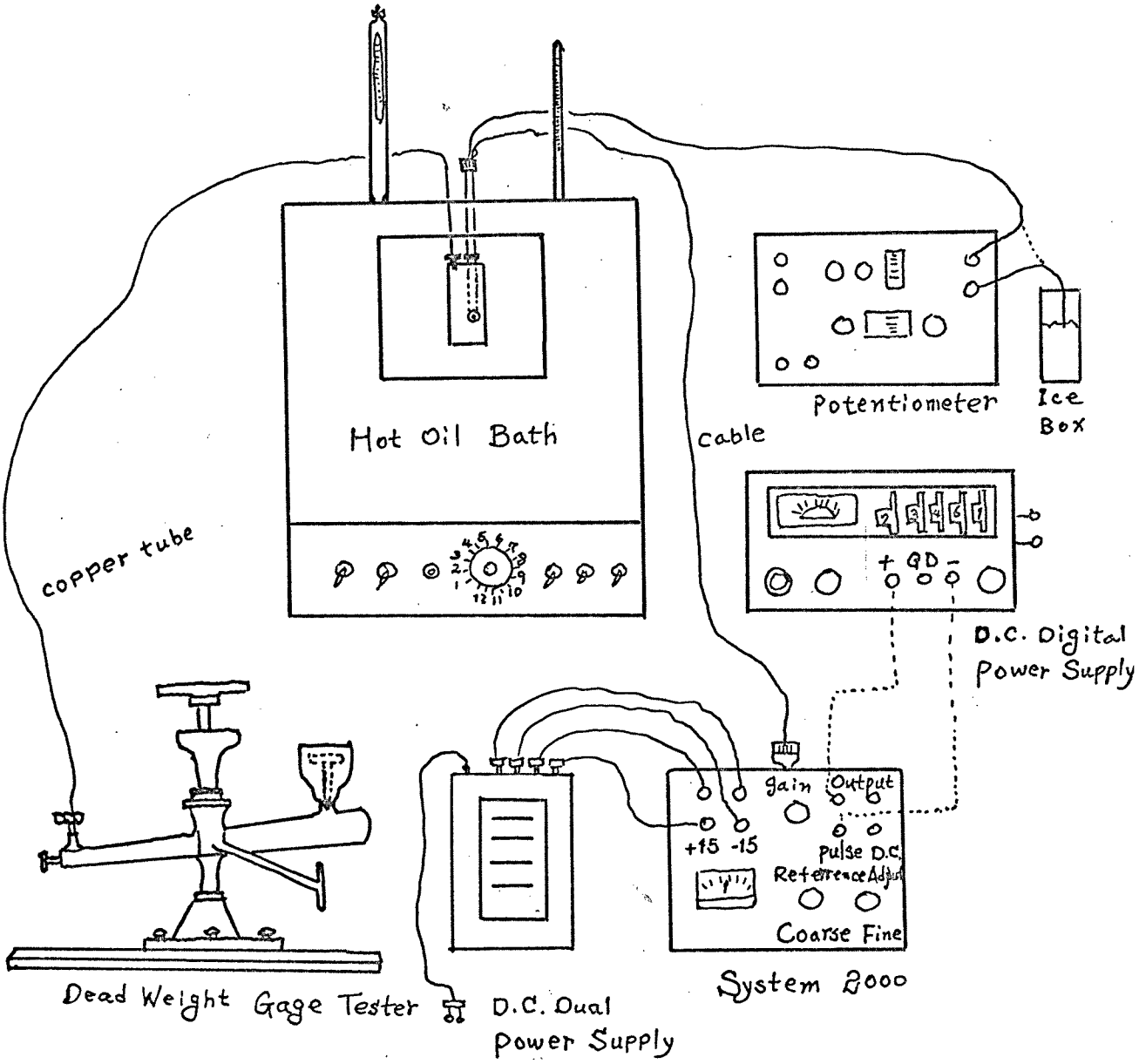

FIG. 8 TRANSDUCER CALIBRATION SYSTEM

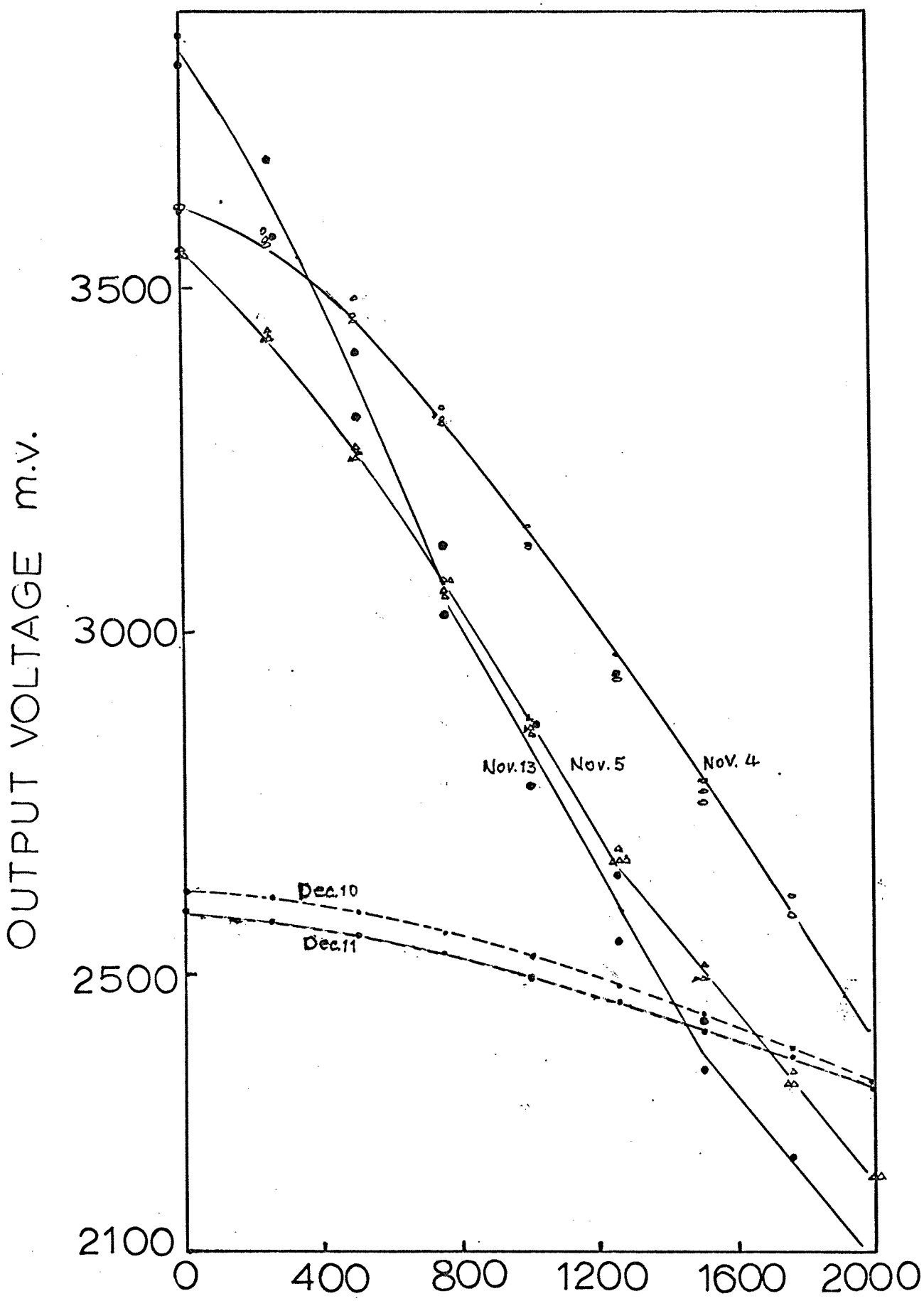

FIG. 9 CALIBRATION CURVE

and auxiliary. Replacement of the cable did not alleviate the problem. A typical set of data are shown in Figure 9. As can be seen, results shifted considerably over a given time period.

Continued results of the type found in Figure 8 led to the conclusion that there was some change in the actual core behavior during calibration. A modified calibration chamber was made to test a total of fifteen transducers during one run. The curves still shifted. Attempts were then made to fill the transducer with polymer melt. This too proved unsuccessful. Finally, it was decided to calibrate the transducers in place after each run in the test device itself.

b. Actual Test Procedure

The first step in the procedure was to heat the test section to the desired level. This was done for a period of five hours so as to attain steady state. In this procedure the oil circulating pump was started and all available heaters were turned to full power. After steady state was attained, a thermoregulator was found to be able to control the temperature. The section between the extruder and the gear pump was heated with high temperature electric tape.

Next, the extruder and gear pump combination was started. The pressure between the extruder and gear pump was maintained at 500 psi. It took approximately fifty minutes to replace the

polymer melt in the test section with a flow rate of 225 grams/minute.

When the system was operating on a steady state basis, temperatures and pressures were recorded. In addition, frequent checks were made of the weight rate of flow. At each flow rate several repeat measurements of temperature and pressure were made. Calibration checks were made of the pressure transducers following each run.

2. Heat Transfer Experimental Procedure

The experimental procedure used in the present work is described below.

Before any measurements were made the thermocouples were all calibrated. This was done in hot oil, boiling water, at the ice point and at room temperature in isolated and closed units. A potentiometer was used to determine the temperatures. This instrument had a sensitivity of 0.00001 volts.

Prior to actual heat transfer studies a considerable amount of preliminary work was necessary. One of the initial steps was to bring the entire system up to temperature. This was done by starting the oil circulating pump (Figure 10) and turning on all availabel electrical heaters to full power. After steady state was attained in the oil system, a thermoregulator was found to be able to acceptably control the temperature. As was noted earlier, the oil jacketed system heated not only the flow test

section but also the gear pump. The section between the extruder and gear pump was heated with high temperature electrical tape.

Temperature was also brought up both in the extruder and the line segment between it and the gear pump.

After about a five hour heating period flow was started through the system. At low flow rates the polymer rate was approximated by a tachometer attached to the shaft of the pump. It was especially important to synchronize the speeds of the metering pump and extruder so that there was neither bubbling in the polymer flow nor an accumulation. This process was aided by observing the extruder pressure gages and another in the line between the extruder and gear pump. It took approximately an hour to bring the whole system to final steady state operation.

Before any temperatures were actually recorded, all thermocouples were first read and checked at the multipoint switch boxes. Next, all wall temperatures, oil heat exchanger temperatures, gear pump jacket temperatures were checked. When no serious fluctuations were observed, thermocouple readings were taken. At one flow rate thirty profile thermocouples, the wall thermocouples and a thermocouple for average inlet temperature were all read in continuous rounds of readings. Flow rate was then changed and the system was brought to steady state before another set of readings was made.

It should be noted that flow rate control was excellent. For a given set of five flow rate samples there was less than 1 per cent deviation.

D. Materials and Equipment

1. Materials

Polyethylene

El Rexene-low density polyethylene, type PE 107, pellets, lot # C-11857, melt index 1.0 gr/10 min., sp. gr. 0.920 at room temperature, elastic modulus 18,500 psi.

Dart Industry Inc. -Rexall Chemical Co., Paramus, N. J.

This low density polyethylene was chosen for the study of inlet flow behavior and used throughout the experiment.

Polymethyl Methacrylate

Plexiglas VM 100, pellets, density 74.2 lb_m/ft^3 at 23°C melt index 4.0 gr/10min. at condition H, Flow Temperature 284°F

Rohm and Haas Co., Philadelphia, Pa. 19105

Used for the study of heat transfer

Mobiltherm 600

Sp. gr. at 212°F 0.90, B.P. 760°F, Flash Point, coc, 360°F, specific heat 0.580(500°F) Btu/lb °F

Mobil Oil Corporation, N.Y., N. Y. 10036

Used as heating medium in the heating unit.

Other materials used:

Thermocouple wire, Iron-Constantan and Chromel-Alumel, 316 stainless tube, Swage lock, ceramic tube of 0.070" with 6 bores, 36 gage lead wire, shrinking tube, Bendix connector, Teflon tube, epoxy resin, insulation materials, pipes, fittings and valves.

2. Apparatus and Equipment

Extruder

Die diameter 2", single step screw, 220v, 3PH, 60Hz, r.p.m. 30/132

Prodex Corporation, Fords, N. J.

To melt the polyethylene and push it to the test section.

Variable Speed Transmission

Input r.p.m. 1750, output r.p.m. 230-0, Model No. 250 MR 2.8, Serial No. 39058688

Graham Transmission Incorporation, Menomonee Falls, Wis.

To vary the gear pump rotation so that it can control the flow rate of the melt.

Motor

r.p.m. 1725/1425, 1.5, 220v, 3PH, 60Hz

Doerr Electric Corporation, Cedarburg, Wisconsin

To run the Variable Speed Transmission

Zenith Two Gear Fixed Mounting Hot Pump

Type HLB 4729-20, 20cc/rev.

Zenith Products Co., West Newton, Mass.

To mix uniformly the polymer melt from the extruder and to prevent the flow fluctuation.

Electric Heating Tape

H-2105-Type H, 1" with x 6" length, 230v, 864w

Scientific Glass Apparatus Co., Bloomfield, N. J.

To heat the pipe between the extruder and the gear pump.

Rupture Disc

3/16" solder type, bursting pressure 3783 psig at 72°F, (est. 3556 psig at 525°F), Tag A 2319-2, Date 3-6-70

Fike Metal Products Co., North Plainfield, N.J. 07060

Installed between extruder and gear pump for safety.

Tachometer

Zero-Max Tachometer, two speed ranges 0-100 and 0-500 r.p.m. Mod. No. B-215

Zero-Max Company, Minneapolis, Minn.

To synchronize the r.p.m. of gear pump and extruder.

Worthington Rotary Pump

20 cc/rev., 15 GPM, Model No. 3Ga 8771B

Worthington Corporation, Harrison, N. J.

To supply and circulate mobiltherm 600 throughout the equipment.

Immersion Heaters

2000 w/unit, 220 volts. Each heaters is consisted of 3 unit to make 6 Kw.

Fisher Scientific Co.

To supply the necessary heat to the oil, Mobiltherm 600.

Century Squirrel-Cage Induction Polyphase Motor

r.p.m. 1755/1460, hp 2, 220-440v, 60Hz

Centry Electric Co., St. Louis, Mo.

To run the oil circulating rotary pump.

Triple Beam Balance

Max. Cap. 2610 gr

Ohaus Scale Corp., Union, N. J.

To weigh the melt bar which were cut at certain time interval. Flow rate was calculated from the result.

Potentiometer

Type K-3, Catalog No. 7557-A

Leeds and Northrup, Philadelphia, Pa.

To measure the wall temperature.

Temperature Bath

Model H-1 High temperature bath

Cannon Instrument Co., State College, Pa.

To keep the temperature constant of transducers during calibration.

Dual D. C. Power Supply

Input voltage: 105-125 VAC, 47-420 cps, single phase

output voltage: 12.0-18.0 VDC at a maximum load current of 0.400 amps.

Power/Mate Corp., Hackensack, N. J.

To supply ± 15 VDC to System 2000

D. C. Differential Voltmeter/Ratiometer

Ranges: ± 1V, ±100V and ± 1000V

Resolution: 6 digit readout yields resolution of 1ppm of range

Models 3420B

Accuracy: 30day : ±(0.002% of reading + 0.0002% of range)

at 23°C ± 1°C

Hewlett-Packard Company, Loveland, Colorado 80537

To check the accuracy of Dual D.C. Power supply and D. C. Digital Power Supply.

D. C. Digital Power Supply

Model 6112A

Input: 105-125/210-250 VAC, single phase, 48-63 Hz, 0.5A, 52w

output:0-40 volts at 0-500 mA

Output Controls: 0.1" + 1 mv of the output voltage

Hewlett Packard Co., Paramus, N. J.

To measure the output voltage from System 2000 by nulling the output voltage.

System 2000

Meter Scales: 0-100%, 0-5 VDC

Output: 0-5 DC volts, FS, pulse 1.5 volts nominal

Power Input ± 15 VDC ± 0.2 v, 50 ma

International Technical Industries, Santa Cruz, Calif. 95060

To measure D. C. output voltage which is equivalent to certain pressure by supplying and receiving signals to and from the transducer.

Transducer (Sensor 500)

Repeatability ± 0.5% FS, Resolution infinite, size 0.05" ODx 0.03" IDx0.01, weight 0.0015 gr.

International Technical Industries, Santa Cruz, Calif. 95060

To sense the pressure in the medium.

Ashcroft Dead Weight Gauge Tester

Range 0-2000psi, pressure increment step 250 psi

Manning, Maxwell & Moore Inc., Stratford, Connecticut

To calibrate the transducers.

Hypodermic Tubing

Stainless steel hypodermic needle tubing, eight wall. 0.0623 in. I. D., 0.0630 in. O. D.

Becton Dickinson Co., Rutherford, N. J.

Used to reinforce the profile thermocouples and prevent bending.

Multi-Point Thermocouple Switch Box

24 point for thermocouple connections, model No. 3311353.

Thermo Electric Co., Inc., Saddlebrook, N. J.

Used to connect all the thermocouple extension wire to the potentiometer.

Profile Thermocouples

Iron-Constantan, grounded Conax thermocouples, stainless steel sheath, 0.0625 in. O.D., Model No. J-ss6-G-PJFC-6.

Thermo Electric Co., Inc., Saddlebrook, N.J.

Used to measure the radial temperature of flowing polymer.

IV. RESULTS AND DISCUSSION

A. Entrance Region Studies

1. Results

Typical results for the entrance region tests are given in Tables III through VI. The pressure data calibrations are given in Figures 15 through 20. As can be seen, the results are inconclusive. Note in certain cases no pressure was recorded. This, of course, conflicts with physical reality. In addition, the pressure behavior follows no meaningful pattern. The continued difficulties indicate that the pressure measuring system is not capable of being used in molten polymer systems.

2. Discussion

As noted previously, the pressure results simply do not make sense. In attempting to determine error sources only two possibilities seemed to exist. One was the effect of temperature, the other the devices and instrumentation.

The response range on span and 1mv-equivalent pressure for each transducer in the range of 0-2000psi are shown in Table VII for further discussion.

TABLE III PRESSURE MEASUREMENT OF THE FIRST RUN

Flow Rate: W = 211 gr/min

Shear Rate: 3.7/sec

Position No. in Fig. 6	Transducer No.	Consecutive Output Voltage						Equivalent Press. from Fig. 15 &16 (psi)
P2	N-1	2.4660	2.4568	2.4552	2.4544	2.4536	2.4534	600
P4	N-4	2.6423	2.6329	2.6350	2.6460	2.6342	2.6375	None
P5	N-6	3.1623	3.1700	3.1676	3.1800	3.1800	3.1798	None
P6	O-1	2.1158	2.1204	2.1160	2.1086	2.1112	2.1000	700
P7	N-7	2.7744	2.7730	2.7742	2.7717	2.7627	2.7523	200
P8	N-8	3.3862	3.3838	3.3767	3.3913	3.3830	3.3830	None
P9	O-2	2.0758	2.0883	2.0810	2.0753	2.0658	2.0600	1250
P10	N-3	2.2981	2.2971	2.2958	2.2914	2.2934	2.2954	None

TABLE IV TEMPERATURE MEASUREMENT OF THE FIRST RUN

Flow Rate: 225 gr/min.

Shear Rate: 3.7/sec

Position No. in Fig. 6	Temperature measured consecutively °F					
P1	430.6	431.0	431.0	429.2	427.6	424.6
	423.3	422.3	423.0	424.3	424.5	430.3
	430.3	424.3	424.6	424.0	424.3	424.0
T5	427.3	427.3	427.3	427.0	425.6	424.0
	421.3	420.2	418.2	419.6	420.3	420.6
	420.6	421.0	421.0	420.7	420.6	420.6
T4	429.4	429.2	429.3	429.4	427.0	421.7
	423.0	421.5	420.0	422.0	422.3	423.0
	422.6	423.0	420.7	420.6	420.6	420.3
P11	423.3	423.3	423.0	422.6	421.6	420.6
	418.5	418.2	417.6	418.5	419.0	419.3
	419.3	418.5	418.3	418.2	418.0	418.0

TABLE V PRESSURE MEASUREMENT OF THE SECOND RUN

Flow Rate: 225 gr/min

Shear Rate: 3.7/sec

Position No. in Fig. 6	Transducer No.	Consecutive Output Voltage(mV) and Temperature(^{o}F)						Equivalent Press. from Fig. 17-20(psi)
P13'	N-6	3.1100	3.1040	3.1030	3.0963	3.0950	3.0958	1200
	^{o}F	425.5	425	425	425	424.5	424	
P2	N-1	2.4024	2.3824	2.3860	2.3892	2.3863	2.3852	None
	^{o}F	422	422	421.5	421	422	421.5	
P6	O-1	2.0395	2.0392	2.0360	2.0392	2.0386	2.0396	500
	^{o}F	429.5	430	429.5	429.5	429.5	429.5	
P7	N-7	2.7100	2.7066	2.6991	2.6960	2.6912	2.6936	670
	^{o}F	424	424	424	424	424	424	
P8	N-4	2.5810	2.5750	2.5702	2.5722	2.5660	2.5652	790
	^{o}F	423	423	423	423	423	423	
P9	O-2	2.0164	1.9992	1.9990	2.0090	1.9972	2.000	110
	^{o}F	422.5	423	423	423	423	423	
P10	N-3	2.2410	2.2300	2.2254	2.2250	2.2237	2.2230	1050
	^{o}F							

More: Temperature and Pressure were measured at the same time.

TABLE VI TEMPERATURE MEASUREMENT OF THE SECOND RUN

Flow Rate: 225 gr/min

Shear Rate: 3.7/sec

Position No. in Fig. 6	Temperature in $^{o}_{F}$ the Axial Direction					
T0	423.6	423.3	424.3			
T1	424.7	425.7	425.3			
T2	421.7	422.3	422.7			
T3	423.3	423.0	424.0			
P11	526.3	426.3	426.7	426.0	426.3	426.3
	426.7	427.0	426.3	426.7		
T4	422.0	422.2	422.6			
T5	425.0	425.3	425.6			
T6	422.0	422.0	422.7			
T7	416.3	416.3	417.0			
T8	424.6	424.7	425.0			
T9	423.0	423.2	423.6			
T10	412.3	412.6	413.0			
T11	417.0	417.3	418.0			
T12	429.6	420.6	420.2			

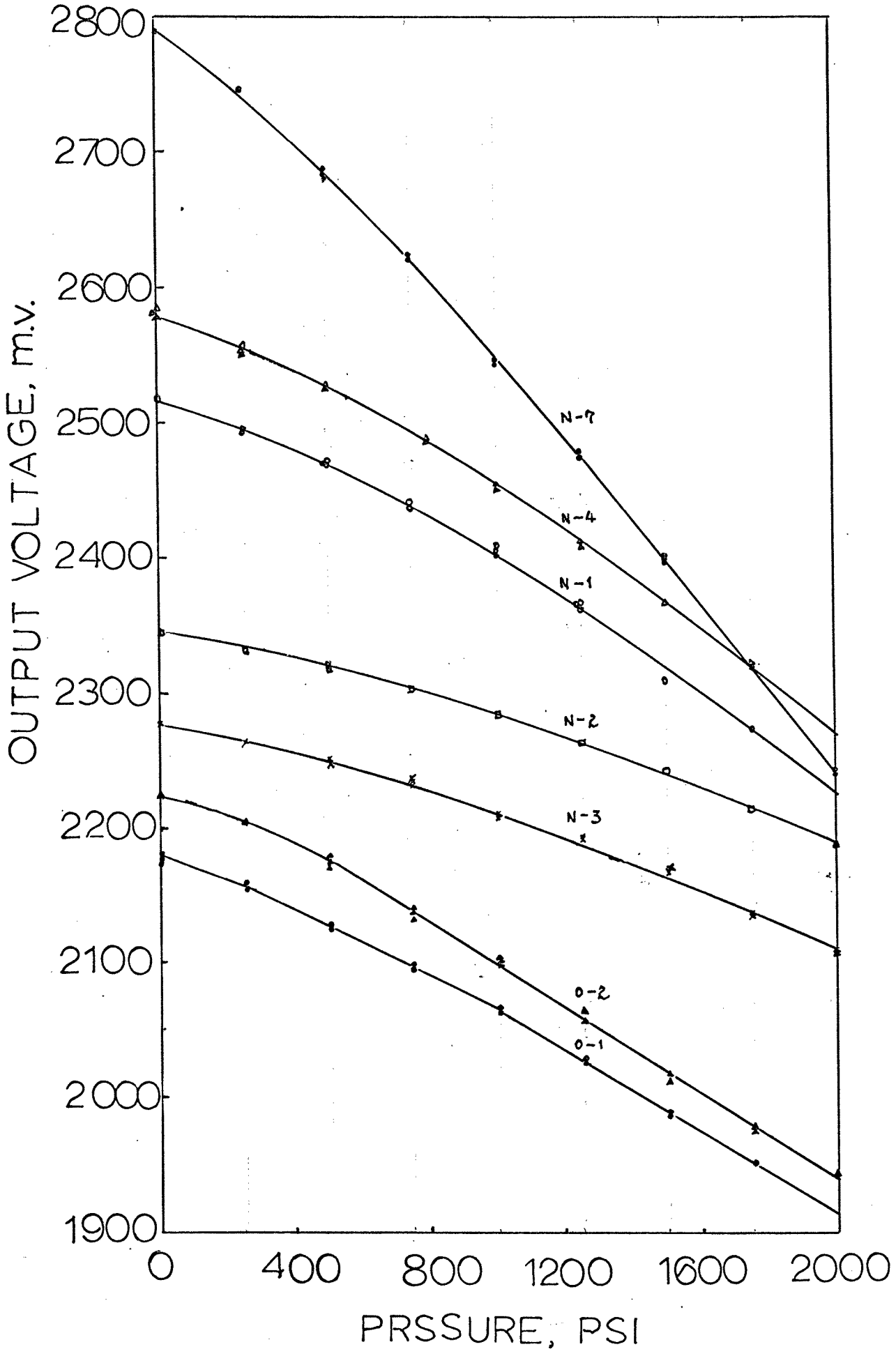

FIGURE 15 Calibration Curve before the Run

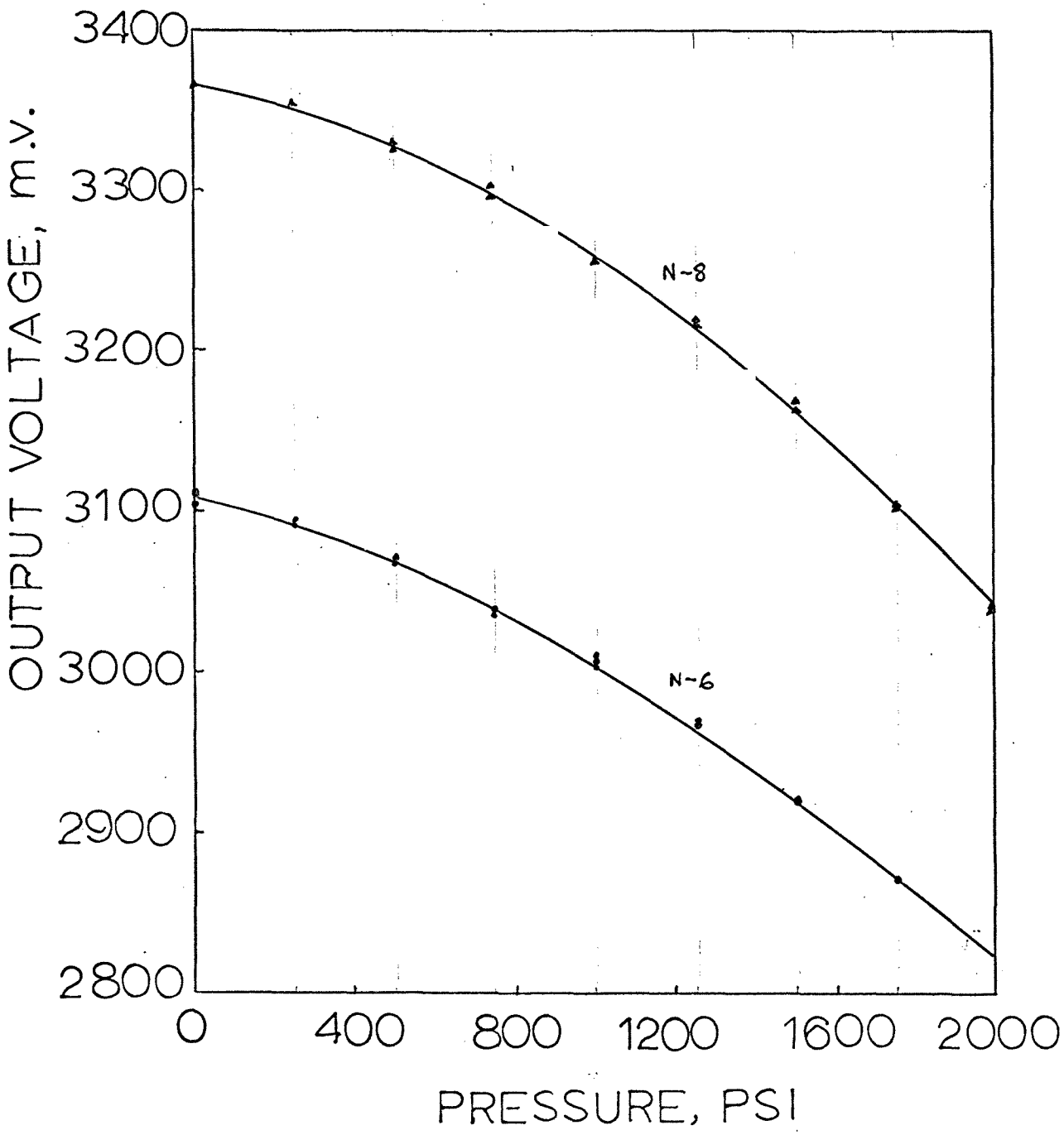

FIGURE 16 Calibration Curve before the Run

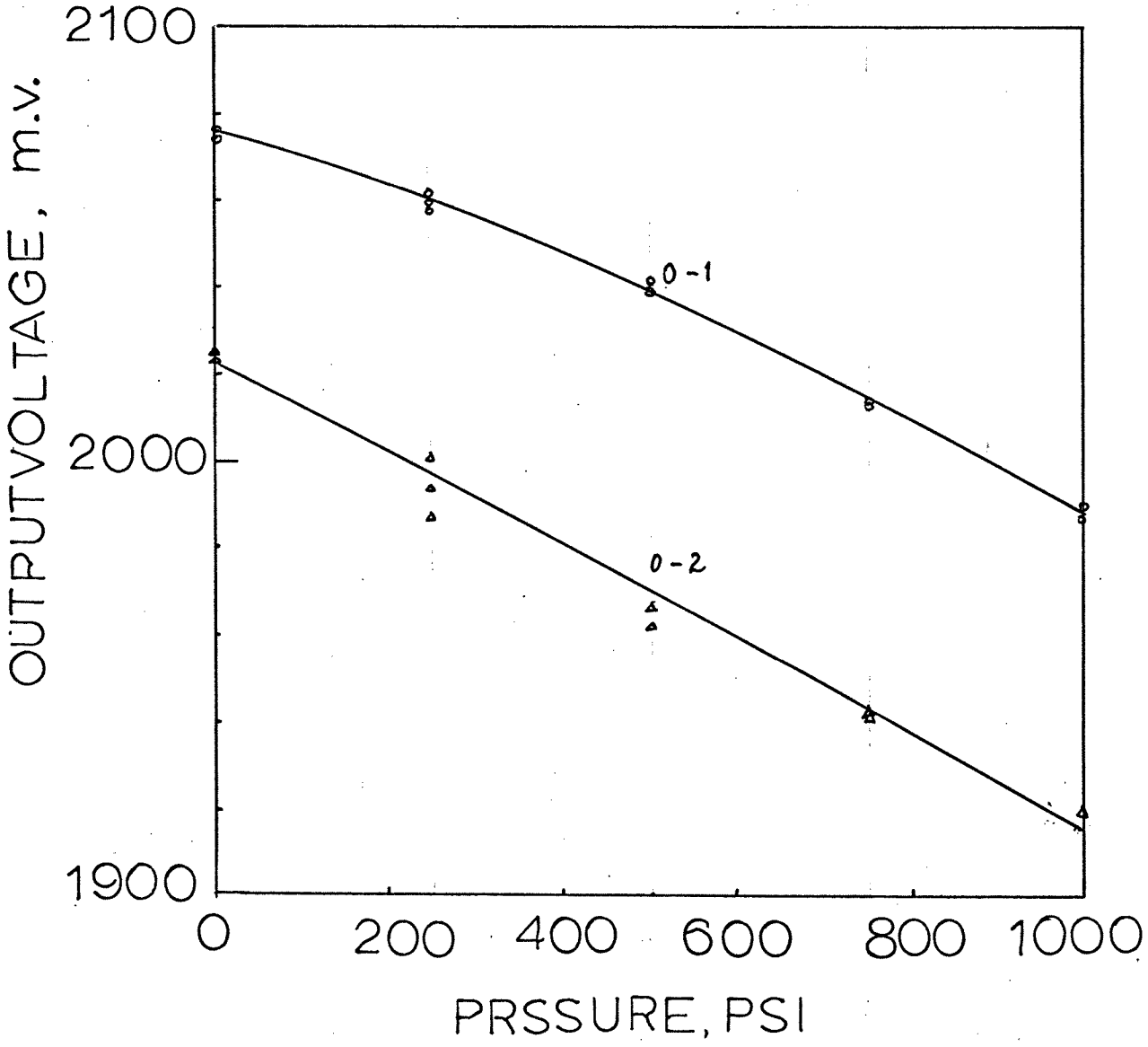

FIGURE 17 Calibration Curve after the Run

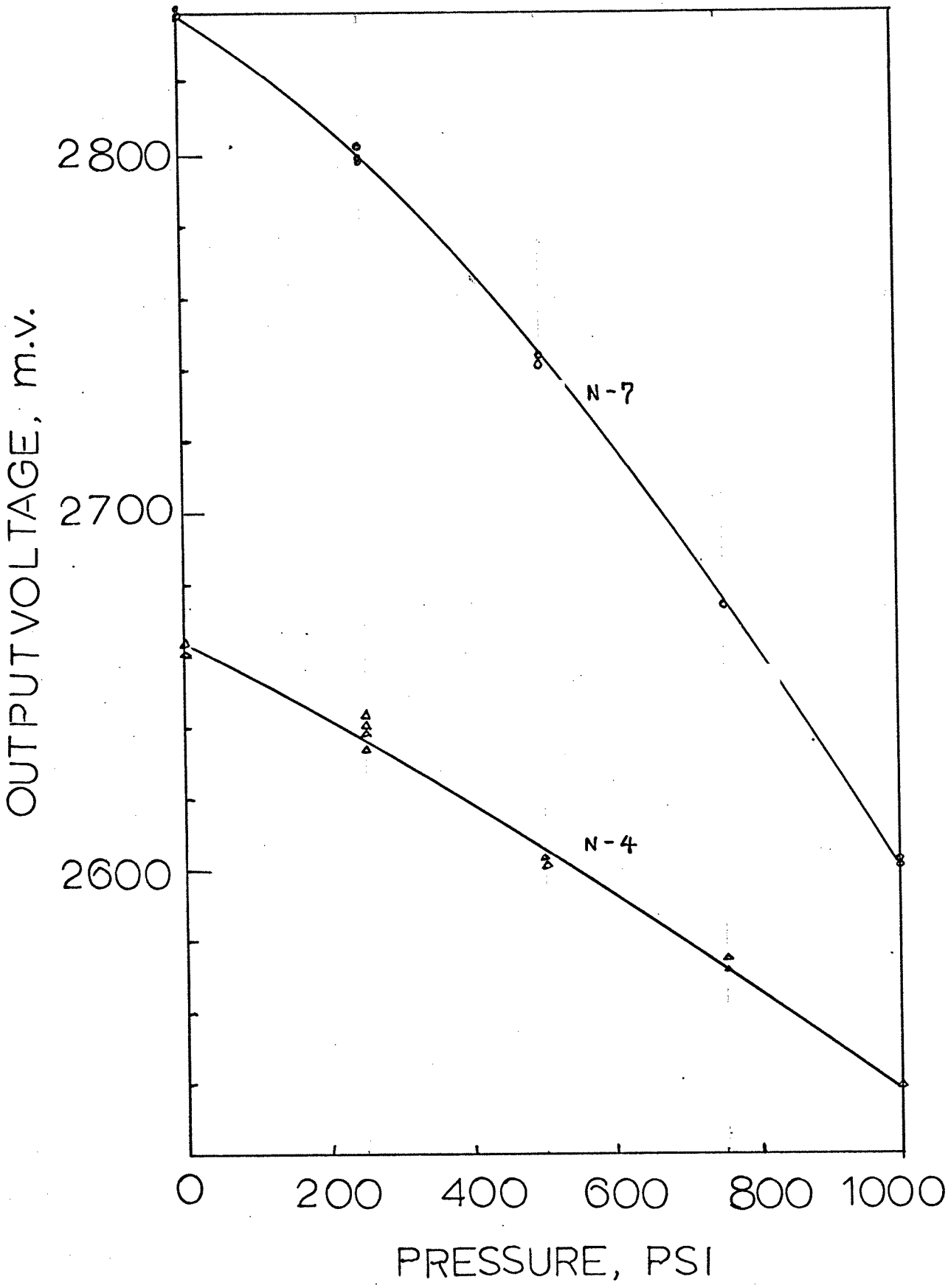

FIGURE 18 Calibration Curve after the Run

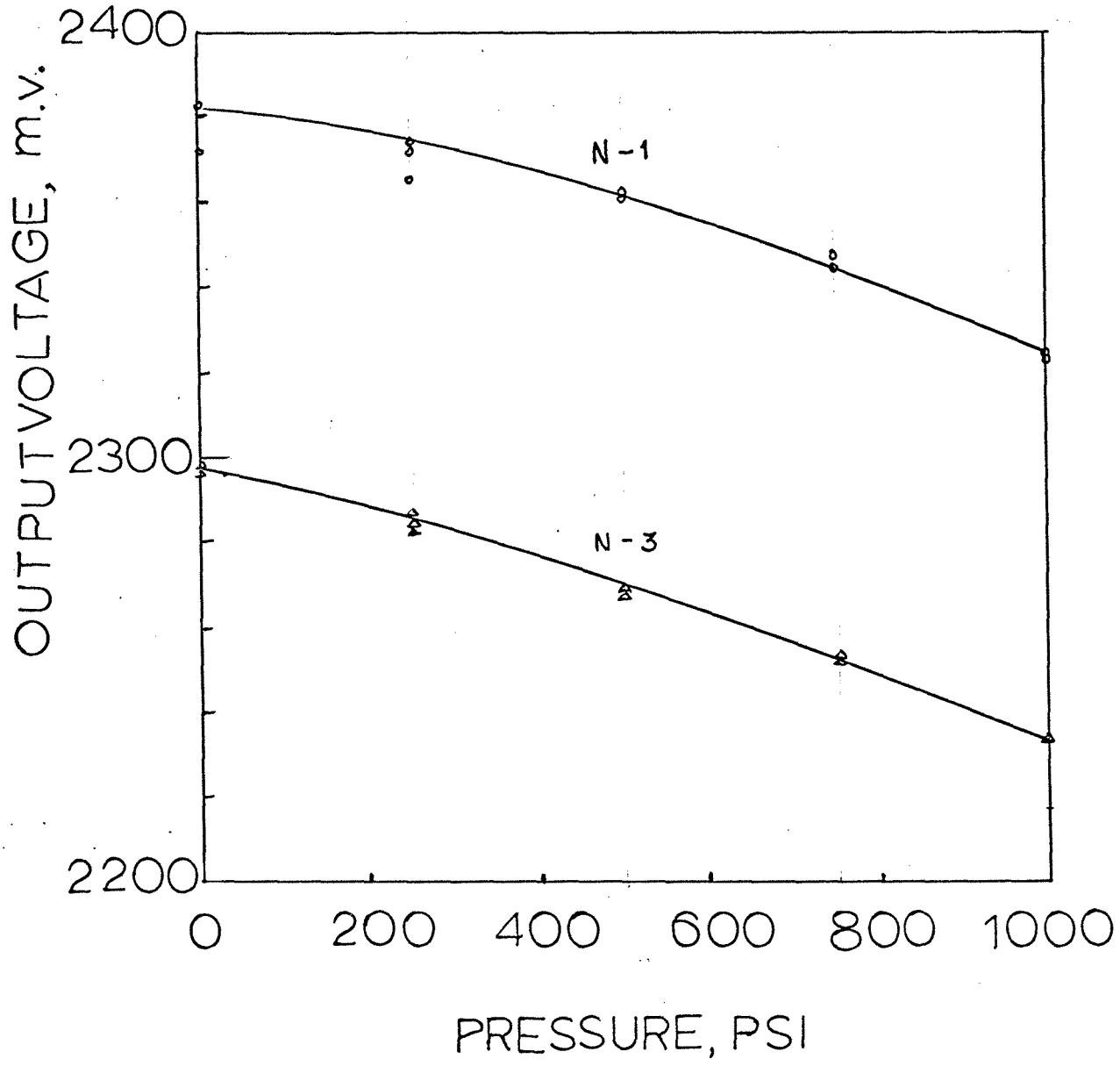

FIGURE 19 Calibration Curve after the Run

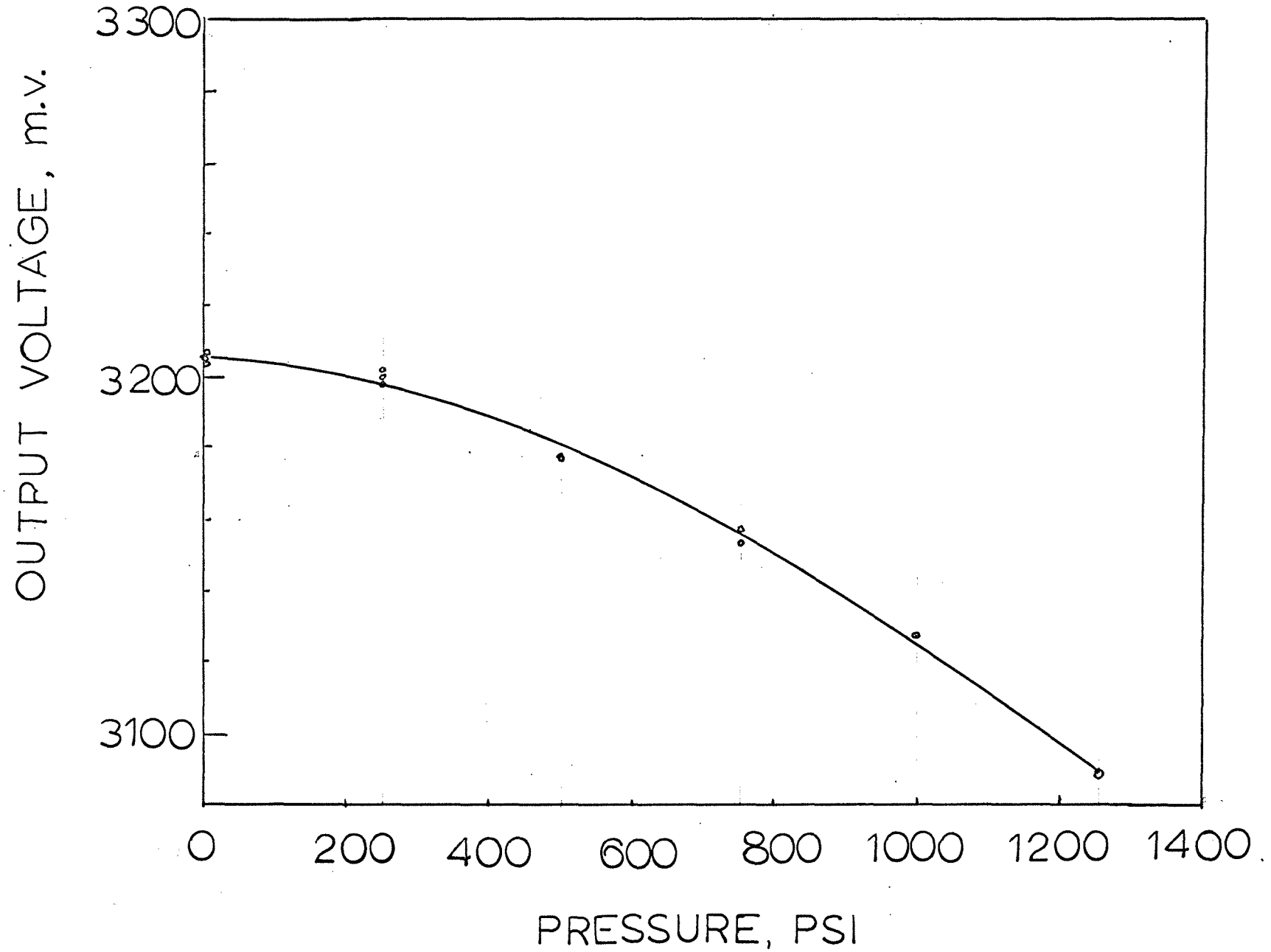

FIGURE 20 Calibration Curve after the Run

TABLE VII SPAN AND 1mv-EQUIVALENT PRESSURE

Transducer No.	N-1	N-2	N-3	N-4	N-6	N-7	N-8	O-1	O-2
Span(mv)	277	153	169	315	281	546	325	258	284
1mv = psi	7.23	13.0	11.9	6.4	7.1	3.7	6.2	7.8	7.1

The possible effect of temperature was checked by determining the thermal sensitivity of the transducers at atmospheric pressure. Results of this testing are given below and in Figure 21.

TABLE VIII PRESSURE EQUIVALENT TO 1°F

Transducer No.	N-6	N-4	N-1
Temperature Range °F	329.5-317	357.3-340.5	374-360.5
T°F	12.5	16.8	13.5
T/50=°F/%	0.25	0.336	0.27
1°F = %	4.0	2.98	3.7
Equivalent mv (1% = 0.6mv)	2.40	1.79	2.22
Equivalent Press. from Table VII psi	17.0	11.5	16.0

On the basis of these data a 1°F error in temperature could yield a 10 to 30psi error in pressure. It should be added,

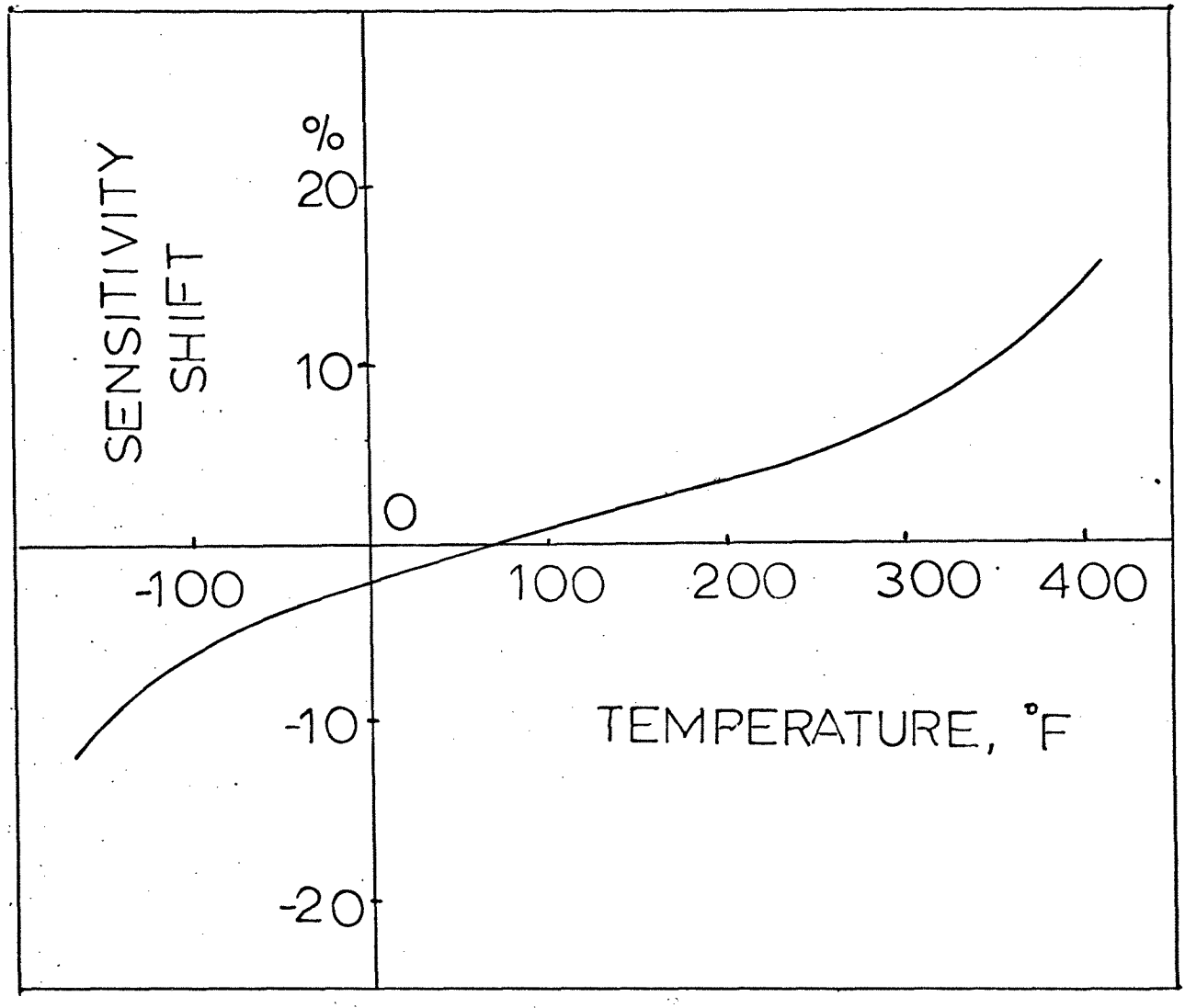

Figure 21. Thermal Sensitivity Shift (Typical)

however, that temperature errors are not too likely since considerable attention had veen directed to perfecting this technique in an earlier study [51]

Other errors could have resulted from the transducers and auxiliary system. For example, when the D.C. digital power supply was checked with a D.C. digital voltmeter it was found that the error developed could be as large as 2 mv. (roughly 15-30 psi).

While the errors that could develop from either thermal effects or equipment problems are sizable, they cannot even if cumulative account for the large deviation found in this work.

The only conclusion that can be reached is that the ITI device simply cannot be used under the severe conditions of a flowing polymer melt. This incidentally has been a common failing of most pressure transducers that have been proposed for such systems.

A possible way out of the problem is to use a device such as the Taylor pressure bulb(a pneumatic device). The device is rugged and insensitive to temperature. However, the high cost of each bulb precludes even considering such a route because of the many bulbs that would be needed.

B. Heat Transfer Studies

1. Heating of Flowing Thermally Softened Polymer Systems

a. Results

A large amount of data was accumulated for a thermally softened polymethylmethacrylate(Plexiglas VM 100).

Table IX shows raw point temperature data for this material at a flow rate of 155.5 gm/min. and an axial length of 0.527 feet. These data are typical of the measurements made with the apparatus of this investigation. Note the precision of the point temperatures for the repeated runs. This precision is especially significant since the experimental situation should be the worst possible case (short axial length, low flow rate). The reproducibility of the point temperatures also demonstrates that no free convection occurred during the tests.

Temperature profile curves are shown in Figures 22 through 28. The data are plotted as dimensionless temperature $\frac{T - T_1}{T_w - T_1}$ versus reduced radius $\frac{r}{R}$. Where:

r = point radius

R = tube radius

T = point temperature at r

T_1 = average inlet temperature

T_w = wall temperature

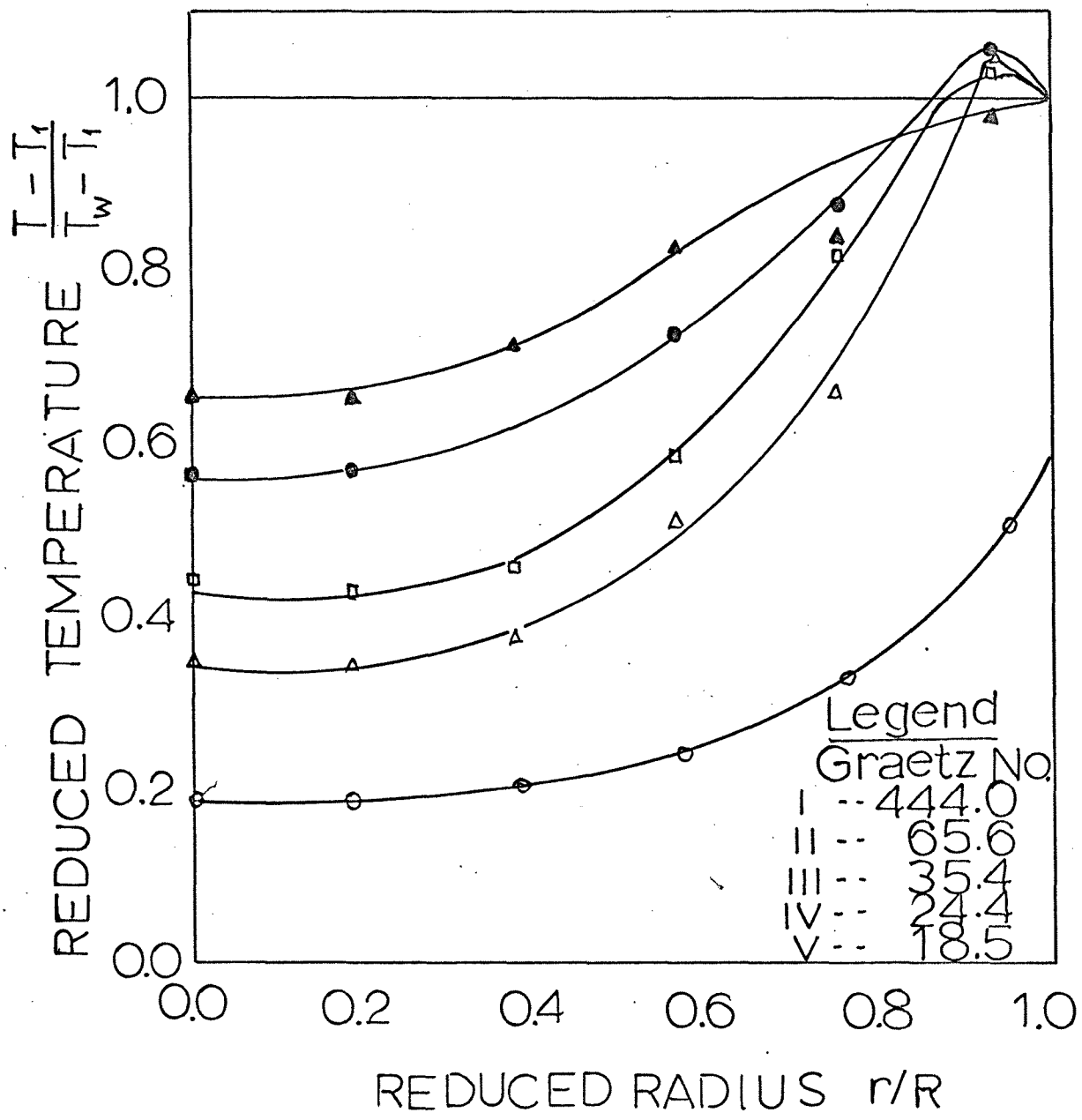

Figure 22. Experimental Dimensionless Temperature Profiles at Different Heat Transfer Lengths with a Flow Rate = 180.9 gr/min.

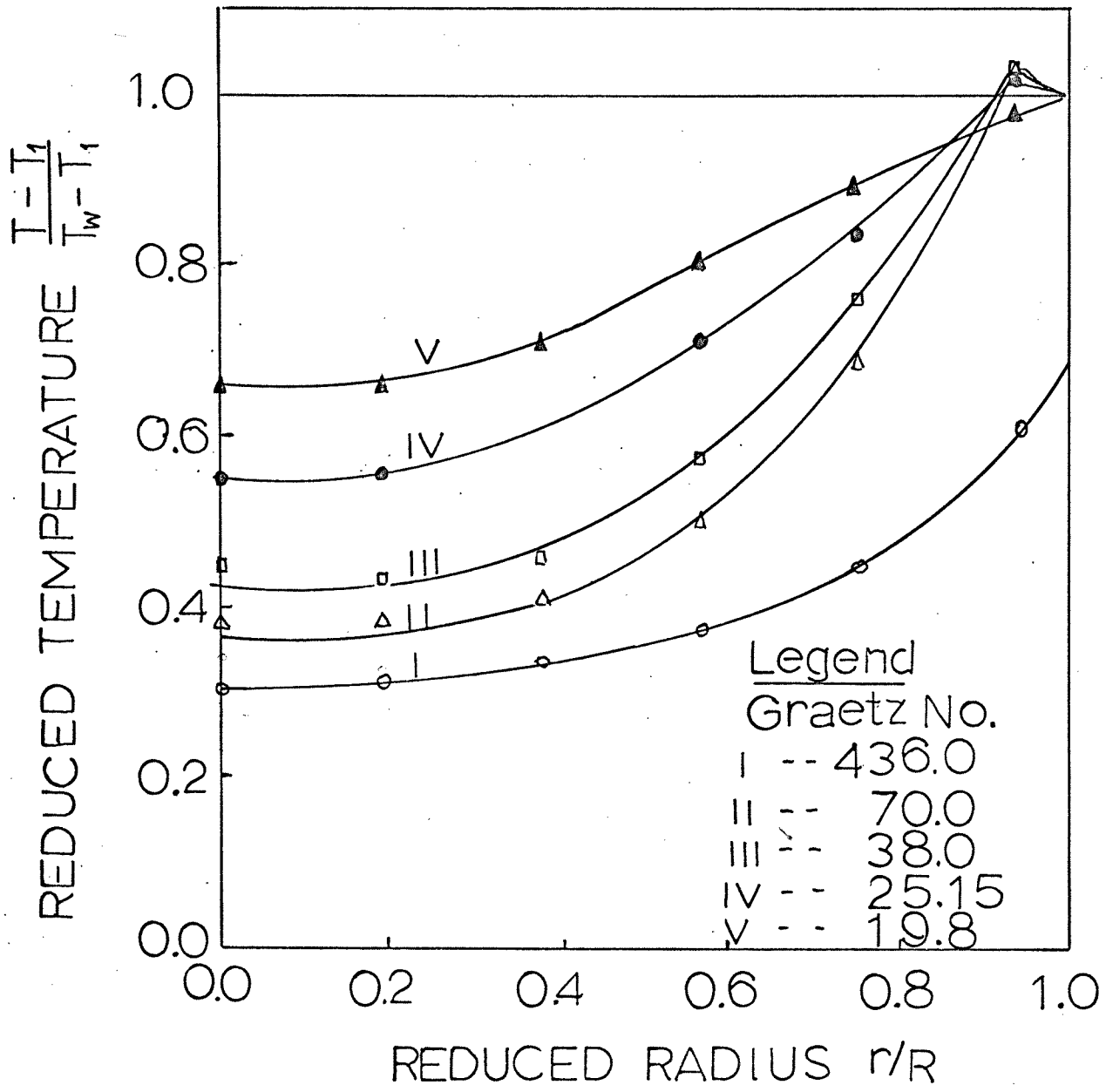

Figure 23. Experimental Dimensionless Temperature Profiles at Different Heat Transfer Lengths with a Flow Rate = 193.5 gr/min.

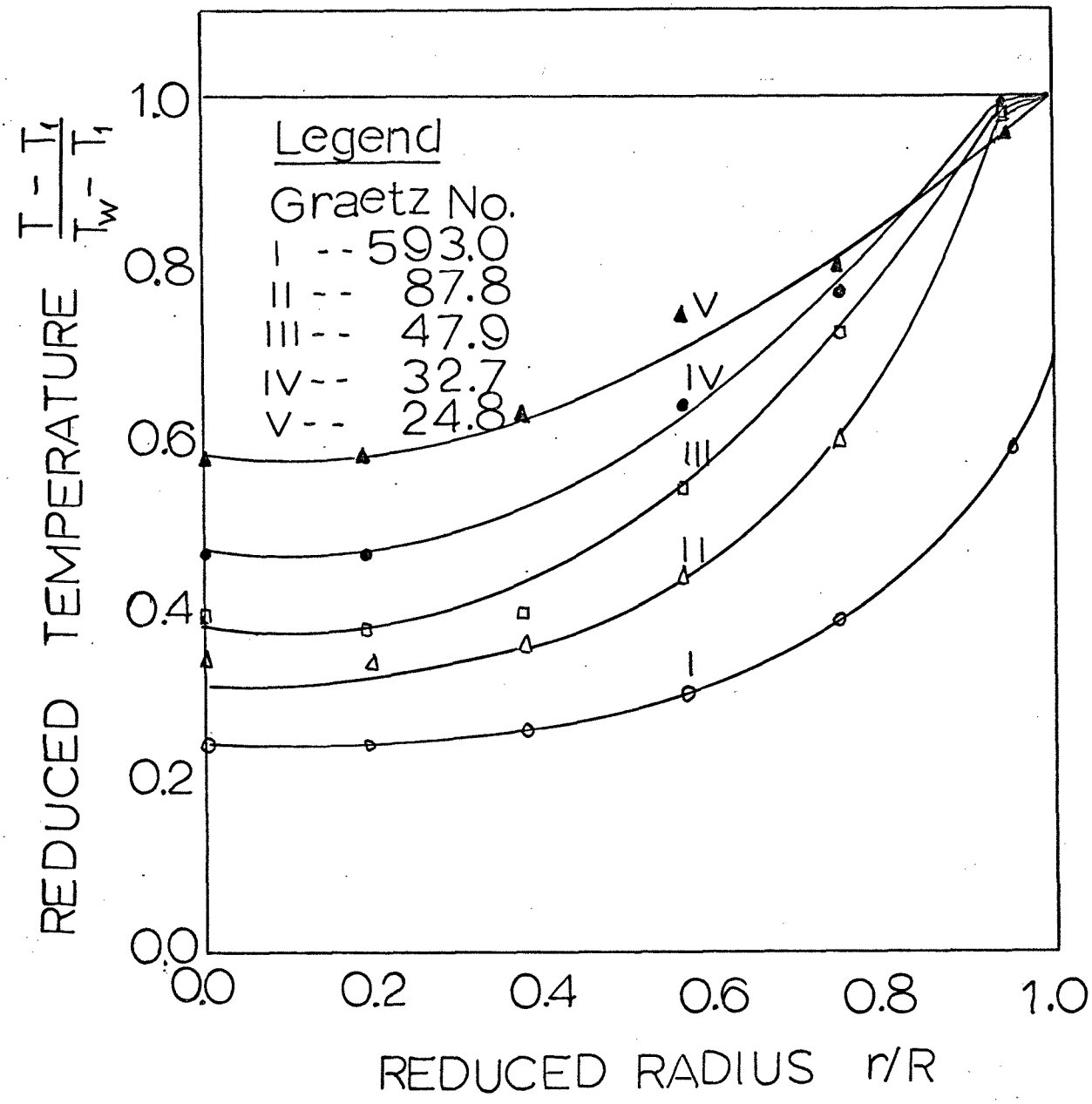

Figure 24. Experimental Dimensionless Temperature Profiles at Different Heat Transfer Lengths with a Flow Rate = 241.9 gr/min.

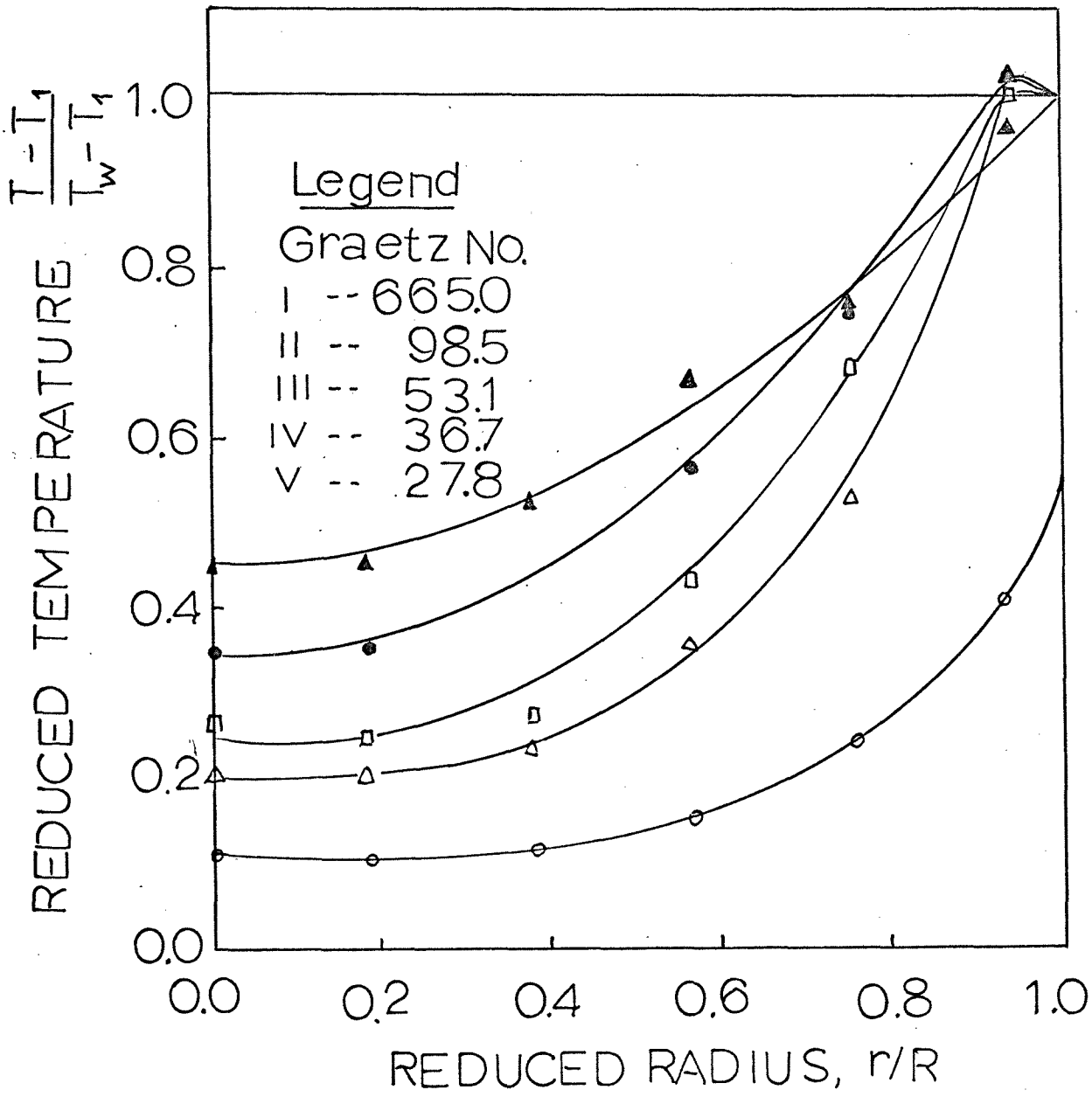

Figure 25. Experimental Dimensionless Temperature Profiles at Different Heat Transfer Lengths with a Flow Rate = 271.5 gr/min.

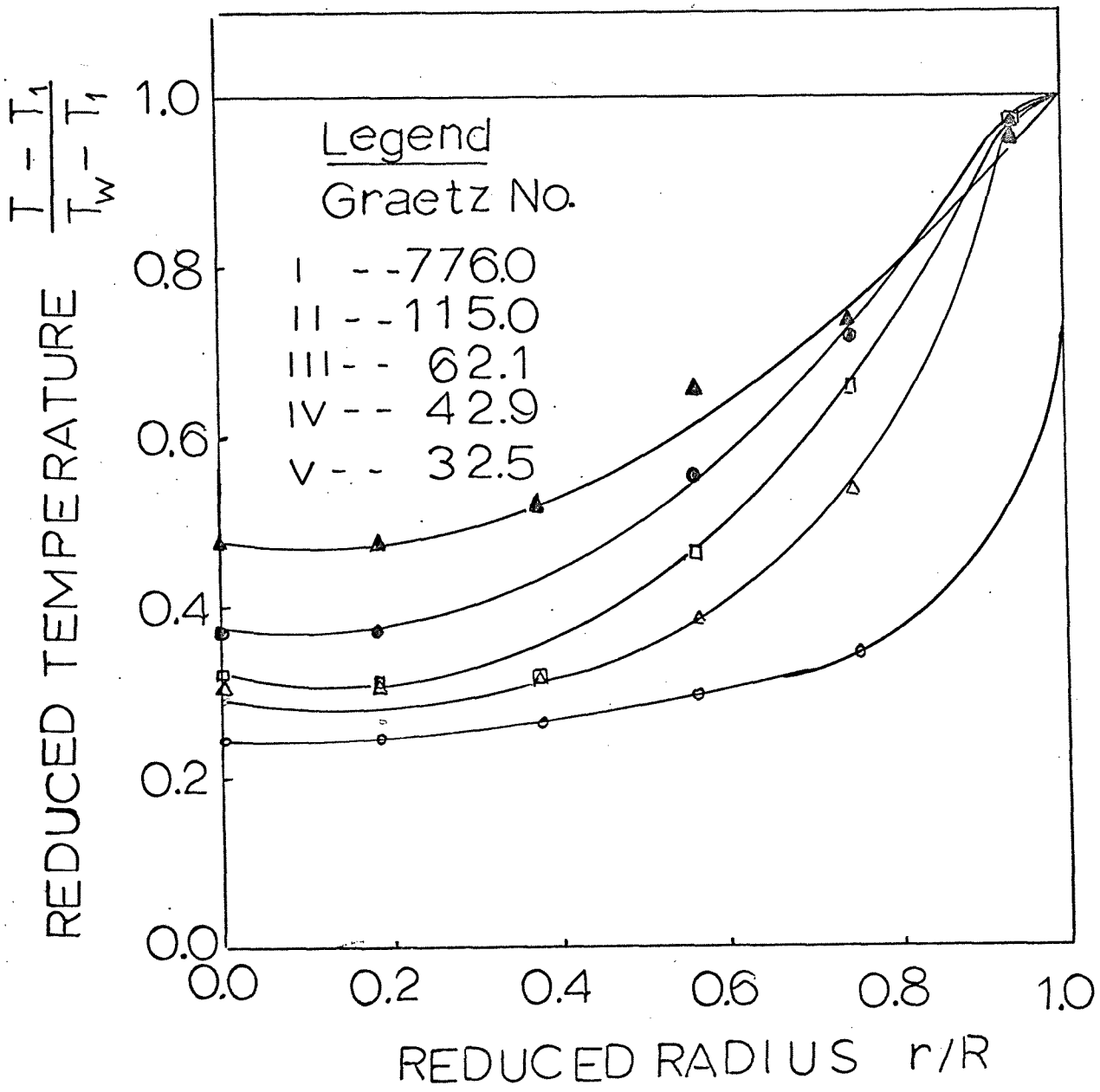

Figure 26. Experimental Dimensionless Temperature Profiles at Different Heat Transfer Lengths with a Flow Rate= 316.4 gr/min.

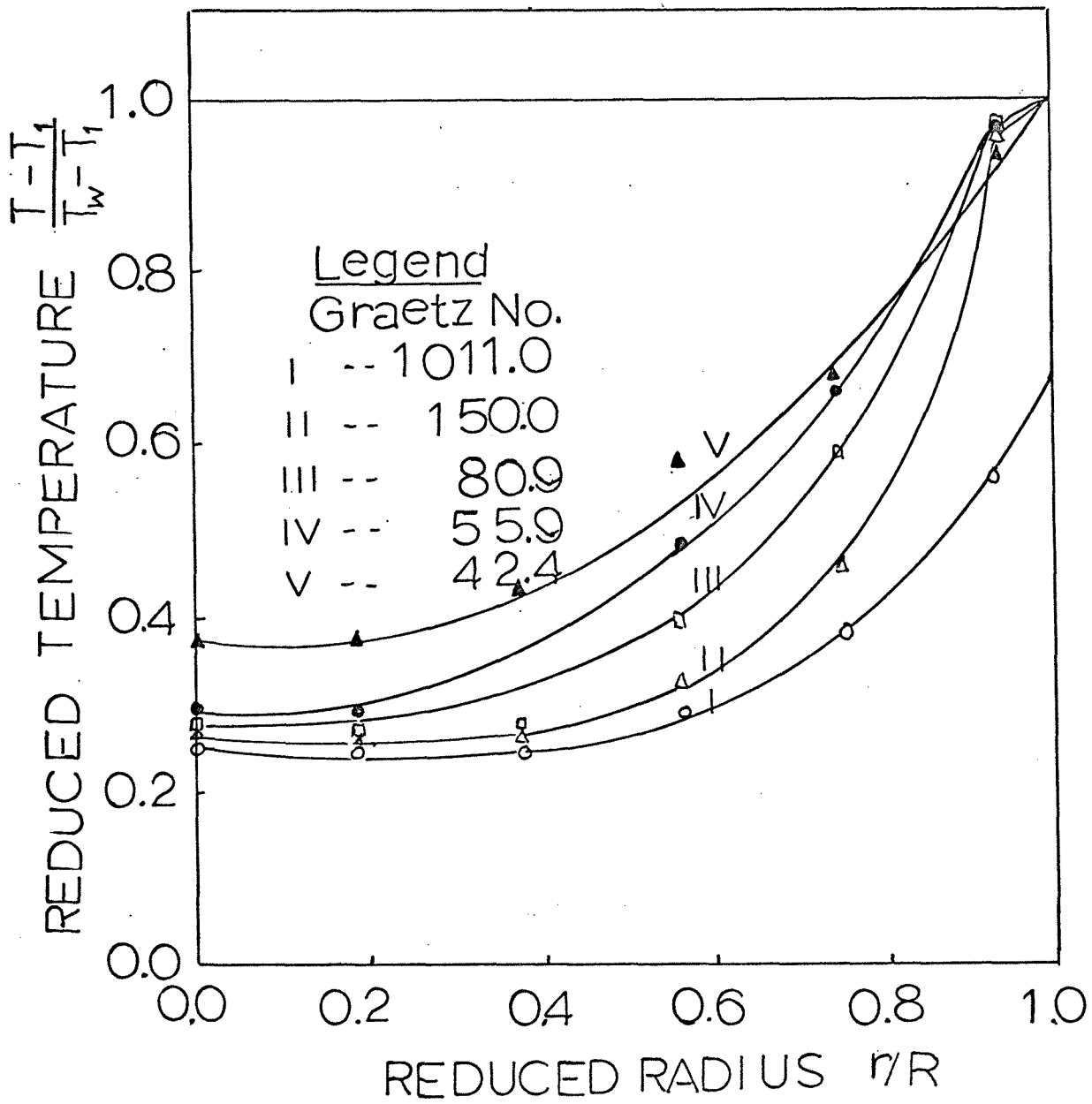

Figure 27. Experimental Dimensionless Temperature Profiles at Different Heat Transfer Lengths with a Flow Rate = 413.4 gr/min.

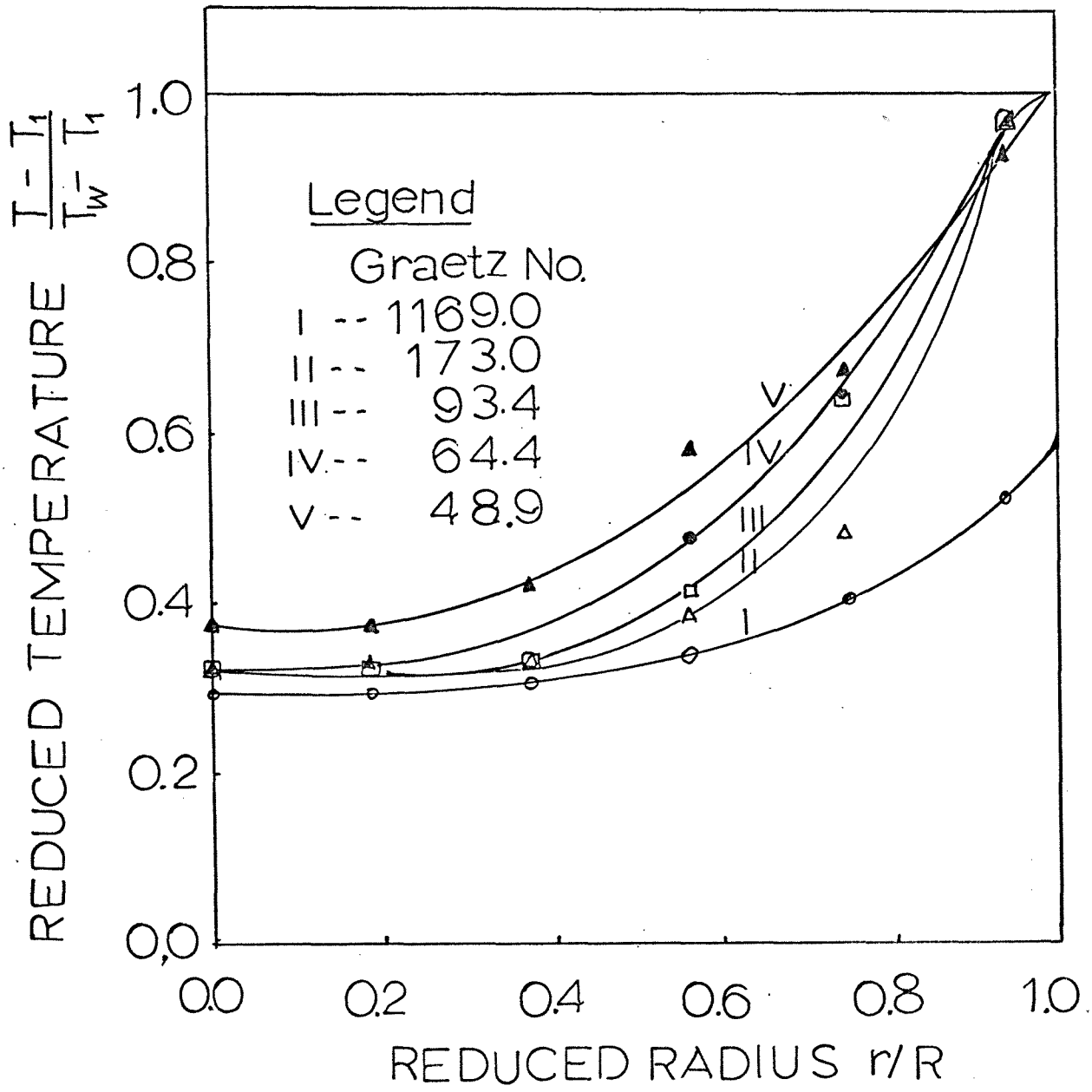

Figure 28. Experimental Dimensionless Temperature Profiles at Different Heat Transfer Lengths with a Flow Rate = 477.0 gr/min.

Each graph is at a given weight flow indicated on the figure. The parameter for each of the curves is the Graetz number $\frac{wC_p}{kL}$.

Where w = weight flow rate

C_p = polymer specific heat

k = thermal conductivity

L = acial length

Table IX

Flow Rate = 193.5 grams/minute

Axial Length = 3.560 ft.

	Test 3 (T_{inlet} = 435°F, T_{wall} = 467.7°F)	Test 4 (T_{inlet} = 434.7°F, T_{wall} = 467.0°F)
Reduced Radius	T_{point} °F	T_{point} °F
0.000	447.2	447.2
0.186	447.3	447.0
0.373	448.2	448.0
0.560	451.2	451.0
0.746	456.8	456.3
0.931	467.7	467.8

b. Discussion

Each of the figures is at a constant weight flow rate (varied from 180.9 to 477.0 gm/min). As a result, each of the curves on a given figure represents a different heat transfer axial length. The lowest curve is measured 0.527 feet from the gear pump. The other curves are at 3.560, 6.600, 9.560 and 12.600 feet, respectively. Likewise, since Graetz number is inversely proportional to length, the lowest curve represents the highest Graetz number and the top curve the lowest value.

The overall pattern given by any set of curves represents the development of the temperature profile with increasing axial length at a constant flow rate. As would be expected, point temperature at a given reduced radius increases with increasing axial length.

It can also be seen that a point temperature at a constant, r/R, and axial length decreases with increasing weight flow rate. This occurs because of the decrease in residence time with increasing flow rate.

Certain other aspects of the curves in Figures should also be noted. These are:

1. Temperature profiles at the 0.525 foot length are almost flat. (Most temperature change occurs at the wall.)

2. A depression in temperature at the center of the tube (r/R from 0.0 to 0.4) occurs.

3. A peak in temperature appears near the wall.

The almost flat profiles occurring at the 0.525 foot length show that the temperature profiles is not developed at this axial length. It also shows that the profile at the gear pump exit is flat as was predicted. It is interesting to compare the behavior of the temperature profile at the 0.525 foot length to that predicted from Kay's correlation.[51]

The correlation, when extended to non-Newtonian fluids, predicts entrance lengths of 10^{-2} to 10^{-1} feet for development of temperature profiles for the flow conditions of Figures 22 through 28. As can be seen, the actual length required is at least an order of magnitude greater than the correlation value.

Before considering the other two aspects of Figures (center depression and peak near wall), mention should be made of the factor of viscous dissipation. This factor depends on the dissipation function, ϕ_v , which in cylindrical co-ordinates for Newtonian fluids is

$$\phi_v = 2\mu\left\{\left(\frac{\partial V_r}{\partial r}\right)^2 + \left[\frac{1}{r}\left(\frac{\partial V_\theta}{\partial \theta} + V_r\right)\right]^2 + \left(\frac{\partial V_z}{\partial z}\right)^2\right\}$$

$$+\mu\left\{\left(\frac{\partial V_\theta}{\partial z} + \frac{1}{r}\frac{\partial V_z}{\partial \theta}\right)^2 + \left(\frac{\partial V_z}{\partial r} + \frac{\partial V_r}{\partial z}\right)^2 \right. \qquad (163)$$

$$\left. + \left[\frac{1}{r}\frac{\partial V_r}{\partial \theta} + r\frac{\partial}{\partial r}\left(\frac{V_\theta}{r}\right)\right]^2\right\}$$

where Vr, V_θ , Vz = radial, angular, axial velocity components

r, θ , z = cylindrical co-ordinates

μ = viscosity

For a non-Newtonian fluid that obeys the power law

$$\tau = K \left|\frac{\partial V_z}{\partial r}\right|^{n-1}\left(-\frac{\partial V_z}{\partial r}\right) \qquad (1)$$

(where τ = shear stress; K = consistency index;

n = power law index) and in which there is only axial flow

$$\phi_v = K \left|\frac{\partial V_z}{\partial r}\right|^{n+1}\left(-\frac{\partial V_z}{\partial r}\right) \qquad (164)$$

As can be seen the dissipation factor is directly proportional to the velocity gradient raised to a power greater than unity. This means that heating due to viscous dissipation will be the greatest near the wall(steep velocity gradient) and least in the center (shallow velocity gradient).

An additional factor which must be taken into consideration is fluid thermal expansion. If a fluid has a significant thermal expansion actual cooling can occur.

Now consider the shape of the temperature profile curves in light of the foregoing. In the tube center heat generation by viscous dissipation is small and as a result is easily removed by the thermal expansion process. Furthermore, this process serves to further flatten the fluid velocity profile

which decreases even further the viscous heating. The net result is that thermal expansion can ultimately depress the center line temperature.

Next, in the region near the wall viscous dissipation is at a maximum. As this effect builds up, heat is transferred to the main body of the fluid. However, owing to the poor fluid thermal diffusivity, the temperature builds up until it actually peaks.

The effect of viscous dissipation can be demonstrated in another way. Consider Figures 29 and 30, where a reduced temperature $\frac{T - T_w}{T_1 - T_w}$ is plotted versus reduced radius and compared to values computed by Toor[55] at constant Brinkman number. The Brinkman number

$$N_{Br} = B^* = \frac{c_1 \tau_w n}{\kappa R (3n+1)(T_1 - T_w)}$$

(where τ_w = wall shear stress, c_1 = constant) is a measure of viscous dissipation.

As can be seen, the experimental data fall between the curves for zero viscous dissipation ($B^* = 0.0$) and the value of $B^* = -0.5$ near the wall. This demonstrates that viscous dissipation is clearly important in flowing molten polymer systems. The failure of earlier studies[22,23,60] to find large viscous dissipation effects may have been due to low flow rates especially since the present work attained flows several times those of earlier studies.

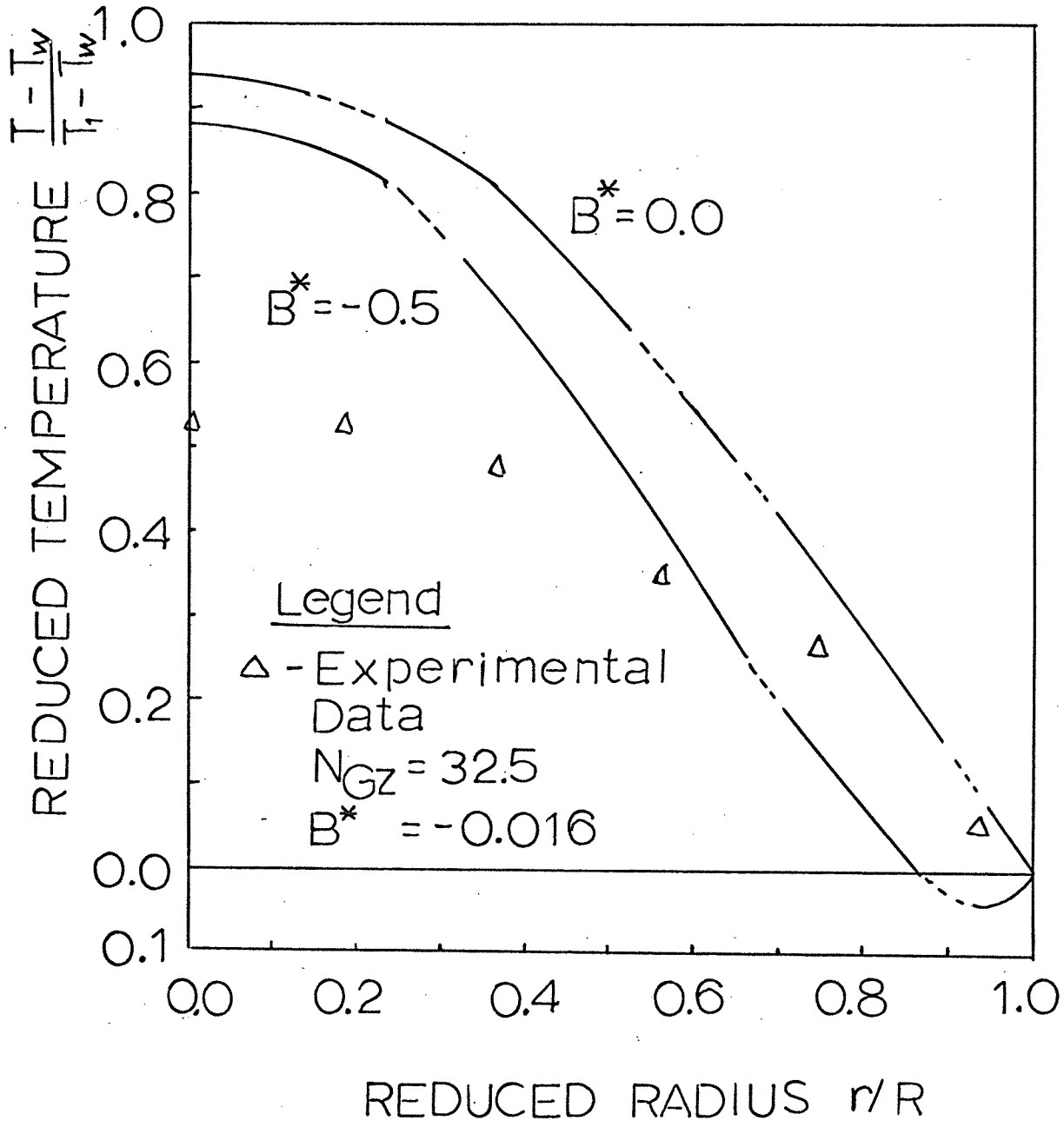

Figure 29. Comparison of Experimental and Calculated Temperature Profiles.

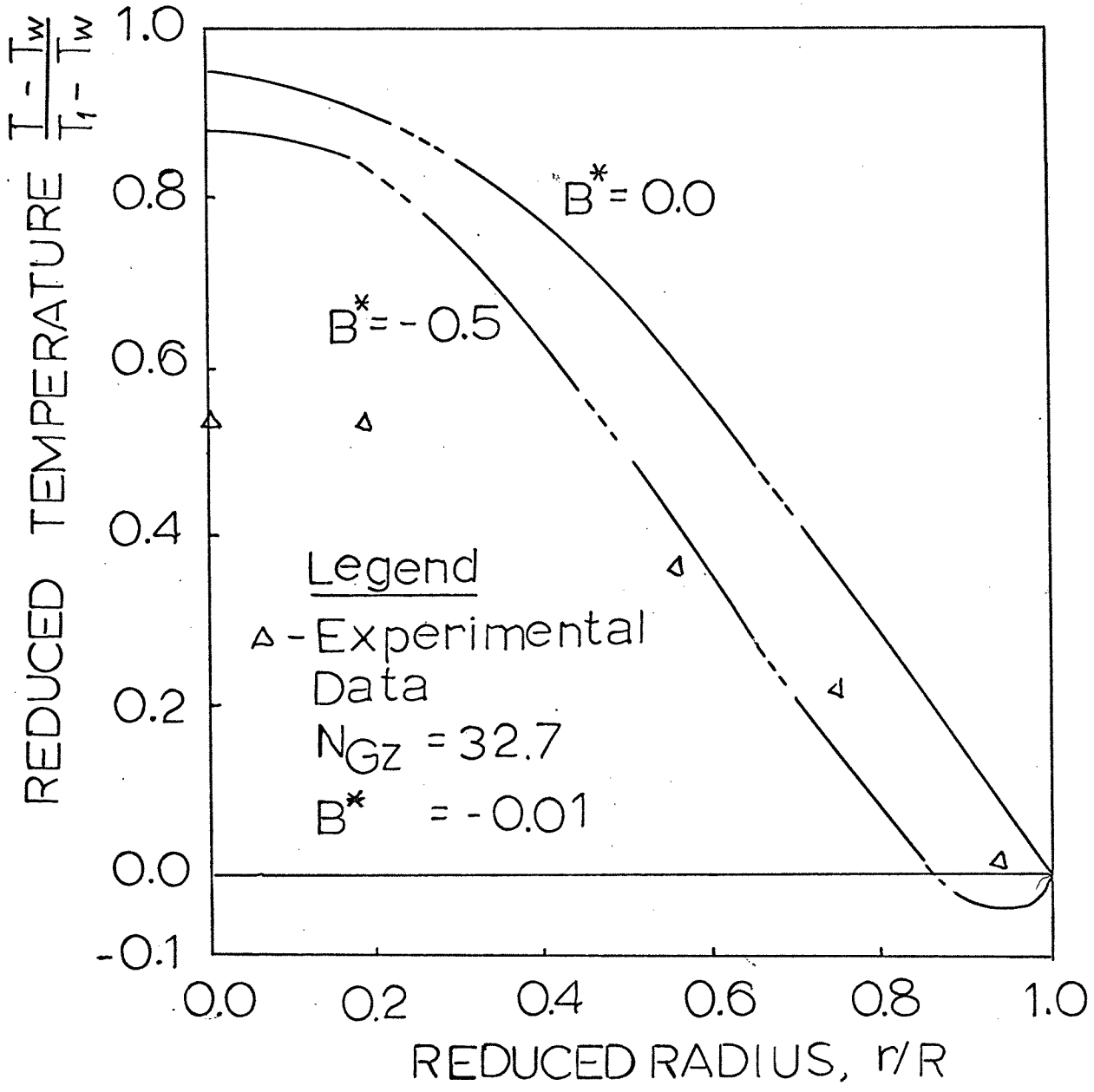

Figure 30. Comparison of Experimental and Calculated Temperature Profiles.

Attention should also be directed to the earlier work of Gee and Lyon.[26] These investigators solved the equations of motion and energy for heat transfer to a flowing thermally softened polymer (Lucite[140] also a polymethylmethancrylate). Figure 31 shows a predicted temperature profile. As can be seen, the slope closely resembles that found in the present work. This would indicate that the Gee-Lyon solution is at least qualitatively correct for heating of flowing thermally softened polymers.

2. Cooling of Flowing Thermally Softened Polymer Systems

a. Results

Data was also taken for the case where the flowing polymer system was cooled. Table X shows raw data for a typical temperature profile. These data are for a flow rate of 197.8 grams/minute and an axial length of 0.527 feet.

As with the heating case the situation ought to be the worst possible case (short axial length, low flow rate) in terms of precision. However, as can be seen, the results are reproducible and quite precise.

Plots of the data as temperature profiles are shown in Figures 32 through 37.

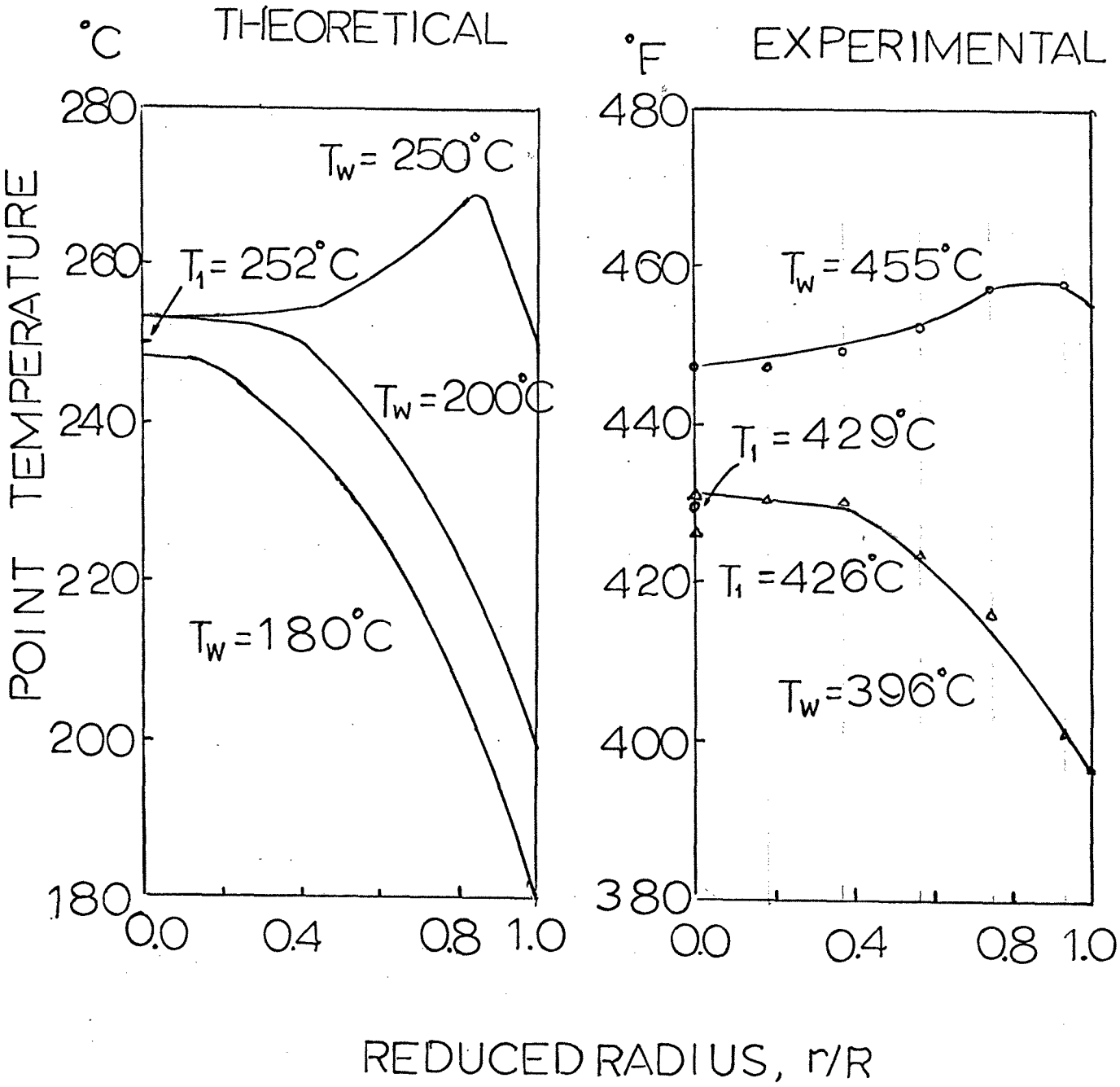

FIG. 31. Comparison of Theoretical and Experimental Point Temperatures at z/L = 1 with wall temperature as parameters

Table X

Flow Rate = 197.8 grams/minute

Reduced Radius	Test 28 (T_{inlet} =423; T_{wall} =384.2) T_{point}, °F	Test 29 (T_{inlet} =424.3 T_{wall} =385.3) T_{point}, °F
0.000	442.0	442.7
0.186	442.0	442.7
0.373	444.8	445.3
0.560	440.6	441.2
0.756	429.4	430.3
0.931	387.0	388.5

b. Discussion

Attention should be called to the ordinate of the temperature profile plots. The denominator of the reduced temperature (T_w-T_1) will always be negative. Hence, the more negative the numerater $(T-T_1)$, the more positive the ratio $\frac{T-T_1}{T_w-T_1}$. This means that the highest positive reduced temperature values are actually the coolest parts of the stream.

In Figures 32 through 37 it can be seen that polymer cooling is a function of axial length. That is, maximum cooling is

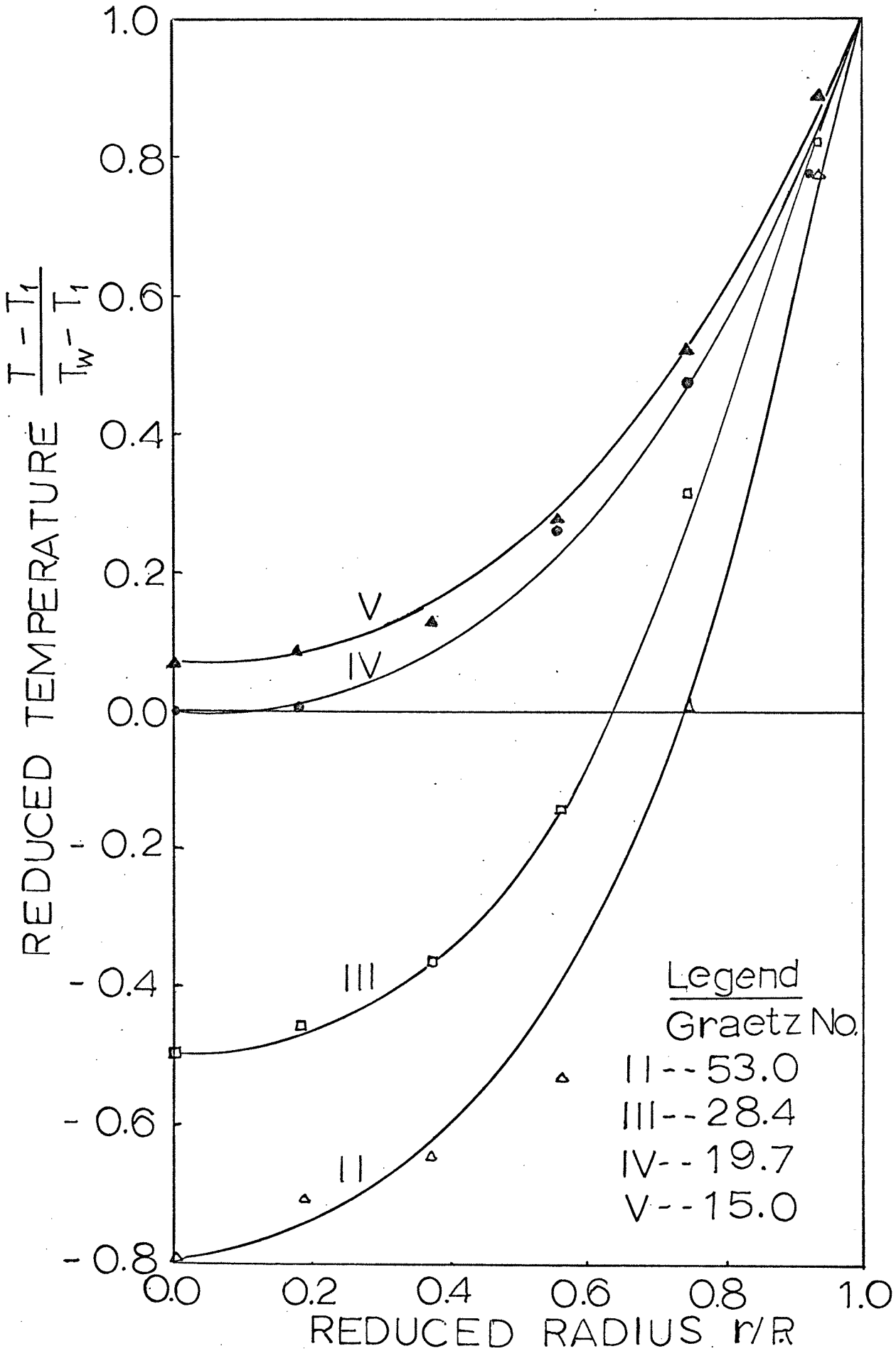

FIGURE 32. Experimental Dimensionless Temperature Profiles at Different Heat Transfer Lengths with a Flow Rate = 158.6 gr/min.

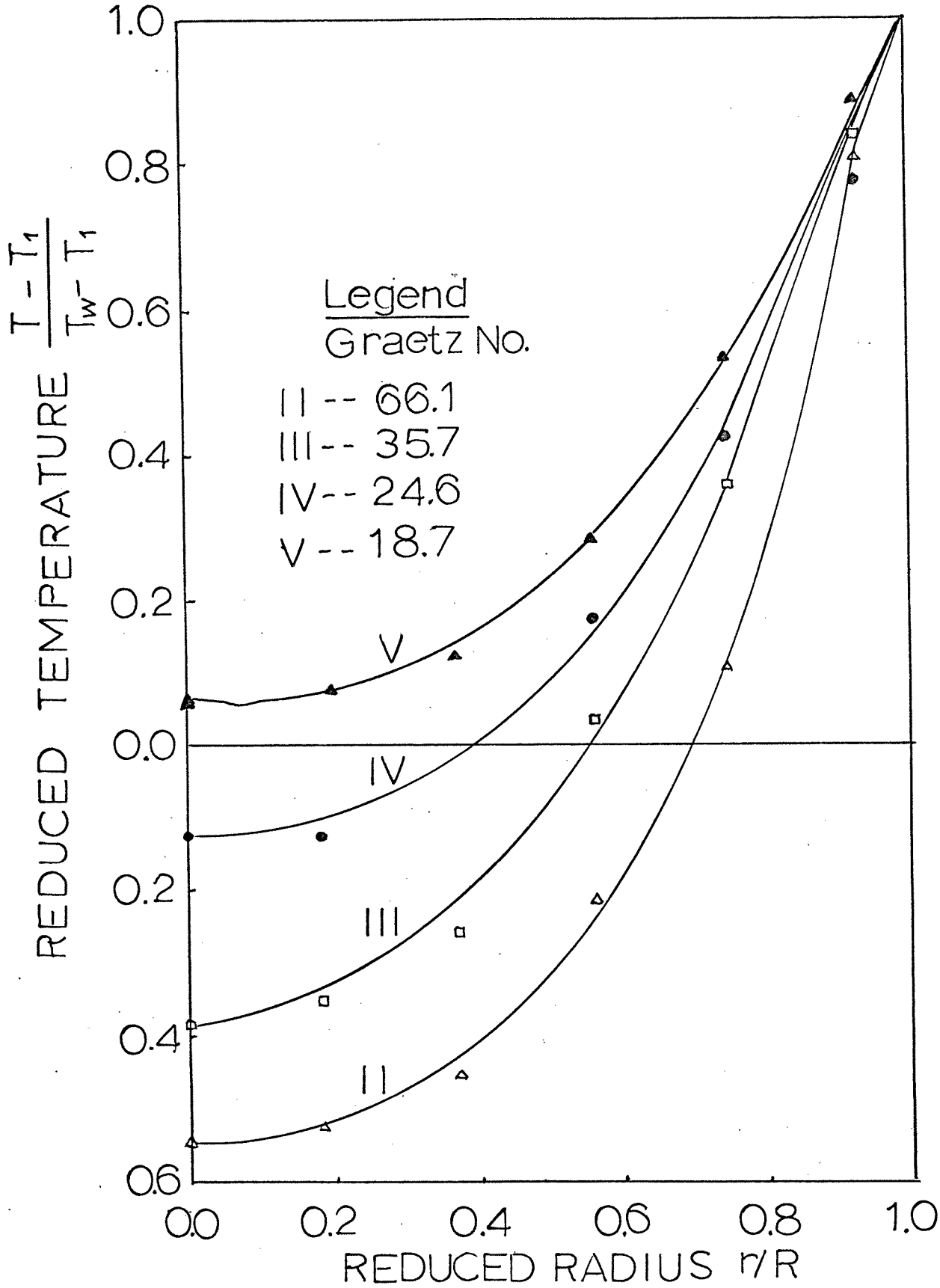

FIGURE 33. Experimental Dimensionless Temperature Profiles at Different Heat Transfer Lengths with a Flow Rate = 197.8 gr/min.

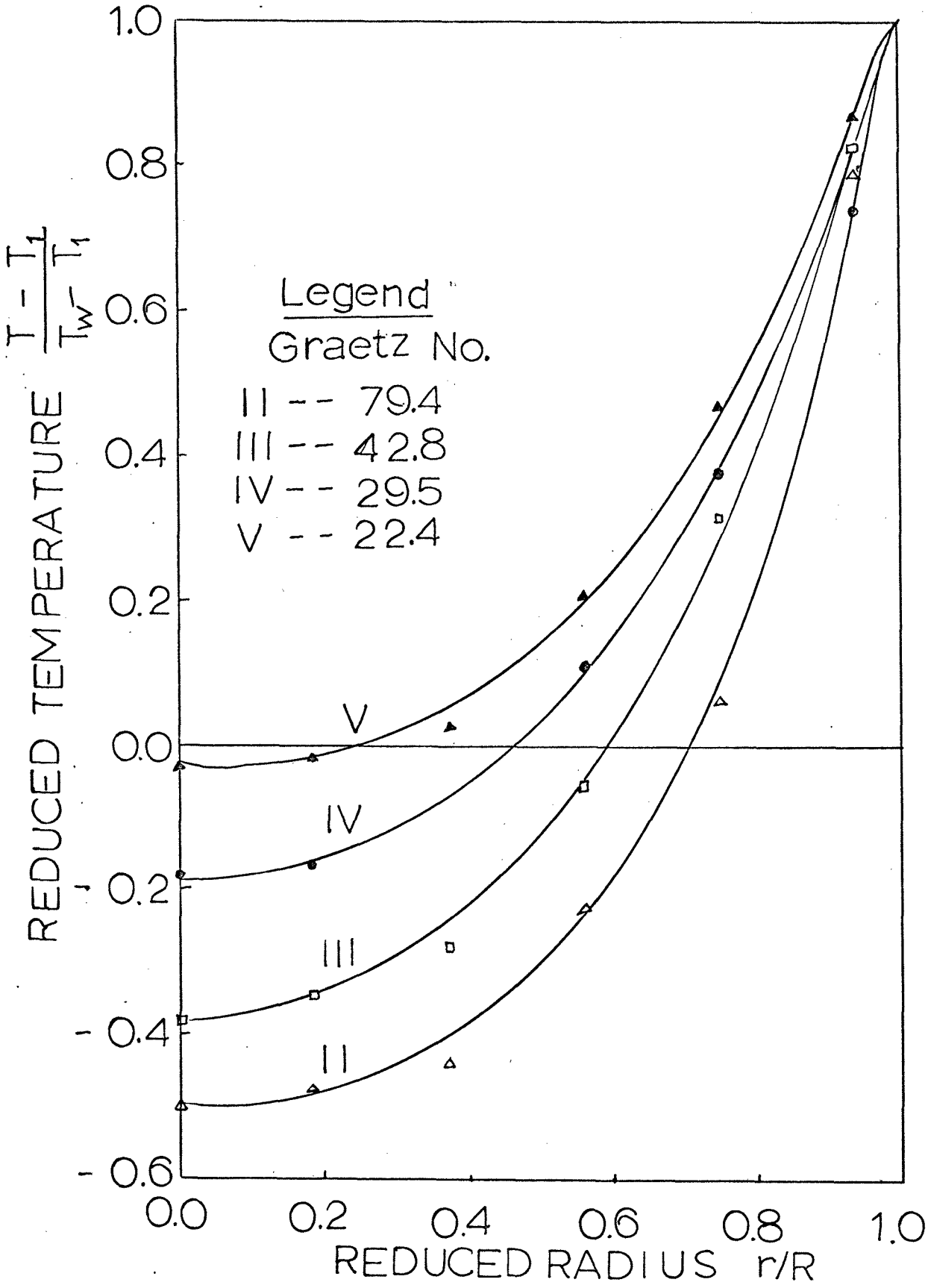

FIGURE 34. Experimental Dimensionless Temperature Profiles at Different Heat Transfer Lengths with a Flow Rate = 237.3 gr/min.

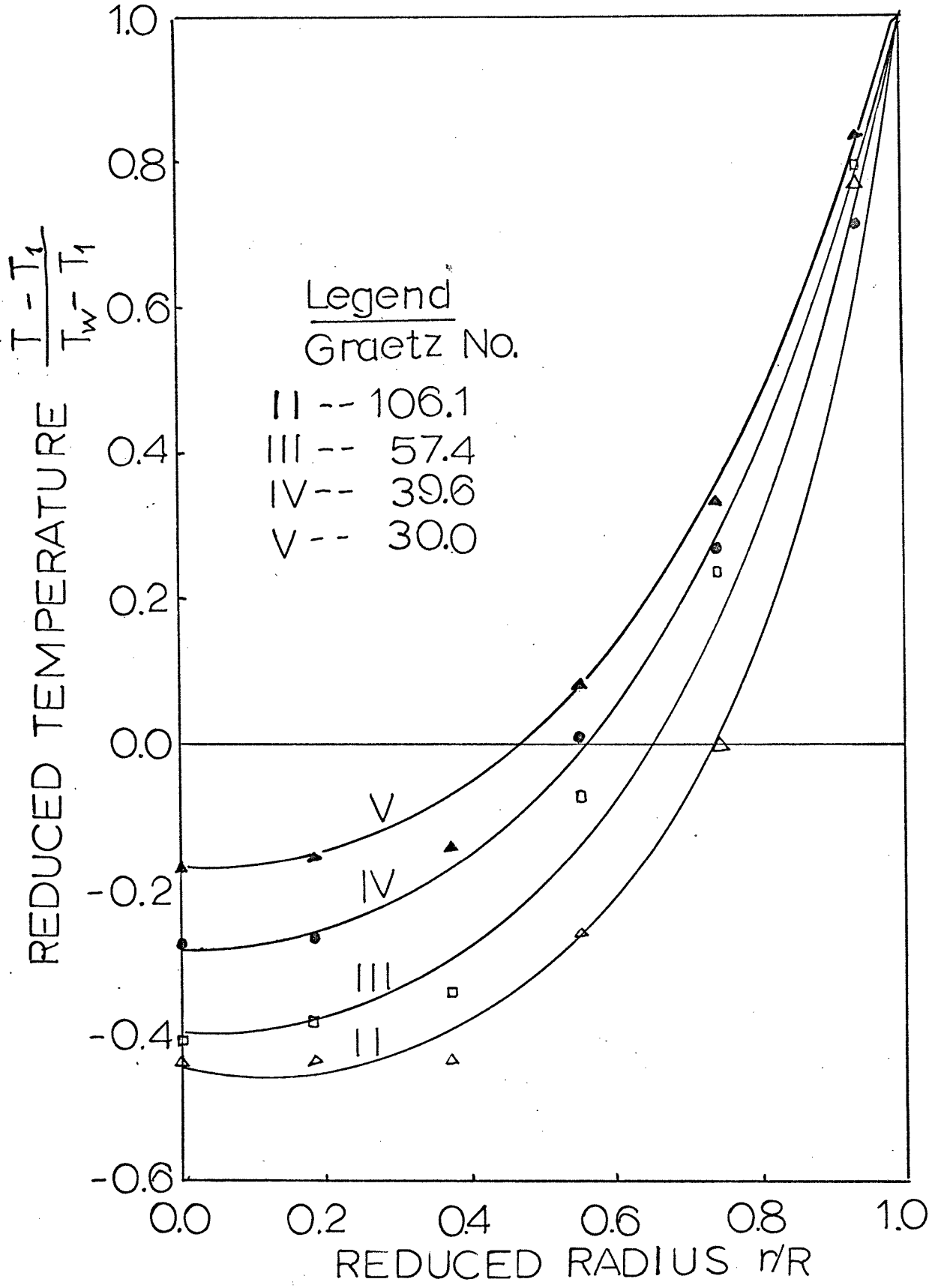

FIGURE 35. Experimental Dimensionless Temperature Profiles at Different Heat Transfer Lengths with a Flow Rate = 317.9 gr/min.

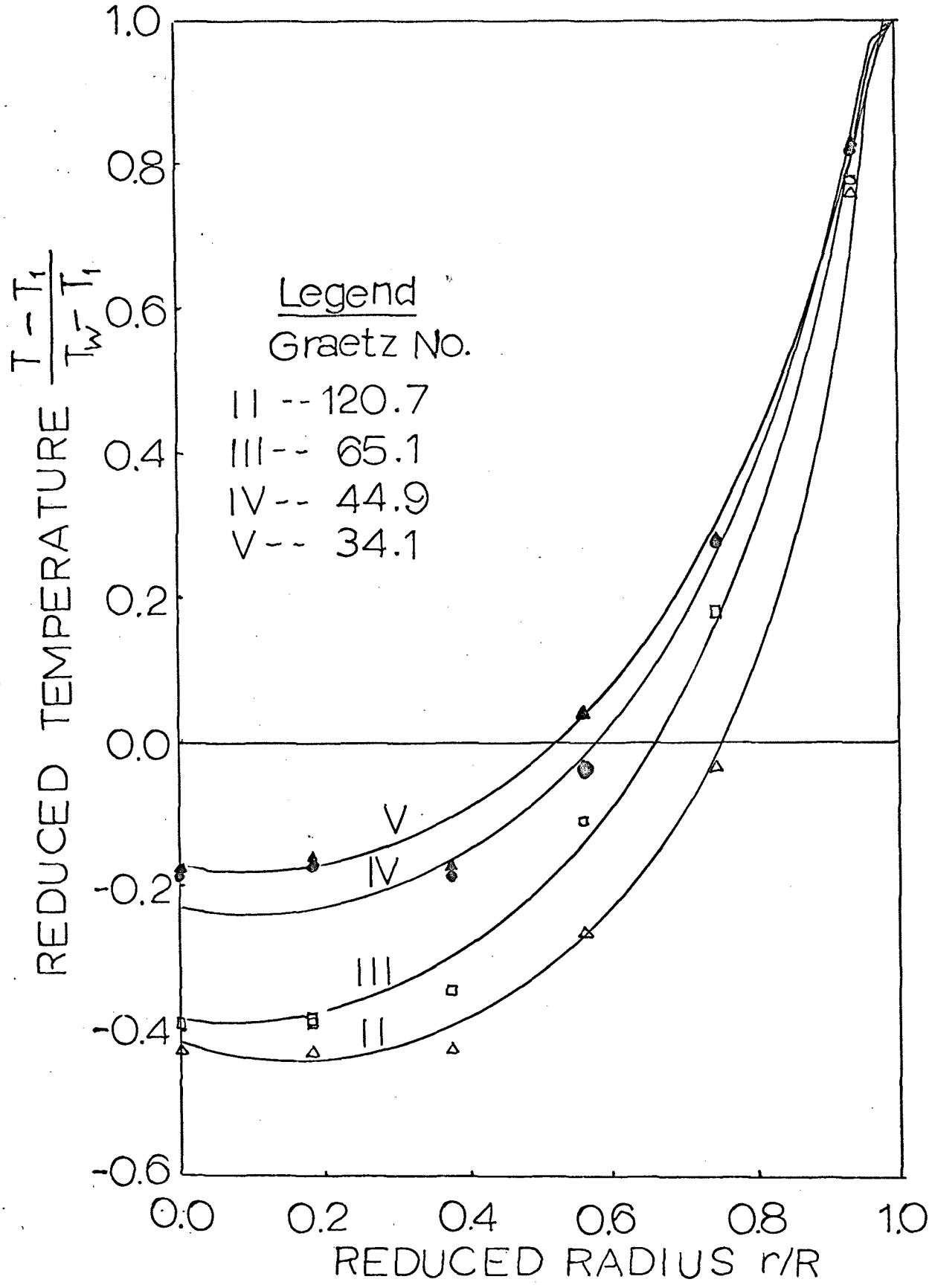

FIGURE 36. Experimental Dimensionless Temperature Profiles at Different Heat Transfer Lengths with a Flow Rate = 360.7 gr/min.

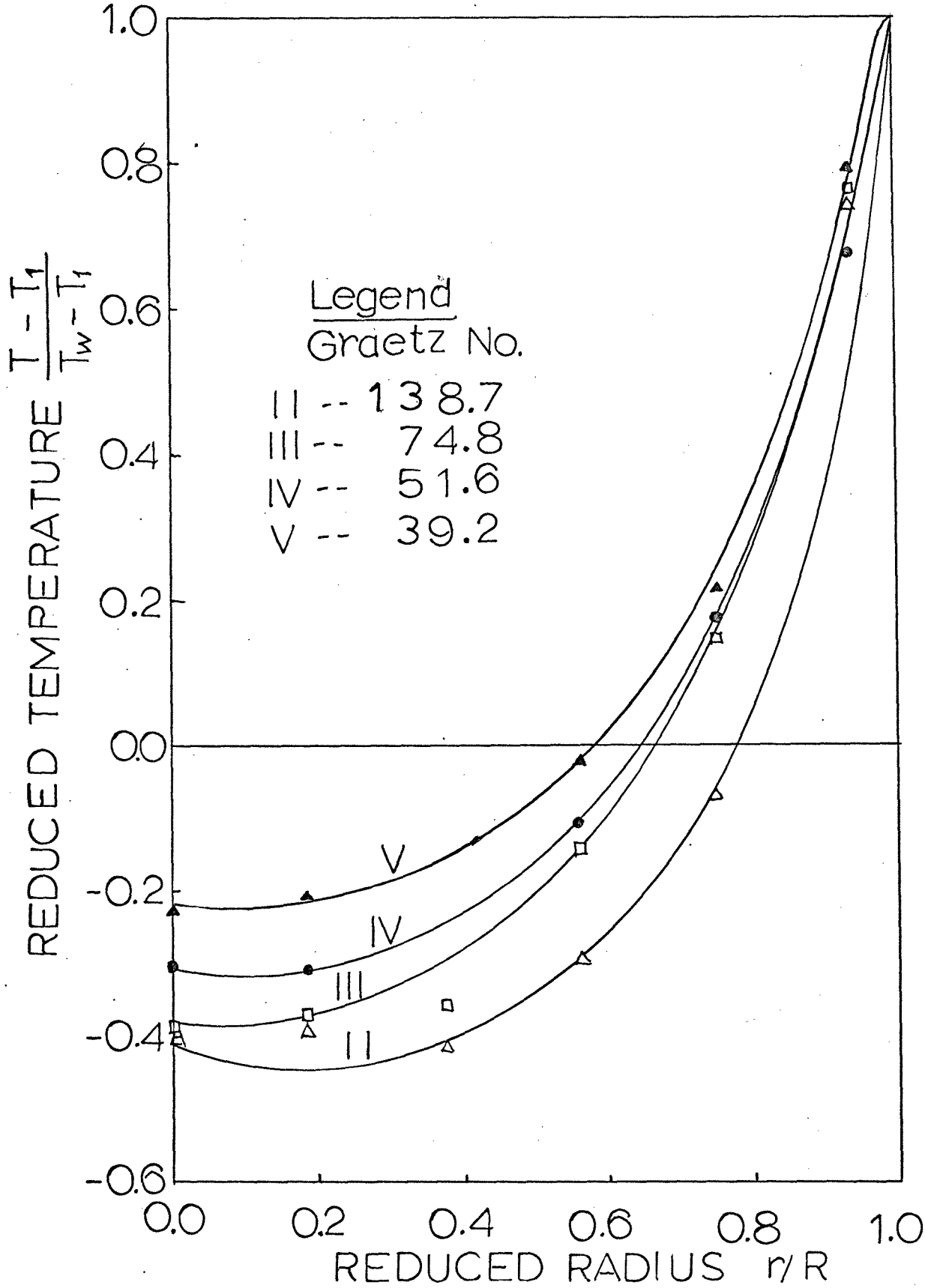

FIGURE 37. Experimental Dimensionless Temperature Profiles at Different Heat Transfer Lengths with a Flow Rate = 414.5 gr/min.

found at the longest axial length. This behavior is as would be expected. The longer the residence time (i.e., longer axial length at constant flow rate), the more cooling that takes place. In addition, as flow rate increases cooling decreases at any given axial length. This again takes place because of reduced residence time.

The shapes of the profiles in Figures 32 through 37 also deserve comment. Unlike the case for heating no special occurrences seem to be evident. There appears for example to be a greatly reduced effect of viscous dissipation. This can be explained because of the alteration of the velocity profile (see Figure 38). As can be seen, the change in profile near the wall will greatly reduce any viscous heating effects. Furthermore, the colder wall will readily act as a heat sink for any viscous heating that does occur. The net result is the type of smooth temperature profile seen in Figures 32 through 37.

Attention should once again be directed to the work of Gee and Lyon.[26] In Figure 31 plots of their predicted temperature profiles for cooling are shown. As can be seen, their curves are qualitatively the same as those found in this work. This point further reinforces the study of Gee and Lyon.

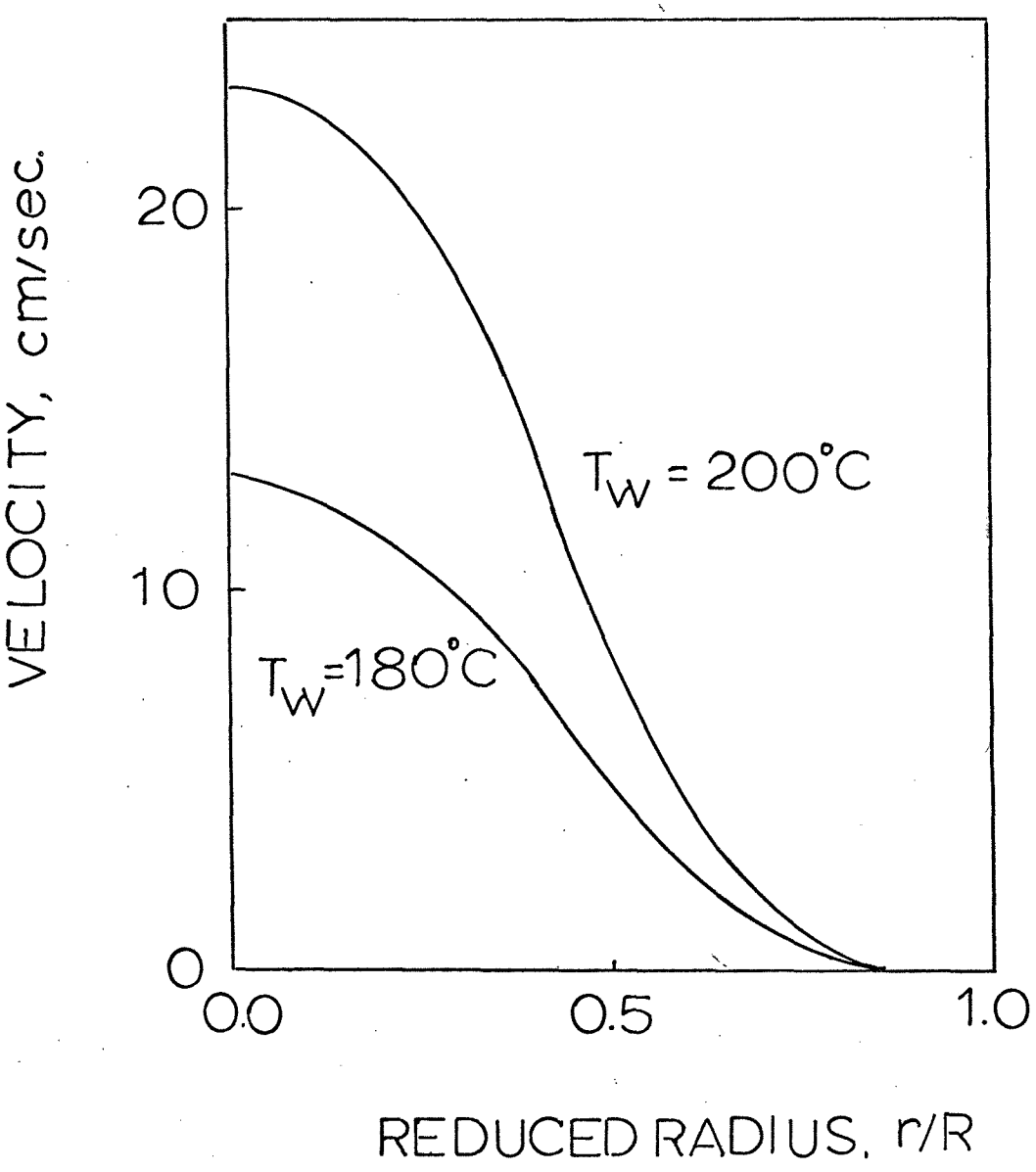

Figure 38. Theoretical Steady State Velocity Distribution at a Reduced Axial Length $\frac{Z}{L}$ = 1 with Initial Temperature T_1 =252°C

Recommendations

Future study should be directed to the stress and velocity field in the entrance region using a proper instrument such as strain gage or by another approach such as birefringent or tracer technique.

It is recommended to study the flow behavior such a manner that the result could be correlated to the physical properties, normal stress differences, and molecular structure.

It is emphasized to control more accurately the boundary conditions of the test section. For example to keep the wall temperature essentially constant it is one way to increase the flow rate of the hot oil or to circulate the oil through each piece of the test section separately.

For the study of heat transfer it would be helpful to do the experiment in different conditions, i.e., polymer inlet temperature and the wall temperature should be same to investigate the true viscous heat generation. It would be another fundamental study to find the heat transfer coefficient of the polymer melt under certain conditions.

There should be some improvement in measuring the temperature so that the axial and radial temperature could be recorded continuously and at the same time.

It is possible to shorten the time needed to heat up the whole system by changing the heating coils with the ones which can supply more heat per unit time.

V. CONCLUSIONS

In this investigation an apparatus has been developed to study the entrance region flow behavior of non-Newtonian fluids, especially for polymer melts by measuring the pressure drop. Although it has left many problems to be solved, a new pressure sensing device was tried to measure the pressure.

Total length of the test section was fifteen feet and inside diameters of small and large pipes were 0.957" and 3.826" respectively. Operating temperature was 425°F. Flow rate was 225 gr/min. Pressure range in calibration was 0 to 2000 psi.

A heat transfer to molten flowing polymer was studied in a heat exchanger of 15 feet and of 0.957 inch I.D. Polymer inlet temperature was controlled between 420°F to 440°F both in heating and cooling experiment. Oil temperature at the melt inlet was maintained by 30°F difference lower and higher for the experiments of cooling and heating effects.

Heat transfer lengths from inlet to the axial position where the measurement was obtained were 0.527, 3.560, 6.600, 9.560 and 12.600 feet respectively. The radial positions at each axial position were r/R = 0.000, 0.186, 0.373, 0.560, 0.746, 0.931 and 1.000. Flow rate range were from 158.6 to 477.0 gr/min.

1. It was tried to develop an apparatus to study the entrance and exit flow behavior.
2. Temperature profiles at the 0.525 foot-length were almost

flat. (Most temperature change occurs at the wall)

3. A depression in temperature at the center of the tube (r/R from 0.0 to 0.4) occurred.

4. A peak in temperature appeared near the wall when heating the polymer melt.

5. When cooling the polymer melt there appeared to be a greatly reduced effect of viscous dissipation due to the alteration of the velocity profile and heat transfer to the cold wall.

6. The polymer melt at the center of the tube could feel the wall temperature which was $30^{\circ}F$ lower than the inlet polymer temperature at a Graetz number less than 22.4.

VI. SUMMARY

Two separate experimental device were required for the present work: one to study the entrance effects in flow in molten polymer systems and the other to investigate the transfer of heat to thermally softened flowing polymer systems. Although two devices were needed some components were common to both. These were a 2" diameter screw extruder, a gear pump-vari-drive combination and a heat unit for the test sections following the gear pump.

For the entrance effects the actual data were to be consisted of the pressure measured at different axial and radial positions. It was concluded from the literature survey that most of the pressure drop in the case of molten polymer system occurs just before the entrance and that the polymer exhibit excess normall stress caused by the contraction to some distance of downstream. To verify this entrance effect a new technical device was tried to measure the pressure drop, but unfortunately it was not successful.

A temperature profile of polymethylmethacrylate were obtained for several flow rates at different axial and radial positions of one inch Schedule 80 stainless steel pipe. It was observed a depression in temperature in the central region of the tube and significant viscous heat generation near the wall when heating the polymer melt. When cooling the polymer there appeared to be a greatly reduced effect of viscous dissipation due to the alteration of the velocity profile and heat transfer to the cold wall.

VII.. BIBLIOGRAPHY

1. Astarita, G. and G. Greco, "Excess Pressure Drop in Laminar Flow Through Sudden Contraction(Newtonian Fluids)", Ind. Eng. Chem. Fund., 7, 27 (1968)

2. _____, and _____, "Excess Presure Drop in Laminar Flow Through Sudden Contraction (Non-Newtonian Fluids)", Ind. Eng. Chem. Fund., 7 595 (1968)

3. Bagley, E. B., "Hooke's Law in Shear and Polymer Melt Fracture", J. Appl. Phys., 31, 1126 (1960)

4. _____, "The Separation of Elastic and Viscous Effects in Polymer Flow", Trans. Soc. Rheol., 5, 355 (1961)

5. _____, and A. M. Birks, "Flow of Polyethylene into a Capillary", J. Appl. Phys., 31,556 (1960)

6. _____, S. H. Storey and D. C. West "Post Extrusion Swelling of Polyethylene", J. Appl. Pol. Sci., 7, 1661 (1963)

7. Beyer, C. E. and R. B. Dahl, "Measurement of Heating Capacities of Injection Molding Machines", Modern Plastics, 30, 124-30, 204 (1952)

8. Bernhardt, E. C., "Processing of Thermoplastic Materials", Reinhold Publishing Co., N.Y., N.Y. (1959)

9. Bird, R. B., "Viscous Heat Effects in Extrusion of Molten Plastics SPE, 11, 35 (1955)

10. _____, W. E. Stewart, and E. N. Lightfoot, "Transport Phenomena", Wiley, New York (1960)

11. Boles, R. L., H. L. Davis and D. C. Bogue, D. C., "Entrance Flows of Polymeric Materials: Pressure Drop and Flow Patterns", Poly. Eng. Sci., 10, 24 (1970)

12. Bogue, D. C., "Entrance Effects and Prediction of Turbulence in Non-Newtonian Flow", Ind. Eng. Chem., 51, 874 (1959)

13. Boussinesq, J. V., "Sur la Manière dont les vitesses, dans un tube cylindrique de section circulaire, évasé à son entrée, se distribuent depuis cette entrée jusqu'aux endroits où se trouve établi un régime uniforme", Compt. Rend. 113, 9-15 (1891)

14. Brinkman, H. C., "Heat Effects in Capillary Flow", Appl. Sci., Res., A2, 120 (1951)

15. Campbell, W. D., and J. C. Slattery, "Flow in the Entrance of Tube", Trans. A. S. M. E. J. of Basic Eng., 85, Series D, 41 (1963)

16. Chong, J. S., E. B. Christiansen, and A. D. Baer, "Flow of Viscous Fluid Through a Circular Aperture", 15, 369 (1971)

17. Christiansen, E. B. and H. E. Lemmon, "Entrance Region Flow", A.I.ChE, 11, 995 (1965)

18. Chu, C. S., M. S. thesis, University of Tennessee, Knoxville, Tennessee (1965)

19. Collins, M. and W. R. Schowalter, "Behavior of Non-Newtonian Fluids in the Entry Region of a Pipe", A. I. ChE. J., 9, 804 (1963)

20. Dodge, D. W., Ph. D. thesis, "Turbulent Flow of Non-Newtonian Fluids in Smooth Round Tubes", University of Delaware, Newark, Delaware (1957)

21. Drew, T. B., J. J. Hogan, and W. H. McAdams, "Heat Transfer in Stream Line Flow", I. E. C., 23, 936 (1931)

22. Forsyth, T. H. and N. F. Murphy, "Experimental Measurement of Temperature Profiles of Molten Flowing Polymers in a Heat Exchanger", Poly. Eng. Sci., 9, 1, 22 (1969)

23. _____ and _____, "Temperature Profile of Profile of Molten Flowing Polymers in a Heat Exchanger", A. I. ChE. J., 15, 5, 958 (1969)

24. Foster, G. N., N. Waldman and R. G. Griskey, "Pressure-Volume-Temperature Behavior of High Density Polyethylene", J. of Appl. Pol. Sci., 10, 201 (1966)

25. Galt, J. and B. Maxwell, "Velocity Profiles for Polyethylene Melts", 41, No. 12, 115 (1964)

26. Gee, R. E. and J. B. Lyon, "A Nonisothermal Flow of Viscous Non-Newtonian Fluids", I. E. C., 49, 956 (1957)

27. Goldstein, S., "Modern Developments in Fluid Dynamics", Vol. 1, P299-308, Dover, N. Y. (1965)

28. Graetz, L., Ann. Physik, 18, 79 (1883)
Drew, T. B., "Mathematical Attacks on Forced Convection Problems", A Review, Trans. of the A. I. ChE, 28, 55-71 (1936)

29. Griskey, R. G. and I. A. Wiehe, "Heat Transfer to Molten Polymers" A. I. ChE. J., 12, 308 (1966)

30. Han, C. D., M. Charles and W. Philippoff, "Measurement of the Axial Pressure Distribution of Molten Polymers in Flow Through a Circular Tube", Trans. Soc. Rheol., 13:4, 455 (1969)

31. Han, C. D., M. Charles, and W. Philippoff, "Rheological Implications of the Exit Pressure and Die Swell in Steady Capillary Flow of Polymer Melts", Trans. Soc. Rheol., 14:3, 393 (1970)

32. Kreith, F. and Eisenstadt, R., "Pressure Drop and Flow Characteristics of Short Capillary Tubes at Low Reynolds Number", Trans. A. S. M. E., 79, 1070 (1957)

33. Langhaar, H. L., "Steady Flow in the Transition Lenght of a Straight Tube", J. Appl. Mech. 9, No. 2, A55-9 (1942)

34. La Nieve H. L., M.S. thesis, "Entrance Effects in Non-Newtonian Pipe Flow", University of Tennessee, Knoxville, Tennessee (1963)

35. La Nieve, H. L. and D. C. Bogue, "Correlation of Capillary Entrance Pressure Drops with Normal Stress Data", J. Appl. Pol. Sci., 12, 353 (1968)

36. Lyche, B. C. and R. B. Bird, "The Graetz-Nusselt Problem for a Power-Law non-Newtonian fluid", Chem. Eng. Sci., 6, 35 (1956)

37. McKelvy, J. M., "Polymer Processing", John Wiley and Sons, Inc., New York (1962)

38. Metzner, A. B., "Advances in Chemical Engineering", Vol. I, Academic Press, New York (1956)

39. _____, E. Lucille Carley, and I. K. Park, "Polymeric Melts", Modern Plastics, 37, No. 11, 133 (1960)

40. _____, E. A. Uebler and C. F. Chan Man Fong, "Converging Flows of Viscoelastic Materials", A. I. ChE. J., 15, 750 (1969)

41. Middleman, S., "The Flow of High Polymers", Interscience Publishers, New York (1968)

42. Perry, J. H., Chemical Engineer's Handbook, 4th Edition, McGraw Hill.

43. Philippoff, W., and F. H. Gaskins, "The Capillary Experiment in Rheology", Trans. Soc. Rheol., 2, 263 (1958)

44. Roscoe, R., "The Flow of Viscous Fluids round Plane Obstacles", Phil. Mag., 40, 338 (1949)

45. Sampson R. A., Phil. Trans. Roy. Soc., 182A, 449 (1891)

46. Schiller L., "Die Entwicklung der laminarion Geschwindigkeitsverteilung und ihre Bedeutung fur Zahigkeitsmessungen", Z. Angew. Mathematik und Mechanik 2 94-106 (1922)

47. Skelland, A. H. P., "Non-Newtonian Flow and Heat Transfer", P122-128, Wiley, N. Y. (1967)

48. Tomita, Y., "On the Additional Loss at the Entry of a Pipe in the Case of Non-Newtonian Laminar Flow", Trans. JSME, 25, 938 (1959)

49. _____, "On the Non-Newtonian Laminar Flow in the Region near the Entrance of a Circular Pipe", Soc. Chem. Engrs. Japan 23,325 (1959)

50. _____, "Analytical Treatments of Non-Newtonian Fluid Flow by Introducing the Conception of Boundary Layer", Bull. JSME, 4, 77 (1961)

51. Saltük, I. K., "Development of an Apparatus to Obtain Temperature Profiles of Molten Flowing Polymer", M.S. thesis, Newark College of Engineering, Newark, New Jersey

52. Schott, H. and W. S. Kaghan, "Temperature Profile of Molten Plastic Flowing in a Cylindrical Duct", SPE J., 20, 139 (1964)

53. Toor, H. L., "The Energy Equation for Viscous Flow", Ind. Eng. Chem., 48, 922 (1956)

54. _____, "Heat Generation and Conduction in the Flow of a Viscous Compressible Liquid", Trans. Soc. Rheology, I, 177 (1957)

55. _____, "Heat Transfer in Forced Convection with Internal Heat Generation", A. I. ChE. J., 4, 319 (1958)

56. Vaughn, R. D., "Heat Transfer to Non-Newtonian Fluids", Ph. D. thesis, University of Delaware, Newark, Delaware (1956)

57. Weissberg, H. L., "End Correction for Slow Viscous Flow through Long Tubes", Phys. Fluids, 5, 1033 (1962)

58. Weltman, R. and T. Keller, "Pressure Losses of Titania and Magnesium Slurries in Pipes and Pipeline Transitions", Natl. Advisory Comm. Aeronaut. In 3889 (1957)

59. Westover, R. F., "Processing Properties", in "Processing of Thermoplastic Materials" by E. C. Bernhardt, Reinhold Publishing Co., New York, N. Y. (1959)

60. Wiehe, I. A., M.S. thesis, "Development of an Apparatus for Measuring Heat Transfer to Molten Polymers", Virginia Polytechnic Institute, Blacksburg, Virginia (1965)

61. Wilkinson, W. L., "Non-Newtonian Fluids", Pergamon Press, New York (1960)

APPENDIX A

NOTATION

A = Newtonian Viscosity at $0^{\circ}K$, poise

A = cross sectional area

A = an empirical constant depending on the nature of the fluid, $lb_f\text{-sec}/ft^2$

$a = \frac{n+1}{n}$, constant in Equation (64)

a = constant in Equation (140)

b = constant in Equation (140)

B_r = Brinkman number for Newtonian fluids

B_r' = Brinkman number for non-Newtonian fluid

C_p = heat capacity of the fluid, $\frac{Btu}{lb_m \cdot {}^{\circ}F}$

$(C_p)_o$ = heat capacity of fluid at constant pressure at $0^{\circ}C.$, ergs/gram$^{\circ}K$

D = diameter of the tube

E_v = viscous dissipation energy

E_e = elastic energy

E = activation energy

$e = n + \frac{s_R}{2}$

E_p = energy consumed due to the expansion, $lb_f/ft^2\text{-sec}$.

F = Rheological constant in Equation (185), $\left(\frac{ft^2}{lb}\right)^{m-1}/hr$

F = energy dissipated by friction

F = velocity, function of $\left(\frac{r}{R}\right)$

f = friction factor

f = function of η in Equation(65)

G = shear modulus

Gr = Graetz number, dimensionless

Ge = gravitational constant

h_a = heat transfer coefficient

H = the energy of activation for flow, ft lb_f/lb-mole

J_o = Bessel function of the zeroth order

J_1 = Bessel function of the first order

k = thermal conductivity of the fluid, $\frac{Btu}{ft\ ^{o}R\ hr}$

K = consistency index in Equation (3)

K_i= constants in Equation (67)

L = tube length or heat transfer length, ft

l = rheological constant, $\frac{1}{n}$

M and M' = constants in Equation (70)

m = kinetic energy correction factor in Equation (103)

m = rheological constant in Equation (155), dimensionless

N_{Re} = Reynolds number, dimensionless

N_{Re}' = generalized Reynolds number for power law fluid, $\frac{D^n V^{2-n} \rho}{g_c K 8^{n-1}}$

N_{Re}'' = generalized Reynolds number, $\frac{D^{n'} V^{2-n'} \rho}{g_c K' 8^{n'-1}}$

N_u = Nusselt number, $\frac{h_a D}{k}$

n = flow behavior index

n' = constant defined in Equation(50)

n = Couette correction in Equation (107)

P = pressure, lb_f/in^2

P_{ij} = deviatoric stress

Q = volume flow rate, ft^3/sec

q = rate of convective heat transfer, Btu/hr

R = pipe radius, ft

R_e^* = generalized Reynolds number in Equation (96)

r = radius, variable, ft

S = cross sectional area of the tube

s = recoverable shear

T_{ii} = total normal stress

T = temperature

T_b = bulk temperature of the fluid

T_w = wall temperature

T_1 = inlet temperature of the polymer

t = temperature, variable

t = spherical coordinate in Equation (91)

U = core velocity

u^* = perturbation velocity in Equation (69)

u = radial velocity in Equation (73)

V = average velocity, ft/sec

v_z = velocity in the axial direction, variable, ft/sec

W = $f(\theta)$ in Equation (74)

w = flow rate, gr/min

x = distance in the axial direction

x = spherical coordinate in Equation (90)

x_d = entrance length

y = distance from the wall of a tube, R-r

y = reduced radius, $\frac{r}{R}$

Greek

α = thermal diffusivity of the fluid, cm^2/sec

α_0 = thermal diffusivity at 0^oC

$\alpha_0, \alpha_1, \alpha_2$ = kinetic energy correction factor

α_1 = constant in Equation (83)

β = compressibility, $\frac{1}{psia}$

$\dot{\gamma}$ = rate of shear, sec^{-1}

$\dot{\gamma}_w$ = shear rate at the wall, sec^{-1}

δ = boundary layer thickness

$\delta^+ = \frac{\delta}{R}$

ϵ = coefficient of thermal expansion

ϵ = Couette correction

ξ = dimensionless distance, $\left(\frac{K}{\rho C_p V_{max} R^2} \right)$

η = dimensionless variables in Equation(66)

η = apparent or plastic viscosity

η_j = jth root of J_0

$\theta = \dfrac{T - T_w}{T_1 - T_w}$ reduced temperature, dimensionless

λ = relaxation time

μ = Newtonian viscosity

ρ = density of the fluid, lb/ft^3

ρ' = reduced radius, $\dfrac{r}{R}$

α = dimensionless variable in Equation(66)

τ = shear stress, lb_f/ft^2

τ_w = shear stress at the wall, lb_f/ft^2

ϕ = function defined in Equation (17)

ϕ = C_b in Equation (82)

ϕ = spherical coordinate in Equation (91)

$\psi = \dfrac{U}{V} - 1$

ψ = stream function

ω = vorticity

APPENDIX B SAMPLE CALCULATION

All the physical properties were calculated at bulk temperature, which is defined as

$$T_b = 1/2\ (T_w - T_1)$$

The average inlet temperature and the average wall temperature were used as the inlet and the wall temperatures in the above equation.

for the heating effect: $T_b = 231^{\circ}C = 448^{\circ}F$

for the cooling effect: $T_b = 208.5^{\circ}C = 407.5^{\circ}F$

Rheological Data

The constants in poser law were calculated from the flow curve of Plexiglas VM 100 in Westover's "Processing Properties".[58] By extrapolating to $448^{\circ}F$ one can get

$$n = \frac{\log \tau_{w_1} - \log \tau_{w_2}}{\log \dot{\gamma}_1 - \log \dot{\gamma}_2} = \frac{\log 1.1 - \log 0.27}{\log 10 - \log 1} = 0.61$$

The consistency index, K, is the value of intercept at $\dot{\gamma} = 1$.

Density

Density was taken from the processing properties of Westover's.[58]

$\rho = 66.0$ lb/ft^3 at $T_b = 448^{\circ}F$

$\rho = 66.8$ lb/ft^3 at $T_b = 407.5^{\circ}F$

Thermal Diffusivity

The thermal diffusivity was calculated using Equation(140) with the proper constants.[35]

$\alpha = 4.01 \times 10^{-4}$ cm^2/sec at $T_b = 448$ F

$$\alpha = 4.30 \times 10^{-4} \text{ cm}^2/\text{sec} \quad \text{at} \quad T_b = 407.5^\circ\text{F}$$

Specific Heat

The data for specific heat were taken from the Processing Properties of Westover's.[58]

$$C_p = 0.88 \text{ Btu/lb}_m{}^\circ\text{F} \quad \text{at} \quad T_b = 448^\circ\text{F}$$

$$C_p = 0.85 \text{ Btu/lb}_m{}^\circ\text{F} \quad \text{at} \quad T_b = 407.5^\circ\text{F}$$

Thermal Conductivity

This physical property was evaluated by the following relationship using the values obtained above.

$$K = \rho C_p \alpha$$

$$K = 0.09 \text{ Btu/ft } ^\circ\text{R hr} \quad \text{at} \quad T_b = 448^\circ\text{F}$$

$$K = 0.0945 \text{ Btu/ft}^\circ\text{R hr} \quad \text{at} \quad T_b = 407.5^\circ\text{F}$$

Evaluation of Temperature

All the data were taken in Millivolts and converted to degrees Fahrenheit referring to the tables of National Bureau of Standards Circular 561.

Calculation of Reduced Temperatures

One reduced temperature was determined in the following manner.

$$\text{Reduced temperature} = \frac{T - T_1}{T_w - T_1}$$

where

T = probe temperature

T_1 = polymer inlet temperature

T_w = wall temperature

The other reduced temperature was evaluated by subtracting the first reduced temperature from unity. Substituting data from Table XI , Test 8 on page 173 at a reduced radius of 0.186,

$$T_{r1} = \frac{T - T_1}{T_w - T_1} = \frac{441.8 - 430.2}{467.2 - 430.2} = 0.314$$

$$T_{r2} = \frac{T_w - T}{T_w - T_1} = 1 - T_{r1} = 1 - 0.314 = 0.686$$

Graetz Number

The Graetz numbers were determined by dividing the product of the average flow rate and the heat capacity by the product of the thermal conductivity and the heat transfer lengths. Using the data from test run 7 at a heat transfer length of 3.560 ft on page 173 the following s are obtained.

$$N_{Gz} = \frac{WC_p}{kL} = \frac{241.9 \frac{gr}{min}\ 0.88 \frac{Btu}{lbm\,°F}\ \frac{60}{453} \frac{lbm}{gr} \frac{min}{hr}}{0.09 \frac{Btu}{ft\,°R\,hr}\ 3.56\,ft} = 87.8$$

Calculation of Brinkman Number(Viscous Heating Factor)

$$Br^* = \frac{\tau_w W n}{(3n+1) k \rho \pi R (T_1 - T_w)}$$

From the previous calculation

$$n = 0.61$$

$$k = 0.09 \text{ Btu/ft}^\circ\text{R hr}$$

$$\rho = 66.0 \text{ lb/ft}^3$$

$$R = 0.957 \text{ in.}$$

$$Br^* = \frac{\tau_w W n}{(3n+1) k R \pi \rho (T_1 - T_w)}$$

$$= \frac{0.61\ \tau_w \frac{lbf}{in^2}\ W \frac{gr}{min}\ 144 \frac{in^2}{ft^2}\ \frac{60\,lb}{453.6\,hr} \frac{min}{gr}}{(2.83)(0.09) \frac{Btu}{ft\,°R\,hr}\ \frac{0.957}{12} ft\,(3.14)\,(66) \frac{lb}{ft^3} (T_1 - T_w)°F\ 778 \frac{ft\,lbf}{Btu}}$$

$$= 3.548 \times 10^{-3} \frac{\tau_w W}{T_1 - T_w}$$

For the test run 10 on page 213,

$$T_1 - T_w = 430.8 - 473.3 = -42.5^\circ\text{F}$$

$$w = 316.4 \text{ gr/min.}$$

At this flow rate the shear rate, 8V/D, was calculated to be 3.9/sec. and the corresponding wall shear stress is 0.60 lb_f/in^2 from Westover's "Processing Properties".[58] Substituting the obtained data into the above equation gives a value of -0.016.

TABLE XI

Data Obtained for Molten Plexiglas VM 100

At a Reduced Length of 0.042 and a Heat Transfer Length of 0.527

Test No.	Reduced Radius	Inlet Temperature		Wall Temperature		Probe Temperature		Flow Rate
		m.v	°F	m.v	°F	m.v	°F	gr/min
1	0.000	12.03	432.3	12.26	440.0	12.345	442.5	193.5
	0.186					12.335	442.15	
	0.373					12.460	446.3	
	0.560					12.480	447.0	
	0.746					12.43	445.3	
	0.931					12.08	434.0	
2	0.000	12.10	434.7	12.34	442.3	12.40	444.3	193.5
	0.186					12.39	444.0	
	0.373					12.515	448.2	
	0.560					12.535	448.8	
	0.746					12.48	447.0	
	0.931					12.14	436.0	

3	0.000	12.11	435.0	12.42	445.0	12.43	445.3	193.5
	0.186					12.415	444.8	
	0.373					12.55	449.3	
	0.560					12.56	449.7	
	0.746					12.51	448.0	
	0.931					12.195	437.8	
4	0.000	12.10	434.7	12.445	445.8	12.43	445.3	193.5
	0.186					12.415	444.8	
	0.373					12.54	449.0	
	0.560					12.56	449.7	
	0.746					12.51	448.0	
	0.931					12.205	438.2	
5	0.000	11.95	429.75	12.44	445.7	12.325	441.8	241.9
	0.186					12.31	441.3	
	0.373					12.39	444.0	
	0.560					12.42	445.0	
	0.746					12.365	443.2	
	0.931					12.15	435.2	

6	0.000	11.95	429.75	12.45	446.0	12.325	441.8	241.9
	0.186					12.31	441.3	
	0.373					12.39	444.0	
	0.560					12.425	445.2	
	0.746					12.36	443.0	
	0.931					12.15	436.3	
7	0.000	11.925	429.1	12.45	446.0	12.33	442.0	241.9
	0.186					12.32	441.7	
	0.373					12.395	444.2	
	0.560					12.425	445.2	
	0.746					12.36	443.0	
	0.931					12.15	436.3	
8	0.000	11.965	430.2	12.43	445.3	12.345	442.5	316.4
	0.186					12.33	442.0	
	0.373					12.38	443.7	
	0.560					12.415	444.8	
	0.746					12.35	442.7	
	0.931					12.15	436.3	

9	0.000	11.975	430.5	12.44	445.7	12.355	442.8	316.4
	0.186					12.355	442.2	
	0.373					12.39	444.0	
	0.560					12.42	445.0	
	0.746					12.36	443.0	
	0.931					12.165	436.8	
10	0.000	11.985	430.8	12.45	446.0	12.36	443.0	316.4
	0.186					12.345	442.5	
	0.373					12.395	444.2	
	0.560					12.43	445.3	
	0.746					12.37	443.3	
	0.931					12.17	437.0	
11	0.000	12.04	432.7	12.46	446.3	12.41	444.7	413.4
	0.186					12.39	444.0	
	0.373					12.41	444.7	
	0.560					12.46	446.3	
	0.746					12.355	442.8	
	0.931					12.23	439.0	

12	0.000	12.045	432.8	12.46	446.3	12.40	444.3	413.4
	0.186					12.38	443.7	
	0.373					12.41	444.7	
	0.560					12.47	446.7	
	0.746					12.36	443.0	
	0.931					12.24	439.3	
13	0.000	12.10	434.7	12.465	446.5	12.40	444.3	413.4
	0.186					12.385	443.8	
	0.373					12.435	445.5	
	0.560					12.48	447.0	
	0.746					12.37	443.3	
	0.931					12.24	439.3	
14	0.000	12.22	438.7	12.485	447.2	12.56	449.7	477.0
	0.186					12.55	449.3	
	0.373					12.56	449.7	
	0.560					12.615	451.4	
	0.746					12.505	447.8	
	0.931					12.31	441.3	

15	0.000	12.235	439.2	12.51	448.0	12.60	451.0	477.0
	0.186					12.585	450.5	
	0.373					12.595	450.8	
	0.560					12.65	452.3	
	0.746					12.54	449.0	
	0.931					12.35	442.7	
16	0.000	12.22	438.7	12.52	448.3	12.58	450.3	477.0
	0.186					12.52	450.0	
	0.373					12.59	450.7	
	0.560					12.63	451.7	
	0.746					12.54	449.0	
	0.931					12.355	442.8	
17	0.000	11.93	429.25	11.75	423.3	12.085	434.2	180.9
	0.186					12.085	434.2	
	0.373					12.22	438.7	
	0.560					12.20	438.0	
	0.746					12.05	433.0	
	0.931					11.445	413.5	

18	0.000	11.88	427.8	11.705	421.8	12.06	433.3	180.9
	0.186					12.05	433.0	
	0.373					12.195	437.8	
	0.560					12.18	437.3	
	0.746					12.00	431.3	
	0.931					11.39	411.7	
19	0.000	11.865	427.2	11.685	421.2	12.04	432.7	180.9
	0.186					12.04	432.7	
	0.373					12.19	437.7	
	0.560					12.17	437.0	
	0.746					11.985	430.8	
	0.931					11.36	410.7	
20	0.000	11.825	425.8	11.63	419.3	11.91	428.7	270.4
	0.186					11.90	428.3	
	0.373					12.055	433.2	
	0.560					12.12	435.3	
	0.746					12.02	432.0	
	0.931					11.36	410.7	

21	0.000	11.835	426.2	11.635	419.5	11.91	428.7	270.4
	0.186					11.905	428.5	
	0.373					12.06	433.3	
	0.560					12.13	435.7	
	0.746					12.025	432.2	
	0.931					11.365	410.8	
22	0.000	11.845	426.5	11.645	419.8	11.93	429.3	271.5
	0.186					11.92	429.0	
	0.373					12.07	433.7	
	0.560					12.14	436.0	
	0.746					12.035	432.5	
	0.931					11.37	411.0	
23	0.000	11.855	426.8	11.415	412.5	12.02	432.0	382.0
	0.186					12.01	431.7	
	0.373					12.07	433.7	
	0.560					12.195	437.8	
	0.746					12.155	436.5	
	0.931					11.28	408.0	

24	0.000	11.855	426.8	11.51	415.7	12.02	432.0	382.0
	0.186					12.005	431.5	
	0.373					12.065	433.5	
	0.560					12.13	435.7	
	0.746					12.105	434.8	
	0.931					11.34	410.0	
25	0.000	11.375	411.2	10.565	385.1	11.895	428.2	158.6
	0.186					11.89	428.0	
	0.373					11.98	430.7	
	0.560					11.845	426.5	
	0.746					11.54	416.7	
	0.931					10.485	382.5	
26	0.000	11.46	414.0	10.49	382.7	12.08	434.0	158.6
	0.186					12.08	434.0	
	0.373					12.17	437.0	
	0.560					12.01	431.7	
	0.746					11.64	419.7	
	0.931					10.455	381.5	

27	0.000	11.52	416.0	10.465	381.8	12.14	436.0	158.6
	0.186					12.13	435.7	
	0.373					12.21	438.3	
	0.560					12.05	433.0	
	0.746					11.68	421.0	
	0.931					10.465	381.8	
28	0.000	11.74	423.0	10.535	384.2	12.33	442.0	197.8
	0.186					12.33	442.0	
	0.373					12.415	444.8	
	0.560					12.285	440.6	
	0.746					11.935	429.4	
	0.931					10.63	387.0	
29	0.000	11.78	424.3	10.57	385.25	12.35	442.7	197.8
	0.186					12.35	442.7	
	0.373					12.43	445.3	
	0.560					12.305	441.2	
	0.746					11.97	430.3	
	0.931					10.675	388.5	

30	0.000	11.755	423.5	10.60	386.0	12.235	439.2	237.3
	0.186					12.235	439.2	
	0.373					12.325	441.8	
	0.560					12.27	440.25	
	0.746					12.00	431.3	
	0.931					10.76	423.7	
31	0.000	11.73	422.7	10.585	385.6	12.18	437.3	237.3
	0.186					12.18	437.3	
	0.373					12.275	440.4	
	0.560					12.225	438.8	
	0.746					11.96	430.0	
	0.931					10.78	392.0	
32	0.000	11.83	426.0	10.575	385.4	12.25	439.7	317.9
	0.186					12.255	439.8	
	0.373					12.36	443.0	
	0.560					12.385	443.8	
	0.746					12.09	434.3	
	0.931					10.78	392.0	

33	0.000	11.83	426.0	10.575	385.4	12.26	440.0	317.9
	0.186					12.26	440.0	
	0.373					12.365	443.2	
	0.560					12.39	444.0	
	0.746					12.095	434.5	
	0.931					10.78	392.0	
34	0.000	11.84	426.3	10.57	385.25	12.235	439.2	360.7
	0.186					12.235	439.2	
	0.373					12.345	442.5	
	0.560					12.39	444.0	
	0.746					12.125	435.5	
	0.931					10.80	392.7	
35	0.000	11.815	425.5	10.555	384.8	12.21	438.3	360.7
	0.186					12.205	438.2	
	0.373					12.315	441.5	
	0.560					12.345	442.5	
	0.746					12.095	434.5	
	0.931					10.775	391.7	

36	0.000	11.87	427.3	10.545	384.5	12.27	440.25	414.5
	0.186					12.27	440.25	
	0.373					12.48	447.0	
	0.560					12.425	445.2	
	0.746					12.18	437.3	
	0.931					10.80	392.7	
37	0.000	11.86	427.0	10.55	384.7	12.26	440.0	414.5
	0.186					12.26	440.0	
	0.373					12.47	446.7	
	0.560					12.415	444.8	
	0.746					12.175	437.2	
	0.931					10.805	392.8	

Data Obtained for Molten Plexiglas VM 100

At a Reduced Length of 0.282 and a Heat Transfer Length of 3.56'

Test No.	Reduced Radius	Inlet Temperature		Wall Temperature		Probe Temperature		Flow Rate
		m.v.	°F	m.v.	°F	m.v.	°F	gr/min
1	0.000	12.03	432.3	12.93	461.7	12.405	444.5	193.5
	0.186					12.405	444.5	
	0.373					12.435	445.5	
	0.560					12.50	447.7	
	0.746					12.67	453.0	
	0.931					12.965	462.5	
2	0.000	12.10	434.7	13.04	465.0	12.455	446.2	193.5
	0.186					12.45	446.0	
	0.373					12.48	447.0	
	0.560					12.56	449.7	
	0.746					12.74	455.3	
	0.931					13.07	466.0	

3	0.000	12.11	435.0	13.12	467.7	12.485	447.2	193.5
	0.186					12.49	447.3	
	0.373					12.515	448.2	
	0.560					12.605	451.2	
	0.746					12.785	456.8	
	0.931					13.12	467.7	
4	0.000	12.10	434.7	13.12	467.0	12.485	447.2	193.5
	0.186					12.48	447.0	
	0.373					12.51	448.0	
	0.560					12.60	451.0	
	0.746					12.78	456.7	
	0.931					13.125	467.8	
5	0.000	11.95	429.75	13.12	467.8	12.34	442.3	241.9
	0.186					12.34	442.3	
	0.373					12.355	442.8	
	0.560					12.45	446.0	
	0.746					12.64	452.0	
	0.931					13.10	467.0	

6	0.000	11.95	429.75	13.125	467.8	12.345	442.5	241.9
	0.186					12.34	442.3	
	0.373					12.36	443.0	
	0.560					12.45	446.0	
	0.746					12.645	452.2	
	0.931					13.10	467.0	
7	0.000	11.925	429.1	13.13	468.0	12.345	442.5	241.9
	0.186					12.34	442.3	
	0.373					12.355	442.8	
	0.560					12.45	446.0	
	0.746					12.645	452.3	
	0.931					13.10	467.0	
8	0.000	11.965	430.2	13.105	467.2	12.33	442.0	316.4
	0.186					12.325	441.8	
	0.373					12.33	442.0	
	0.560					12.41	444.7	
	0.746					12.575	450.2	
	0.931					13.07	466.0	

9	0.000	11.975	430.5	13.115	467.5	12.34	442.3	316.4
	0.186					12.35	442.7	
	0.373					12.34	442.3	
	0.560					12.42	445.0	
	0.746					12.585	450.5	
	0.931					13.08	466.3	
10	0.000	11.985	430.8	13.115	467.5	12.34	442.3	316.4
	0.186					12.34	442.3	
	0.373					12.345	442.5	
	0.560					12.42	445.0	
	0.746					12.585	450.5	
	0.931					13.08	466.3	
11	0.000	12.04	432.7	13.115	467.5	12.365	443.2	413.4
	0.186					12.365	443.2	
	0.373					12.36	443.0	
	0.560					12.43	445.3	
	0.746					12.55	449.3	
	0.931					13.07	466.0	

12	0.000	12.045	432.8	13.11	467.3	12.36	443.0	413.4
	0.186					12.36	443.0	
	0.373					12.355	442.8	
	0.560					12.42	445.0	
	0.746					12.54	449.0	
	0.931					13.065	465.8	
13	0.000	12.10	434.7	13.115	467.5	12.37	443.3	413.4
	0.186					12.37	443.3	
	0.373					12.365	443.2	
	0.560					12.43	445.3	
	0.746					12.555	449.5	
	0.931					13.07	466.0	
14	0.000	12.22	438.7	13.11	467.3	12.52	448.3	477.0
	0.186					12.515	448.2	
	0.373					12.51	448.0	
	0.560					12.565	449.8	
	0.746					12.65	452.3	
	0.931					13.08	466.3	

15	0.000	12.235	439.2	13.12	467.8	12.55	449.3	477.0
	0.186					12.545	449.2	
	0.373					12.54	449.0	
	0.560					12.60	451.0	
	0.746					12.685	453.5	
	0.931					13.10	467.0	
16	0.000	12.22	438.7	13.125	467.8	12.535	448.8	477.0
	0.186					12.525	448.5	
	0.373					12.52	448.3	
	0.560					12.58	450.3	
	0.746					12.68	453.3	
	0.931					13.105	467.2	
17	0.000	11.93	429.25	12.63	451.75	12.16	436.7	180.9
	0.186					12.16	436.7	
	0.373					12.18	437.3	
	0.560					12.28	440.5	
	0.746					12.40	444.3	
	0.931					12.67	453.0	

18	0.000	11.88	427.8	12.62	451.5	12.135	435.8	180.9
	0.186					12.13	435.7	
	0.373					12.155	436.5	
	0.560					12.25	439.7	
	0.746					12.37	443.3	
	0.931					12.66	452.7	
19	0.000	11.865	427.2	12.62	451.5	12.13	435.7	180.9
	0.186					12.125	435.5	
	0.373					12.15	436.3	
	0.560					12.245	439.5	
	0.746					12.365	443.2	
	0.931					12.66	452.7	
20	0.000	11.825	425.8	12.605	451.1	11.99	431.0	270.4
	0.186					11.985	430.8	
	0.373					12.02	432.0	
	0.560					12.11	435.0	
	0.746					12.23	439.0	
	0.931					12.625	451.6	

21	0.000	11.835	426.2	12.615	451.4	11.995	431.2	270.4
	0.186					11.985	430.8	
	0.373					12.02	432.0	
	0.560					12.11	435.0	
	0.746					12.235	439.2	
	0.931					12.635	451.9	
22	0.000	11.845	426.5	12.625	451.6	12.01	431.7	271.5
	0.186					12.005	431.5	
	0.373					12.035	432.5	
	0.560					12.125	435.5	
	0.746					12.25	439.7	
	0.931					12.645	452.2	
23	0.000	11.855	426.8	12.33	442.0	12.04	432.7	382.0
	0.186					12.03	432.3	
	0.373					12.08	434.0	
	0.560					12.115	435.2	
	0.746					12.175	437.2	
	0.931					12.40	444.3	

24	0.000	11.855	426.8	12.32	441.7	12.03	432.3	382.0
	0.186					12.025	432.2	
	0.373					12.055	433.2	
	0.560					12.10	434.7	
	0.746					12.18	437.3	
	0.931					12.475	446.8	
25	0.000	11.375	411.2	11.03	400.0	11.85	426.7	158.6
	0.186					11.835	426.2	
	0.373					11.79	424.7	
	0.560					11.64	419.7	
	0.746					11.49	415.0	
	0.931					11.14	403.7	
26	0.000	11.46	414.0	10.90	396.0	12.025	432.2	158.6
	0.186					12.000	431.3	
	0.373					11.94	429.25	
	0.560					11.735	422.8	
	0.746					11.52	416.0	
	0.931					11.04	400.3	

27	0.000	11.52	416.0	10.835	393.8	12.07	433.7	158.6
	0.186					12.045	432.8	
	0.373					11.97	430.3	
	0.560					11.75	423.3	
	0.746					11.515	415.8	
	0.931					10.99	398.7	
28	0.000	11.74	423.0	10.81	393.0	12.29	440.75	197.8
	0.186					12.27	440.25	
	0.373					12.20	438.0	
	0.560					11.97	430.3	
	0.746					11.67	420.7	
	0.931					11.00	399.0	
29	0.000	11.78	424.3	10.81	393.0	12.31	441.3	197.8
	0.186					12.29	440.75	
	0.373					12.215	438.5	
	0.560					11.99	431.0	
	0.746					11.68	421.0	
	0.931					11.00	399.0	

30	0.000	11.755	423.5	10.80	392.7	12.23	439.0	237.3
	0.186					12.215	438.5	
	0.373					12.18	437.3	
	0.560					11.98	430.7	
	0.746					11.70	421.7	
	0.931					11.005	399.2	
31	0.000	11.73	422.7	10.80	392.7	12.19	437.7	237.3
	0.186					12.17	437.0	
	0.373					12.14	436.0	
	0.560					11.935	429.4	
	0.746					11.675	420.8	
	0.931					11.000	399.0	
32	0.000	11.83	426.0	10.805	392.8	12.28	440.5	317.9
	0.186					12.27	440.25	
	0.373					12.275	440.4	
	0.560					12.095	434.5	
	0.746					11.835	426.2	
	0.931					11.045	400.5	

33	0.000	11.83	426.0	10.80	392.7	12.285	440.6	317.9
	0.186					12.275	440.4	
	0.373					12.28	440.5	
	0.560					12.10	434.7	
	0.746					11.83	426.0	
	0.931					11.04	400.3	
34	0.000	11.84	426.3	10.805	392.8	12.265	440.1	360.7
	0.186					12.255	439.8	
	0.373					12.275	440.4	
	0.560					12.11	435.0	
	0.746					11.865	427.3	
	0.931					11.055	400.8	
35	0.000	11.815	425.5	10.81	393.0	12.235	439.2	360.7
	0.186					12.235	439.2	
	0.373					12.24	439.3	
	0.560					12.085	434.2	
	0.746					11.85	426.7	
	0.931					11.055	400.8	

36	0.000	11.87	427.3	10.815	393.2	12.295	440.9	414.5
	0.186					12.29	440.75	
	0.373					12.315	441.5	
	0.560					12.18	437.3	
	0.746					11.95	429.75	
	0.931					11.085	401.8	
37	0.000	11.86	427.0	10.81	393.1	12.285	440.6	414.5
	0.186					12.28	440.5	
	0.373					12.305	441.2	
	0.560					12.17	437.0	
	0.746					11.94	429.5	
	0.931					11.08	401.7	

Data Obtained for Molten Plexiglas VM 100

At a Reduced Length of 0.523 and a Heat Transfer Length of 6.600

Test No.	Reduced Radius	Inlet Temperature		Wall Temperature		Probe Temperature		Flow Rate
		m.v.	°F	m.v.	°F	m.v.	°F	gr/min
1	0.000	12.03	432.3	13.01	464.0	12.50	447.7	193.5
	0.186					12.485	447.2	
	0.373					12.515	448.2	
	0.560					12.64	452.0	
	0.746					12.825	458.2	
	0.931					13.035	464.8	
2	0.000	12.10	434.7	13.13	468.0	12.56	449.7	193.5
	0.186					12.54	449.0	
	0.373					12.57	450.0	
	0.560					12.71	454.3	
	0.746					12.91	461.0	
	0.931					13.15	468.7	

3	0.000	12.11	435.0	13.185	469.8	12.60	451.0	193.5
	0.186					12.585	450.5	
	0.373					12.615	451.4	
	0.560					12.76	456.0	
	0.746					12.95	462.25	
	0.931					13.185	469.8	
4	0.000	12.10	434.7	13.185	470.8	12.60	451.0	193.5
	0.186					12.58	450.3	
	0.373					12.61	451.25	
	0.560					12.75	455.7	
	0.746					12.95	462.25	
	0.931					13.18	469.7	
5	0.000	11.95	429.75	13.18	469.7	12.42	445.0	241.9
	0.186					12.40	444.3	
	0.373					12.43	445.3	
	0.560					12.595	450.8	
	0.746					12.83	458.3	
	0.931					13.15	468.7	

6	0.000	11.95	429.75	13.195	470.2	12.425	445.2	241.9
	0.186					12.405	444.5	
	0.373					12.435	445.5	
	0.560					12.60	451.0	
	0.746					12.84	458.7	
	0.931					13.165	469.2	
7	0.000	11.925	429.1	13.19	470.0	12.42	445.0	241.9
	0.186					12.40	444.3	
	0.373					12.43	445.3	
	0.560					12.60	451.0	
	0.746					12.835	458.5	
	0.931					13.165	469.2	
8	0.000	11.965	430.2	13.17	469.3	12.36	443.0	316.4
	0.186					12.34	442.3	
	0.373					12.36	443.0	
	0.560					12.52	448.3	
	0.746					12.76	456.0	
	0.931					13.13	468.0	

9	0.000	11.975	430.5	13.175	469.5	12.375	443.5	316.4
	0.186					12.35	442.7	
	0.373					12.37	443.3	
	0.560					12.53	448.7	
	0.746					12.77	456.3	
	0.931					13.135	468.2	
10	0.000	11.985	430.8	13.18	469.7	12.37	443.3	316.4
	0.186					12.35	442.7	
	0.373					12.37	443.3	
	0.560					12.53	448.7	
	0.746					12.77	456.3	
	0.931					13.145	468.5	
11	0.000	12.04	432.7	13.18	469.7	12.37	443.3	413.4
	0.186					12.35	442.7	
	0.373					12.355	442.8	
	0.560					12.50	447.7	
	0.746					12.72	454.7	
	0.931					13.13	468.0	

12	0.000	12.045	432.8	13.17	469.3	12.36	443.0	413.4
	0.186					12.345	442.5	
	0.373					12.35	442.7	
	0.560					12.49	447.3	
	0.746					12.71	454.3	
	0.931					13.125	467.8	
13	0.000	12.10	434.7	13.175	469.5	12.38	443.7	413.4
	0.186					12.36	443.0	
	0.373					12.365	443.2	
	0.560					12.505	447.8	
	0.746					12.725	454.8	
	0.931					13.125	467.8	
14	0.000	12.22	438.7	13.175	469.5	12.51	448.0	477.0
	0.186					12.49	447.3	
	0.373					12.485	447.2	
	0.560					12.60	451.0	
	0.746					12.785	456.8	
	0.931					13.14	468.3	

15	0.000	12.235	439.2	13.185	469.8	12.54	449.0	477.0
	0.186					12.52	448.3	
	0.373					12.515	448.2	
	0.560					12.63	451.75	
	0.746					12.84	458.7	
	0.931					13.155	468.8	
16	0.000	12.22	438.7	13.185	469.8	12.52	448.3	477.0
	0.186					12.50	447.7	
	0.373					12.50	447.7	
	0.560					12.62	451.5	
	0.746					12.81	457.8	
	0.931					13.15	467.2	
17	0.000	11.93	429.25	12.72	454.7	12.27	440.25	180.9
	0.186					12.25	439.7	
	0.373					12.27	440.25	
	0.560					12.39	444.0	
	0.746					12.565	450.9	
	0.931					12.735	455.2	

18	0.000	11.88	427.8	12.705	454.2	12.245	439.5	180.9
	0.186					12.225	438.8	
	0.373					12.245	439.5	
	0.560					12.365	443.2	
	0.746					12.545	449.2	
	0.931					12.72	454.7	
19	0.000	11.865	427.2	12.72	454.7	12.24	439.2	180.9
	0.186					12.22	438.7	
	0.373					12.245	439.5	
	0.560					12.365	443.2	
	0.746					12.55	449.3	
	0.931					12.735	455.2	
20	0.000	11.825	425.8	12.70	454.0	12.06	433.3	270.4
	0.186					12.04	432.7	
	0.373					12.07	433.7	
	0.560					12.20	438.0	
	0.746					12.42	445.0	
	0.931					12.695	453.8	

21	0.000	11.835	426.2	12.70	454.0	12.065	433.5	270.4
	0.186					12.045	432.8	
	0.373					12.07	433.7	
	0.560					12.20	438.0	
	0.746					12.42	445.0	
	0.931					12.695	453.8	
22	0.000	11.845	426.5	12.71	454.3	12.08	434.0	271.5
	0.186					12.055	433.2	
	0.373					12.08	434.0	
	0.560					12.21	438.3	
	0.746					12.43	445.3	
	0.931					12.71	454.3	
23	0.000	11.855	426.8	12.42	445.0	12.05	433.0	382.0
	0.186					12.035	432.5	
	0.373					12.05	433.0	
	0.560					12.125	435.5	
	0.746					12.275	440.4	
	0.931					12.46	446.3	

24	0.000	11.855	426.8	12.51	448.0	12.05	433.0	382.0
	0.186					12.025	432.2	
	0.373					12.04	432.7	
	0.560					12.13	435.7	
	0.746					12.30	441.0	
	0.931					12.535	448.8	
25	0.000	11.375	411.2	11.06	401.0	11.67	420.7	158.6
	0.186					11.65	420.0	
	0.373					11.61	418.75	
	0.560					11.475	414.5	
	0.746					11.35	410.3	
	0.931					11.145	403.8	
26	0.000	11.46	414.0	10.935	396.8	11.82	425.7	158.6
	0.186					11.795	424.8	
	0.373					11.74	423.0	
	0.560					11.535	416.5	
	0.746					11.34	410.0	
	0.931					11.04	400.3	

27	0.000	11.52	416.0	10.865	394.8	11.845	426.5	158.6
	0.186					11.82	425.7	
	0.373					11.76	423.7	
	0.560					11.53	416.3	
	0.746					11.32	409.3	
	0.931					10.985	398.5	
28	0.000	11.74	423.0	10.845	394.2	12.11	435.0	197.8
	0.186					12.08	434.0	
	0.373					12.005	431.5	
	0.560					11.73	422.7	
	0.746					11.435	413.2	
	0.931					11.00	399.0	
29	0.000	11.78	424.3	10.86	394.7	12.13	435.7	197.8
	0.186					12.10	434.7	
	0.373					12.02	432.0	
	0.560					11.745	423.2	
	0.746					11.45	413.7	
	0.931					11.02	399.7	

30	0.000	11.755	423.5	10.845	394.2	12.11	435.0	237.3
	0.186					12.085	434.2	
	0.373					12.025	432.2	
	0.560					11.76	423.7	
	0.746					11.47	414.3	
	0.931					11.01	399.3	
31	0.000	11.73	422.7	10.845	394.2	12.065	433.5	237.3
	0.186					12.04	432.7	
	0.373					11.98	430.7	
	0.560					11.775	424.2	
	0.746					11.45	413.7	
	0.931					11.01	399.3	
32	0.000	11.83	426.0	10.855	394.5	12.225	438.8	317.9
	0.186					12.20	438.0	
	0.373					12.165	436.8	
	0.560					11.905	428.5	
	0.746					11.595	418.4	
	0.931					11.055	400.8	

33	0.000	11.83	426.0	10.855	394.5	12.225	438.8	317.9
	0.186					12.20	438.0	
	0.373					12.165	436.8	
	0.560					11.90	428.3	
	0.746					11.60	418.5	
	0.931					11.06	401.0	
34	0.000	11.84	426.3	10.86	394.7	12.225	438.8	360.7
	0.186					12.20	438.0	
	0.373					12.18	437.3	
	0.560					11.94	429.5	
	0.746					11.645	419.8	
	0.931					11.08	401.7	
35	0.000	11.815	425.5	10.86	394.7	12.195	437.8	360.7
	0.186					12.17	437.0	
	0.373					12.145	436.2	
	0.560					11.915	428.8	
	0.746					11.645	419.8	
	0.931					11.08	401.7	

36	0.000	11.87	427.3	10.865	394.8	12.265	440.1	414.5
	0.186					12.245	439.5	
	0.373					12.23	439.0	
	0.560					12.02	432.0	
	0.746					11.72	422.3	
	0.931					11.105	402.5	
37	0.000	11.86	427.0	10.865	394.8	12.25	439.7	414.5
	0.186					12.23	439.0	
	0.373					12.215	438.5	
	0.560					12.005	431.5	
	0.746					11.715	422.2	
	0.931					11.105	402.5	

Data Obtained for Molten Plexiglas VM 100

At a Reduced Length of 0.758 and a Heat Transfer Length of 9.560'

Test No.	Reduced Radius	Inlet Temperature		Wall Temperature		Probe Temperature		Flow Rate
		m.v.	°F	m.v.	°F	m.v.	°F	gr/min
1	0.000	12.03	432.3	13.08	466.3	12.61	451.25	193.5
	0.186					12.61	451.25	
	0.373					12.46	446.3	
	0.560					12.78	456.7	
	0.746					12.915	461.2	
	0.931					13.12	467.7	
2	0.000	12.10	434.7	13.195	470.2	12.675	453.2	193.5
	0.186					12.68	453.3	
	0.373					12.53	448.7	
	0.560					12.86	459.3	
	0.746					13.01	464.0	
	0.931					13.23	471.3	

3	0.000	12.11	435.0	13.22	471.0	12.72	454.7	193.5
	0.186					12.72	454.7	
	0.373					12.575	450.2	
	0.560					12.905	460.8	
	0.746					13.045	465.2	
	0.931					13.24	471.7	
4	0.000	12.10	434.7	13.22	471.0	12.72	454.7	193.5
	0.186					12.72	454.7	
	0.373					12.565	450.8	
	0.560					12.90	460.7	
	0.746					13.04	465.0	
	0.931					13.24	471.7	
5	0.000	11.95	429.75	13.22	471.0	12.53	448.7	241.9
	0.186					12.53	448.7	
	0.373					12.39	444.0	
	0.560					12.755	455.5	
	0.746					12.93	461.7	
	0.931					13.20	470.3	

6	0.000	11.95	429.75	13.24	471.7	12.54	449.0	241.9
	0.186					12.54	449.0	
	0.373					12.395	444.2	
	0.560					12.77	456.3	
	0.746					12.95	462.25	
	0.931					13.23	471.3	
7	0.000	11.925	429.1	13.235	471.5	12.53	448.7	241.9
	0.186					12.53	448.7	
	0.373					12.39	444.0	
	0.560					12.76	456.0	
	0.746					12.94	462.0	
	0.931					13.22	471.0	
8	0.000	11.965	430.2	13.205	470.8	12.43	445.3	316.4
	0.186					12.43	445.3	
	0.373					12.28	440.5	
	0.560					12.66	452.7	
	0.746					12.85	459.0	
	0.931					13.17	469.3	

9	0.000	11.975	430.5	13.215	470.8	12.435	445.5	316.4
	0.186					12.435	445.5	
	0.373					12.29	440.75	
	0.560					12.67	453.0	
	0.746					12.865	459.5	
	0.931					13.185	469.8	
10	0.000	11.985	430.8	13.22	471.0	12.44	445.7	316.4
	0.186					12.44	445.7	
	0.373					12.295	440.8	
	0.560					12.67	453.0	
	0.746					12.87	459.7	
	0.931					13.185	469.8	
11	0.000	12.04	432.7	13.21	470.8	12.395	444.2	413.4
	0.186					12.395	444.2	
	0.373					12.24	439.3	
	0.560					12.61	451.25	
	0.746					12.80	457.3	
	0.931					13.16	469.0	

12	0.000	12.045	432.8	13.21	470.7	12.385	443.8	413.4
	0.186					12.385	443.8	
	0.373					12.235	439.2	
	0.560					12.61	451.3	
	0.746					12.805	457.8	
	0.931					13.16	469.0	
13	0.000	12.10	434.7	13.22	471.0	12.40	444.3	413.4
	0.186					12.40	444.3	
	0.373					12.24	439.3	
	0.560					12.62	451.7	
	0.746					12.81	457.7	
	0.931					13.175	469.5	
14	0.000	12.22	438.7	13.21	470.7	12.51	448.0	477.0
	0.186					12.51	448.0	
	0.373					12.54	449.0	
	0.560					12.70	454.0	
	0.746					12.865	459.5	
	0.931					13.175	469.5	

15	0.000	12.235	439.2	13.22	471.0	12.54	449.0	477.0
	0.186					12.54	449.0	
	0.373					12.32	443.3	
	0.560					12.72	454.7	
	0.746					12.885	460.2	
	0.931					13.19	470.0	
16	0.000	12.22	438.7	13.23	471.3	12.525	448.5	477.0
	0.186					12.525	448.5	
	0.373					12.355	442.8	
	0.560					12.71	454.3	
	0.746					12.875	459.7	
	0.931					13.20	470.3	
17	0.000	11.93	429.25	12.73	455.0	12.38	443.7	180.9
	0.186					12.38	443.7	
	0.373					12.22	438.7	
	0.560					12.515	448.2	
	0.746					12.62	451.5	
	0.931					12.775	456.5	

18	0.000	11.88	427.8	12.72	454.7	12.35	442.7	180.9
	0.186					12.35	442.7	
	0.373					12.185	437.5	
	0.560					12.49	447.3	
	0.746					12.60	451.0	
	0.931					12.76	456.0	
19	0.000	11.865	427.2	12.725	454.8	12.35	442.7	180.9
	0.186					12.35	442.7	
	0.373					12.19	437.7	
	0.560					12.49	447.3	
	0.746					12.605	451.2	
	0.931					12.765	456.2	
20	0.000	11.825	425.8	12.705	454.2	12.14	436.0	270.4
	0.186					12.14	436.0	
	0.373					11.99	431.0	
	0.560					12.32	441.7	
	0.746					12.475	446.8	
	0.931					12.72	454.7	

21	0.000	11.835	426.2	12.72	454.7	12.145	436.2	270.4
	0.186					12.145	436.2	
	0.373					11.985	430.8	
	0.560					12.325	441.8	
	0.746					12.48	447.0	
	0.931					12.73	455.0	
22	0.000	11.845	426.5	12.715	454.5	12.15	436.3	271.5
	0.186					12.15	436.3	
	0.373					12.00	431.3	
	0.560					12.335	442.2	
	0.746					12.485	447.2	
	0.931					12.725	454.8	
23	0.000	11.855	426.8	12.465	446.5	12.065	433.5	382.0
	0.186					12.065	433.5	
	0.373					11.79	424.7	
	0.560					12.20	438.0	
	0.746					12.325	441.8	
	0.931					12.52	448.3	

24	0.000	11.855	426.8	12.555	449.5	12.06	433.3	382.0
	0.186					12.06	433.3	
	0.373					11.785	424.5	
	0.560					12.215	438.5	
	0.746					12.355	442.8	
	0.931					12.59	450.7	
25	0.000	11.375	411.2	11.055	400.8	11.50	415.3	158.6
	0.186					11.50	415.3	
	0.373					11.185	405.2	
	0.560					11.41	412.3	
	0.746					11.315	409.2	
	0.931					11.18	405.0	
26	0.000	11.46	414.0	10.93	396.75	11.60	418.5	158.6
	0.186					11.60	418.5	
	0.373					11.265	407.6	
	0.560					11.435	413.2	
	0.746					11.285	408.2	
	0.931					11.08	401.7	

27	0.000	11.61	418.75	10.89	395.7	11.61	418.75	158.6
	0.186					11.605	418.6	
	0.373					11.27	407.75	
	0.560					11.42	412.7	
	0.746					11.265	407.8	
	0.931					11.055	400.8	
28	0.000	11.74	423.0	10.87	395.0	11.875	427.5	197.8
	0.186					11.865	427.2	
	0.373					11.51	415.7	
	0.560					11.61	418.7	
	0.746					11.38	411.3	
	0.931					11.08	401.7	
29	0.000	11.78	424.3	10.87	395.0	11.89	428.0	197.8
	0.186					11.89	428.0	
	0.373					11.53	416.3	
	0.560					11.63	419.3	
	0.746					11.40	412.0	
	0.931					11.08	401.7	

30	0.000	11.755	423.5	10.87	395.0	11.92	429.0	237.3
	0.186					11.915	428.8	
	0.373					11.565	417.5	
	0.560					11.67	420.7	
	0.746					11.43	413.0	
	0.931					11.10	402.3	
31	0.000	11.73	422.7	10.865	394.8	11.88	427.7	237.3
	0.186					11.875	427.5	
	0.373					11.58	418.0	
	0.560					11.64	419.7	
	0.746					11.41	412.3	
	0.931					11.095	402:2	
32	0.000	11.83	426.0	10.87	395.0	12.095	434.5	317.9
	0.186					12.09	434.3	
	0.373					11.755	423.5	
	0.560					11.835	426.2	
	0.746					11.57	417.7	
	0.931					11.15	404.0	

33	0.000	11.83	426.0	10.87	395.0	12.095	434.5	317.9
	0.186					12.09	434.3	
	0.373					11.75	423.3	
	0.560					11.84	426.3	
	0.746					11.57	417.7	
	0.931					11.15	404.0	
34	0.000	11.84	426.3	10.87	395.0	12.115	435.2	360.7
	0.186					12.11	435.0	
	0.373					11.79	424.7	
	0.560					11.88	427.7	
	0.746					11.615	418.9	
	0.931					11.17	404.7	
35	0.000	11.815	425.5	10.92	396.5	11.99	431.0	360.7
	0.186					11.975	430.5	
	0.373					11.99	431.0	
	0.560					11.78	424.3	
	0.746					11.565	417.5	
	0.931					11.085	401.8	

36	0.000	11.87	427.3	10.875	395.2	12.17	437.0	414.5
	0.186					12.17	437.0	
	0.373					11.855	426.8	
	0.560					11.97	430.3	
	0.746					11.70	421.7	
	0.931					11.20	405.7	
37	0.000	11.86	427.0	10.875	395.2	12.165	436.8	414.5
	0.186					12.16	436.7	
	0.373					11.84	426.3	
	0.560					11.965	430.2	
	0.746					11.695	421.5	
	0.931					11.20	405.7	

Data Obtained for Molten Plexiglas VM 100.

At a Reduced Length of 1.000 and a Heat Transfer Length of 12.600'

Test No.	Reduced Radius	Inlet Temperature		Wall Temperature		Probe Temperature		Flow Rate
		m.v.	°F	m.v.	°F	m.v.	°F	gr/min
1	0.000	12.03	432.3	13.165	469.2	12.77	456.3	193.5
	0.186					12.77	456.3	
	0.373					12.82	458.0	
	0.560					12.94	462.0	
	0.746					12.99	463.3	
	0.931					13.15	468.7	
2	0.000	12.10	434.7	13.28	473.0	12.85	459.0	193.5
	0.186					12.85	459.0	
	0.373					12.905	460.8	
	0.560					13.035	464.8	
	0.746					13.095	466.8	
	0.931					13.26	472.3	

3	0.000	12.11	435.0	13.30	473.7	12.90	460.7	193.5
	0.186					12.90	460.7	
	0.373					12.955	462.4	
	0.560					13.075	466.2	
	0.746					13.12	467.7	
	0.931					13.27	472.7	
4	0.000	12.10	434.7	13.29	473.3	12.89	460.3	193.5
	0.186					12.89	460.3	
	0.373					12.945	462.2	
	0.560					13.07	466.0	
	0.746					13.115	467.5	
	0.931					13.255	472.2	
5	0.000	11.95	429.75	13.30	473.7	12.72	454.7	241.9
	0.186					12.72	454.7	
	0.373					12.785	456.8	
	0.560					12.935	461.8	
	0.746					13.02	464.3	
	0.931					13.24	471.7	

6	0.000	11.95	429.75	13.315	474.2	12.73	455.0	241.9
	0.186					12.73	455.0	
	0.373					12.80	457.3	
	0.560					12.95	462.25	
	0.746					13.04	465.0	
	0.931					13.255	472.2	
7	0.000	11.925	429.1	13.305	473.8	12.725	454.8	241.9
	0.186					12.725	454.8	
	0.373					12.79	457.0	
	0.560					12.945	462.1	
	0.746					13.03	464.7	
	0.931					13.245	471.8	
8	0.000	11.965	430.2	13.28	473.0	12.59	450.7	316.4
	0.186					12.59	450.7	
	0.373					12.66	452.7	
	0.560					12.83	458.3	
	0.746					12.93	461.7	
	0.931					13.21	470.7	

9	0.000	11.975	430.5	13.29	473.3	12.60	451.0	316.4
	0.186					12.60	451.0	
	0.373					12.67	453.0	
	0.560					12.84	458.7	
	0.746					12.945	462.1	
	0.931					13.22	471.0	
10	0.000	11.985	430.8	13.29	473.3	12.60	451.0	316.4
	0.186					12.60	451.0	
	0.373					12.67	453.0	
	0.560					12.84	458.7	
	0.746					12.945	462.1	
	0.931					13.22	471.0	
11	0.000	12.04	432.7	13.28	473.0	12.52	448.3	413.4
	0.186					12.52	448.3	
	0.373					12.585	450.5	
	0.560					12.77	456.3	
	0.746					12.88	460.0	
	0.931					13.195	470.3	

12	0.000	12.045	432.8	13.285	473.2	12.52	448.3	413.4
	0.186					12.52	448.3	
	0.373					12.585	450.5	
	0.560					12.765	456.2	
	0.746					12.875	456.8	
	0.931					13.20	470.3	
13	0.000	12.10	434.7	13.29	473.3	12.53	448.7	413.4
	0.186					12.53	448.7	
	0.373					12.59	450.7	
	0.560					12.775	456.5	
	0.746					12.89	460.3	
	0.931					13.205	470.5	
14	0.000	12.22	438.7	13.285	473.2	12.62	451.5	477.0
	0.186					12.62	451.5	
	0.373					12.665	452.8	
	0.560					12.83	458.3	
	0.746					12.925	461.5	
	0.931					13.21	470.7	

15	0.000	12.235	439.2	13.30	473.7	12.65	452.2	477.0
	0.186					12.65	452.2	
	0.373					12.69	453.7	
	0.560					12.855	459.3	
	0.746					12.94	462.0	
	0.931					13.225	471.2	
16	0.000	12.22	438.7	13.30	473.7	12.63	451.75	477.0
	0.186					12.63	451.75	
	0.373					12.68	453.3	
	0.560					12.845	458.8	
	0.746					12.94	462.0	
	0.931					13.225	471.3	
17	0.000	11.93	429.25	12.73	455.0	12.51	448.0	180.9
	0.186					12.565	450.9	
	0.373					12.665	452.8	
	0.560					12.685	453.5	
	0.746					12.79	457.0	
	0.931					12.81	457.8	

18	0.000	11.88	427.8	12.80	457.3	12.485	447.2	180.9
	0.186					12.48	447.0	
	0.373					12.54	449.0	
	0.560					12.64	452.0	
	0.746					12.67	453.0	
	0.931					12.77	456.3	
19	0.000	11.865	427.2	12.805	457.5	12.485	447.2	180.9
	0.186					12.48	447.0	
	0.373					12.54	449.0	
	0.560					12.645	452.2	
	0.746					12.67	453.0	
	0.931					12.78	456.7	
20	0.000	11.825	425.8	12.79	457.0	12.27	440.25	270.4
	0.186					12.27	440.25	
	0.373					12.34	442.3	
	0.560					12.48	447.0	
	0.746					12.545	449.1	
	0.931					12.745	455.5	

21	0.000	11.835	426.2	12.79	457.0	12.27	440.25	270.4
	0.186					12.27	440.25	
	0.373					12.345	442.5	
	0.560					12.48	447.0	
	0.746					12.55	449.3	
	0.931					12.79	455.3	
22	0.000	11.845	426.5	12.795	457.2	12.28	440.5	271.5
	0.186					12.275	440.4	
	0.373					12.345	442.5	
	0.560					12.48	447.0	
	0.746					12.55	449.3	
	0.931					12.75	455.7	
23	0.000	11.855	426.8	12.545	449.2	12.155	436.5	382.0
	0.186					12.135	435.8	
	0.373					12.205	438.2	
	0.560					12.32	441.7	
	0.746					12.375	443.5	
	0.931					12.54	449.0	

24	0.000	11.855	426.8	12.63	451.75	12.155	436.5	382.0
	0.186					12.15	436.3	
	0.373					12.21	438.3	
	0.560					12.34	442.3	
	0.746					12.41	444.7	
	0.931					12.61	451.25	
25	0.000	11.375	411.2	11.11	402.7	11.43	413.0	158.6
	0.186					11.42	412.7	
	0.373					11.41	412.3	
	0.560					11.38	411.3	
	0.746					11.27	407.75	
	0.931					11.125	403.2	
26	0.000	11.46	414.0	10.975	398.2	11.48	414.7	158.6
	0.186					11.47	414.3	
	0.373					11.45	413.7	
	0.560					11.37	411.0	
	0.746					11.225	406.5	
	0.931					11.02	399.7	

27	0.000	11.52	416.0	10.94	397.0	11.48	414.7	158.6
	0.186					11.47	414.3	
	0.373					11.445	413.5	
	0.560					11.36	410.7	
	0.746					11.21	406.0	
	0.931					11.00	399.0	
28	0.000	11.74	423.0	10.92	396.5	11.715	422.2	197.8
	0.186					11.70	421.7	
	0.373					11.665	420.5	
	0.560					11.525	416.2	
	0.746					11.325	409.5	
	0.931					11.01	399.3	
29	0.000	11.78	424.3	10.925	396.6	11.73	422.7	197.8
	0.186					11.72	422.3	
	0.373					11.675	420.8	
	0.560					11.53	416.3	
	0.746					11.325	409.5	
	0.931					11.02	399.7	

30	0.000	11.755	423.5	10.91	396.25	11.795	424.8	237.3
	0.186					11.78	424.3	
	0.373					11.74	423.0	
	0.560					11.59	418.25	
	0.746					11.375	411.2	
	0.931					11.025	399.8	
31	0.000	11.73	422.7	10.92	396.5	11.755	423.5	237.3
	0.186					11.745	423.2	
	0.373					11.71	422.0	
	0.560					11.56	417.3	
	0.746					11.355	410.5	
	0.931					11.03	400.0	
32	0.000	11.83	426.0	10.915	396.4	11.98	430.7	317.9
	0.186					11.97	430.3	
	0.373					11.965	430.2	
	0.560					11.75	423.3	
	0.746					11.52	416.0	
	0.931					11.07	401.3	

33	0.000	11.83	426.0	10.915	396.4	11.99	431.0	317.9
	0.186					11.975	430.5	
	0.373					11.97	430.3	
	0.560					11.755	423.5	
	0.746					11.52	416.0	
	0.931					11.07	401.3	
34	0.000	11.84	426.3	10.915	396.4	12.015	431.8	360.7
	0.186					12.00	431.3	
	0.373					12.02	432.0	
	0.560					11.80	425.0	
	0.746					11.57	417.7	
	0.931					11.085	401.8	
35	0.000	11.815	425.5	10.92	396.5	11.99	431.0	360.7
	0.186					11.975	430.5	
	0.373					11.99	431.0	
	0.560					11.78	424.3	
	0.746					11.565	417.5	
	0.931					11.085	401.8	

36	0.000	11.87	427.3	10.92	396.5	12.08	434.0	414.5
	0.186					12.07	433.7	
	0.373					12.11	435.0	
	0.560					11.89	428.0	
	0.746					11.67	420.7	
	0.931					11.10	402.3	
37	0.000	11.86	427.0	10.92	396.5	12.075	433.8	414.5
	0.186					12.06	433.3	
	0.373					12.10	434.7	
	0.560					11.88	427.7	
	0.746					11.665	420.5	
	0.931					11.11	402.7	

TABLE XII

Reduced Temperature Obtained for Molten Plexiglas VM 100

Test Number	Reduced Radius	Reduced Temperature$_1$	Reduced Temperature$_2$	Flow Rate	Reduced Length
	Dimensionless	Dimensionless	Dimensionless	gr/min	Dimensionless
	r/R	$\frac{T - T_1}{T_W - T_1}$	$\frac{T - T_W}{T_1 - T_W}$		z/L
1	0.000	0.415	0.585	193.5	0.282
	0.186	0.415	0.585		
	0.373	0.449	0.551		
	0.560	0.524	0.476		
	0.746	0.704	0.296		
	0.931	1.010	-0.010		
	1.000	1.000	0.000		
2	0.000	0.380	0.620	193.5	0.282
	0.186	0.373	0.627		
	0.373	0.406	0.594		
	0.560	0.495	0.505		
	0.746	0.680	0.320		
	0.931	1.033	-0.033		
	1.000	1.000	0.000		
3	0.000	0.373	0.627	193.5	0.282
	0.186	0.376	0.624		
	0.373	0.404	0.596		
	0.560	0.495	0.505		
	0.746	0.667	0.333		
	0.931	1.000	0.000		
	1.000	1.000	0.000		
4	0.000	0.387	0.613	193.5	0.282
	0.186	0.381	0.619		
	0.373	0.412	0.588		
	0.560	0.501	0.499		
	0.746	0.681	0.319		
	0.931	1.025	-0.025		
	1.000	1.000	0.000		

5	0.000	0.330	0.670	241.9	0.282
	0.186	0.330	0.670		
	0.373	0.343	0.657		
	0.560	0.427	0.573		
	0.746	0.585	0.415		
	0.931	0.979	0.021		
	1.000	1.000	0.000		
6	0.000	0.335	0.665	241.9	0.282
	0.186	0.330	0.670		
	0.373	0.348	0.652		
	0.560	0.427	0.573		
	0.746	0.590	0.410		
	0.931	0.979	0.021		
	1.000	1.000	0.000		
7	0.000	0.344	0.656	241.9	0.282
	0.186	0.339	0.661		
	0.373	0.352	0.648		
	0.560	0.434	0.566		
	0.746	0.596	0.404		
	0.931	0.974	0.026		
	1.000	1.000	0.000		
8	0.000	0.319	0.681	316.4	0.282
	0.186	0.314	0.686		
	0.373	0.319	0.681		
	0.560	0.392	0.608		
	0.746	0.541	0.459		
	0.931	0.968	0.032		
	1.000	1.000	0.000		
9	0.000	0.319	0.681	316.4	0.282
	0.186	0.330	0.670		
	0.373	0.319	0.681		
	0.560	0.392	0.608		
	0.746	0.541	0.459		
	0.931	0.968	0.032		
	1.000	1.000	0.000		
10	0.000	0.313	0.687	316.4	0.282
	0.186	0.313	0.687		
	0.373	0.319	0.681		
	0.560	0.387	0.613		
	0.746	0.537	0.463		
	0.931	0.967	0.033		
	1.000	1.000	0.000		

11	0.000	0.302	0.698	413.4	0.282
	0.186	0.302	0.698		
	0.373	0.296	0.704		
	0.560	0.362	0.638		
	0.746	0.477	0.523		
	0.931	0.957	0.043		
	1.000	1.000	0.000		
12	0.000	0.296	0.704	413.4	0.282
	0.186	0.296	0.704		
	0.373	0.290	0.710		
	0.560	0.354	0.646		
	0.746	0.470	0.530		
	0.931	0.957	0.043		
	1.000	1.000	0.000		
13	0.000	0.262	0.738	413.4	0.282
	0.186	0.262	0.738		
	0.373	0.259	0.741		
	0.560	0.323	0.677		
	0.746	0.451	0.549		
	0.931	0.954	0.046		
	1.000	1.000	0.000		
14	0.000	0.336	0.664	477.0	0.282
	0.186	0.332	0.668		
	0.373	0.325	0.675		
	0.560	0.388	0.612		
	0.746	0.476	0.524		
	0.931	0.965	0.035		
	1.000	1.000	0.000		
15	0.000	0.353	0.647	477.0	0.282
	0.186	0.350	0.650		
	0.373	0.343	0.657		
	0.560	0.413	0.587		
	0.746	0.500	0.500		
	0.931	0.972	0.028		
	1.000	1.000	0.000		
16	0.000	0.347	0.653	477.0	0.282
	0.186	0.337	0.663		
	0.373	0.330	0.670		
	0.560	0.399	0.601		
	0.746	0.502	0.498		
	0.931	0.979	0.021		
	1.000	1.000	0.000		

17	0.000	0.331	0.669	180.9	0.282
	0.186	0.331	0.669		
	0.373	0.358	0.642		
	0.560	0.500	0.500		
	0.746	0.669	0.331		
	0.931	1.056	-0.056		
	1.000	1.000	0.000		
18	0.000	0.338	0.662	180.9	0.282
	0.186	0.333	0.667		
	0.373	0.367	0.633		
	0.560	0.502	0.498		
	0.746	0.654	0.346		
	0.931	1.051	-0.051		
	1.000	1.000	0.000		
19	0.000	0.350	0.650	180.9	0.282
	0.186	0.342	0.658		
	0.373	0.374	0.626		
	0.560	0.506	0.494		
	0.746	0.658	0.342		
	0.931	1.049	-0.049		
	1.000	1.000	0.000		
20	0.000	0.206	0.794	270.4	0.282
	0.186	0.198	0.812		
	0.373	0.245	0.755		
	0.560	0.364	0.636		
	0.746	0.522	0.478		
	0.931	1.020	-0.020		
	1.000	1.000	0.000		
21	0.000	0.198	0.802	270.4	0.282
	0.186	0.183	0.817		
	0.373	0.230	0.770		
	0.560	0.349	0.651		
	0.746	0.516	0.484		
	0.931	1.020	-0.020		
	1.000	1.000	0.000		
22	0.000	0.207	0.793	271.5	0.282
	0.186	0.199	0.811		
	0.373	0.239	0.761		
	0.560	0.359	0.641		
	0.746	0.526	0.474		
	0.931	1.024	-0.024		
	1.000	1.000	0.000		

23	0.000	0.388	0.622	382.0	0.282
	0.186	0.362	0.638		
	0.373	0.474	0.526		
	0.560	0.553	0.447		
	0.746	0.684	0.316		
	0.931	1.151	-0.151		
	1.000	1.000	0.000		
24	0.000	0.369	0.631	382.0	0.282
	0.186	0.369	0.631		
	0.373	0.430	0.570		
	0.560	0.530	0.470		
	0.746	0.705	0.295		
	0.931	1.342	-0.342		
	1.000	1.000	0.000		
25	0.000	-1.384	2.384	158.6	0.282
	0.186	-1.339	2.339		
	0.373	-1.205	2.205		
	0.560	-0.7589	1.7589		
	0.746	-0.339	1.339		
	0.931	0.670	0.330		
	1.000	1.000	0.000		
26	0.000	-1.011	2.011	158.6	0.282
	0.186	-0.961	1.961		
	0.373	-0.847	1.847		
	0.560	-0.489	1.489		
	0.746	-0.111	1.111		
	0.931	0.761	0.239		
	1.000	1.000	0.000		
27	0.000	-0.797	1.797	158.6	0.282
	0.186	-0.757	1.757		
	0.373	-0.644	1.644		
	0.560	-0.329	1.329		
	0.746	0.009	0.991		
	0.931	0.779	0.221		
	1.000	1.000	0.000		
28	0.000	-0.592	1.592	197.8	0.282
	0.186	-0.575	1.575		
	0.373	-0.500	1.500		
	0.560	-0.243	1.243		
	0.746	0.077	0.923		
	0.931	0.800	0.200		
	1.000	1.000	0.000		

29	0.000	-0.543	1.543	197.8	0.282
	0.186	-0.526	1.526		
	0.373	-0.454	1.454		
	0.560	-0.214	1.214		
	0.746	0.105	0.895		
	0.931	0.808	0.192		
	1.000	1.000	0.000		
30	0.000	-0.503	1.503	237.3	0.282
	0.186	-0.487	1.487		
	0.373	-0.448	1.448		
	0.560	-0.234	1.234		
	0.746	0.058	0.942		
	0.931	0.789	0.211		
	1.000	1.000	0.000		
31	0.000	-0.50	1.50	237.3	0.282
	0.186	-0.477	1.477		
	0.373	-0.443	1.443		
	0.560	-0.223	1.223		
	0.746	0.063	0.937		
	0.931	0.790	0.210		
	1.000	1.000	0.000		
32	0.000	-0.437	1.437	317.9	0.282
	0.186	-0.429	1.429		
	0.373	-0.434	1.434		
	0.560	-0.256	1.256		
	0.746	-0.006	1.006		
	0.931	0.768	0.232		
	1.000	1.000	0.000		
33	0.000	-0.438	1.438	317.9	0.282
	0.186	-0.432	1.432		
	0.373	-0.435	1.435		
	0.560	-0.261	1.261		
	0.746	0.000	0.000		
	0.931	0.772	0.228		
	1.000	1.000	0.000		
34	0.000	-0.412	1.412	360.7	0.282
	0.186	-0.403	1.403		
	0.373	-0.421	1.421		
	0.560	-0.269	1.269		
	0.746	-0.030	1.030		
	0.931	0.761	0.239		
	1.000	1.000	0.000		

35	0.000	-0.422	1.422	360.7	0.282
	0.186	-0.422	1.422		
	0.373	-0.425	1.425		
	0.560	-0.268	1.268		
	0.746	-0.037	1.037		
	0.931	0.760	0.240		
	1.000	1.000	0.000		
36	0.000	-0.399	1.399	414.5	0.282
	0.186	-0.394	1.394		
	0.373	-0.416	1.416		
	0.560	-0.293	1.293		
	0.746	-0.072	1.072		
	0.931	0.748	0.252		
	1.000	1.000	0.000		
37	0.000	-0.401	1.401	414.5	0.282
	0.186	-0.398	1.398		
	0.373	-0.419	1.419		
	0.560	-0.295	1.295		
	0.746	-0.074	1.074		
	0.931	0.746	0.254		
	1.000	1.000	0.000		

Reduced Temperature Obtained for Molten Plexiglas VM 100

Test Number	Reduced Radius	Reduced Temperature$_1$	Reduced Temperature$_2$	Flow Rate	Reduced Length
	Dimensionless	Dimensionless	Dimensionless	gr/min	Dimensionless
	r/R	$\frac{T - T_1}{T_w - T_1}$	$\frac{T - T_w}{T_1 - T_w}$		z/L
1	0.000	0.486	0.514	193.5	0.523
	0.186	0.470	0.530		
	0.373	0.502	0.498		
	0.560	0.621	0.379		
	0.746	0.817	0.183		
	0.931	1.025	-0.025		
	1.000	1.000	0.000		
2	0.000	0.450	0.550	193.5	0.523
	0.186	0.429	0.571		
	0.373	0.459	0.541		
	0.560	0.610	0.390		
	0.746	0.790	0.210		
	0.931	1.021	-0.021		
	1.000	1.000	0.000		
3	0.000	0.460	0.540	193.5	0.523
	0.186	0.445	0.555		
	0.373	0.471	0.529		
	0.560	0.603	0.397		
	0.746	0.783	0.217		
	0.931	1.000	0.000		
	1.000	1.000	0.000		
4	0.000	0.452	0.548	193.5	0.523
	0.186	0.432	0.568		
	0.373	0.458	0.542		
	0.560	0.582	0.418		
	0.746	0.763	0.237		
	0.931	0.970	0.030		
	1.000	1.000	0.000		

5	0.000	0.382	0.618	241.9	0.523
	0.186	0.364	0.636		
	0.373	0.389	0.611		
	0.560	0.527	0.473		
	0.746	0.715	0.285		
	0.931	0.975	0.025		
	1.000	1.000	0.000		
6	0.000	0.382	0.618	241.9	0.523
	0.186	0.365	0.635		
	0.373	0.389	0.611		
	0.560	0.525	0.475		
	0.746	0.716	0.284		
	0.931	0.975	0.025		
	1.000	1.000	0.000		
7	0.000	0.389	0.611	241.9	0.523
	0.186	0.372	0.628		
	0.373	0.396	0.604		
	0.560	0.535	0.465		
	0.746	0.719	0.281		
	0.931	0.980	0.020		
8	0.000	0.327	0.673	316.4	0.523
	0.186	0.309	0.691		
	0.373	0.327	0.673		
	0.560	0.463	0.537		
	0.746	0.660	0.340		
	0.931	0.967	0.033		
	1.000	1.000	0.000		
9	0.000	0.333	0.667	316.4	0.523
	0.186	0.313	0.687		
	0.373	0.328	0.672		
	0.560	0.467	0.533		
	0.746	0.662	0.338		
	0.931	0.967	0.033		
	1.000	1.000	0.000		
10	0.000	0.321	0.679	316.4	0.523
	0.186	0.306	0.694		
	0.373	0.321	0.679		
	0.560	0.460	0.540		
	0.746	0.656	0.344		
	0.931	0.969	0.031		
	1.000	1.000	0.000		

0.286	0.714	413.4	0.523
0.270	0.730		
0.273	0.727		
0.405	0.595		
0.595	0.405		
0.954	0.046		
1.000	0.000		
0.279	0.721	413.4	0.523
0.266	0.734		
0.271	0.729		
0.397	0.603		
0.589	0.411		
0.959	0.041		
1.000	0.000		
0.259	0.741	413.4	0.523
0.239	0.761		
0.244	0.756		
0.376	0.624		
0.578	0.422		
0.951	0.049		
1.000	0.000		
.302	0.698	477.0	0.523
.279	0.721		
.276	0.724		
.399	0.601		
.588	0.412		
.961	0.039		
1.000	0.000		
.320	0.680	477.0	0.523
.297	0.703		
.294	0.706		
.410	0.590		
.637	0.363		
.967	0.033		
1.000	0.000		
.309	0.691	477.0	0.523
.289	0.711		
.289	0.711		
.412	0.588		
.614	0.386		
.916	0.084		
1.000	0.000		

17	0.000	0.432	0.568	180.9	0.523
	0.186	0.410	0.590		
	0.373	0.432	0.568		
	0.560	0.580	0.420		
	0.746	0.851	0.149		
	0.931	1.020	-0.020		
	1.000	1.000	0.000		
18	0.000	0.443	0.557	180.9	0.523
	0.186	0.417	0.583		
	0.373	0.443	0.557		
	0.560	0.583	0.417		
	0.746	0.811	0.199		
	0.931	1.019	-0.019		
	1.000	1.000	0.000		
19	0.000	0.441	0.559	180.9	0.523
	0.186	0.423	0.577		
	0.373	0.452	0.548		
	0.560	0.588	0.422		
	0.746	0.813	0.187		
	0.931	1.029	-0.029		
	1.000	1.000	0.000		
20	0.000	0.266	0.734	270.4	0.523
	0.186	0.245	0.755		
	0.373	0.280	0.720		
	0.560	0.433	0.567		
	0.746	0.681	0.319		
	0.931	0.993	0.007		
	1.000	1.000	0.000		
21	0.000	0.263	0.737	270.4	0.523
	0.186	0.237	0.763		
	0.373	0.270	0.730		
	0.560	0.424	0.576		
	0.746	0.676	0.324		
	0.931	0.993	0.007		
	1.000	1.000	0.000		
22	0.000	0.270	0.730	271.5	0.523
	0.186	0.241	0.759		
	0.373	0.270	0.730		
	0.560	0.424	0.576		
	0.746	0.676	0.324		
	0.931	1.000	0.000		
	1.000	1.000	0.000		

23	0.000	0.341	0.659	382.0	0.523
	0.186	0.313	0.687		
	0.373	0.341	0.659		
	0.560	0.478	0.522		
	0.746	0.747	0.253		
	0.931	1.071	-0.071		
	1.000	1.000	0.000		
24	0.000	0.292	0.708	382.0	0.523
	0.186	0.254	0.746		
	0.373	0.278	0.722		
	0.560	0.420	0.580		
	0.746	0.670	0.330		
	0.931	1.038	-0.038		
	1.000	1.000	0.000		
25	0.000	-0.931	1.931	158.6	0.523
	0.186	-0.931	1.931		
	0.373	-0.740	1.740		
	0.560	-0.324	1.324		
	0.746	0.088	0.912		
	0.931	0.725	0.275		
	1.000	1.000	0.000		
26	0.000	-0.680	1.680	158.6	0.523
	0.186	-0.628	1.628		
	0.373	-0.523	1.523		
	0.560	-0.145	1.145		
	0.746	0.233	0.767		
	0.931	0.797	0.203		
	1.000	1.000	0.000		
27	0.000	-0.495	1.495	158.6	0.523
	0.186	-0.458	1.458		
	0.373	-0.363	1.363		
	0.560	-0.142	1.142		
	0.746	0.316	0.684		
	0.931	0.825	0.175		
	1.000	1.000	0.000		
28	0.000	-0.417	1.417	197.8	0.523
	0.186	-0.382	1.382		
	0.373	-0.295	1.295		
	0.560	0.010	0.990		
	0.746	0.340	0.660		
	0.931	0.833	0.167		
	1.000	1.000	0.000		

29	0.000	-0.385	1.385	197.8	0.523
	0.186	-0.351	1.351		
	0.373	-0.260	1.260		
	0.560	0.037	0.963		
	0.746	0.358	0.642		
	0.931	0.831	0.169		
	1.000	1.000	0.000		
30	0.000	-0.392	1.392	237.3	0.523
	0.186	-0.365	1.365		
	0.373	-0.297	1.297		
	0.560	-0.007	1.007		
	0.746	0.314	0.686		
	0.931	0.826	0.174		
	1.000	1.000	0.000		
31	0.000	-0.379	1.379	237.3	0.523
	0.186	-0.351	1.351		
	0.373	-0.281	1.281		
	0.560	-0.053	1.053		
	0.746	0.316	0.684		
	0.931	0.821	0.179		
	1.000	1.000	0.000		
32	0.000	-0.406	1.406	317.9	0.523
	0.186	-0.381	1.381		
	0.373	-0.343	1.343		
	0.560	-0.079	1.079		
	0.746	0.241	0.759		
	0.931	0.800	0.200		
	1.000	1.000	0.000		
33	0.000	-0.406	1.406	317.9	0.523
	0.186	-0.381	1.381		
	0.373	-0.343	1.343		
	0.560	-0.073	1.073		
	0.746	0.238	0.762		
	0.931	0.794	0.206		
	1.000	1.000	0.000		
34	0.000	-0.396	1.396	360.7	0.523
	0.186	-0.370	1.370		
	0.373	-0.348	1.348		
	0.560	-0.101	1.101		
	0.746	0.206	0.794		
	0.931	0.778	0.222		
	1.000	1.000	0.000		

35	0.000	-0.399	1.399	360.7	0.523
	0.186	-0.373	1.373		
	0.373	-0.347	1.347		
	0.560	-0.107	1.107		
	0.746	0.185	0.815		
	0.931	0.773	0.227		
	1.000	1.000	0.000		
36	0.000	-0.394	1.394	414.5	0.523
	0.186	-0.375	1.375		
	0.373	-0.360	1.360		
	0.560	-0.145	1.145		
	0.746	0.154	0.846		
	0.931	0.763	0.237		
	1.000	1.000	0.000		
37	0.000	-0.394	1.394	414.5	0.523
	0.186	-0.373	1.373		
	0.373	-0.357	1.357		
	0.560	-0.140	1.140		
	0.746	0.149	0.851		
	0.931	0.761	0.239		
	1.000	1.000	0.000		

Reduced Temperature Obtained for Molten Plexiglas VM 100

Test Number	Reduced Radius	Reduced Temperature$_1$	Reduced Temperature$_2$	Flow Rate	Reduced Length
	Dimensionless	Dimensionless	Dimensionless	gr/min	Dimensionless
	r/R	$\frac{T - T_1}{T_w - T_1}$	$\frac{T - T_w}{T_1 - T_w}$		z/L
1	0.000	0.557	0.443	193.5	0.758
	0.186	0.557	0.443		
	0.373	0.412	0.588		
	0.560	0.718	0.282		
	0.746	0.850	0.150		
	0.931	1.041	-0.041		
	1.000	1.000	0.000		
2	0.000	0.521	0.479	193.5	0.758
	0.186	0.524	0.476		
	0.373	0.394	0.606		
	0.560	0.693	0.307		
	0.746	0.825	0.175		
	0.931	1.031	-0.031		
	1.000	1.000	0.000		
3	0.000	0.547	0.453	193.5	0.758
	0.186	0.547	0.453		
	0.373	0.422	0.578		
	0.560	0.717	0.283		
	0.746	0.839	0.161		
	0.931	1.019	-01019		
	1.000	1.000	0.000		
4	0.000	0.551	0.449	193.5	0.758
	0.186	0.551	0.449		
	0.373	0.446	0.554		
	0.560	0.716	0.284		
	0.746	0.835	0.165		
	0.931	1.019	-0.019		
	1.000	1.000	0.000		

5	0.000	0.459	0.541	241.9	0.758
	0.186	0.459	0.541		
	0.373	0.345	0.655		
	0.560	0.642	0.358		
	0.746	0.775	0.225		
	0.931	0.983	0.017		
	1.000	1.000	0.000		
6	0.000	0.459	0.541	241.9	0.758
	0.186	0.459	0.541		
	0.373	0.344	0.656		
	0.560	0.633	0.367		
	0.746	0.775	0.225		
	0.931	0.990	0.010		
	1.000	1.000	0.000		
7	0.000	0.462	0.538	241.9	0.758
	0.186	0.462	0.538		
	0.373	0.351	0.649		
	0.560	0.634	0.366		
	0.746	0.776	0.224		
	0.931	0.988	0.012		
	1.000	1.000	0.000		
8	0.000	0.372	0.628	316.4	0.758
	0.186	0.372	0.628		
	0.373	0.254	0.746		
	0.560	0.554	0.446		
	0.746	0.709	0.291		
	0.931	0.963	0.037		
	1.000	1.000	0.000		
9	0.000	0.372	0.628	316.4	0.758
	0.186	0.372	0.628		
	0.373	0.254	0.746		
	0.560	0.558	0.442		
	0.746	0.720	0.280		
	0.931	0.975	0.025		
	1.000	1.000	0.000		
10	0.000	0.371	0.629	316.4	0.758
	0.186	0.371	0.629		
	0.373	0.249	0.751		
	0.560	0.552	0.448		
	0.746	0.719	0.281		
	0.931	0.970	0.030		
	1.000	1.000	0.000		

11	0.000	0.302	0.698	413.4	0.758
	0.186	0.302	0.698		
	0.373	0.173	0.827		
	0.560	0.487	0.513		
	0.746	0.646	0.354		
	0.931	0.953	0.047		
	1.000	1.000	0.000		
12	0.000	0.290	0.710	413.4	0.758
	0.186	0.290	0.710		
	0.373	0.169	0.831		
	0.560	0.488	0.512		
	0.746	0.660	0.340		
	0.931	0.955	0.045		
	1.000	1.000	0.000		
13	0.000	0.264	0.736	413.4	0.758
	0.186	0.264	0.736		
	0.373	0.127	0.873		
	0.560	0.468	0.532		
	0.746	0.634	0.366		
	0.931	0.959	0.041		
	1.000	1.000	0.000		
14	0.000	0.291	0.709	477.0	0.758
	0.186	0.291	0.709		
	0.373	0.322	0.678		
	0.560	0.478	0.522		
	0.746	0.650	0.350		
	0.931	0.963	0.037		
	1.000	1.000	0.000		
15	0.000	0.308	0.692	477.0	0.758
	0.186	0.308	0.692		
	0.373	0.129	0.871		
	0.560	0.487	0.513		
	0.746	0.660	0.340		
	0.931	0.969	0.031		
	1.000	1.000	0.000		
16	0.000	0.301	0.699	477.0	0.758
	0.186	0.301	0.699		
	0.373	0.126	0.874		
	0.560	0.479	0.521		
	0.746	0.644	0.356		
	0.931	0.969	0.031		
	1.000	1.000	0.000		

17	0.000	0.561	0.439	180.9	0.758
	0.186	0.561	0.439		
	0.373	0.367	0.633		
	0.560	0.736	0.264		
	0.746	0.864	0.136		
	0.931	1.058	-0.058		
	1.000	1.000	0.000		
18	0.000	0.554	0.446	180.9	0.758
	0.186	0.554	0.446		
	0.373	0.361	0.639		
	0.560	0.725	0.275		
	0.746	0.862	0.138		
	0.931	1.048	-0.048		
	1.000	1.000	0.000		
19	0.000	0.562	0.438	180.9	0.758
	0.186	0.562	0.438		
	0.373	0.380	0.620		
	0.560	0.728	0.272		
	0.746	0.870	0.130		
	0.931	1.051	-0.051		
	1.000	1.000	0.000		
20	0.000	0.359	0.641	270.4	0.758
	0.186	0.359	0.641		
	0.373	0.183	0.817		
	0.560	0.560	0.440		
	0.746	0.739	0.261		
	0.931	1.018	-0.018		
	1.000	1.000	0.000		
21	0.000	0.351	0.649	270.4	0.758
	0.186	0.351	0.649		
	0.373	0.161	0.839		
	0.560	0.547	0.453		
	0.746	0.730	0.270		
	0.931	1.011	-0.011		
	1.000	1.000	0.000		
22	0.000	0.350	0.650	271.5	0.758
	0.186	0.350	0.650		
	0.373	0.171	0.829		
	0.560	0.561	0.439		
	0.746	0.739	0.261		
	0.931	1.011	-0.011		
	1.000	1.000	0.000		

23	0.000	0.340	0.660	382.0	0.758
	0.186	0.340	0.660		
	0.373	-	-		
	0.560	0.569	0.431		
	0.746	0.761	0.239		
	0.931	1.091	-0.091		
	1.000	1.000	0.000		
24	0.000	0.286	0.714	382.0	0.758
	0.186	0.286	0.714		
	0.373	-	-		
	0.560	0.515	0.485		
	0.746	0.705	0.295		
	0.931	1.053	-0.053		
	1.000	1.000	0.000		
25	0.000	-0.394	1.394	158.6	0.758
	0.186	-0.394	1.394		
	0.373	0.577	0.423		
	0.560	0.106	0.894		
	0.746	0.192	0.808		
	0.931	0.596	0.404		
	1.000	1.000	0.000		
26	0.000	-0.261	1.261	158.6	0.758
	0.186	-0.261	1.261		
	0.373	0.371	0.629		
	0.560	0.046	0.954		
	0.746	0.336	0.664		
	0.931	0.713	0.287		
	1.000	1.000	0.000		
27	0.000	0.000	1.000	158.6	0.758
	0.186	0.007	0.993		
	0.373	0.477	0.523		
	0.560	0.262	0.738		
	0.746	0.475	0.525		
	0.931	0.779	0.221		
	1.000	1.000	0.000		
28	0.000	-0.161	1.161	197.8	0.758
	0.186	-0.150	1.150		
	0.373	0.261	0.739		
	0.560	0.154	0.846		
	0.746	0.418	0.582		
	0.931	0.761	0.239		
	1.000	1.000	0.000		

29	0.000	-0.126	1.126	197.8	0.758
	0.186	-0.126	1.126		
	0.373	0.273	0.727		
	0.560	0.171	0.829		
	0.746	0.420	0.580		
	0.931	0.771	0.229		
	1.000	1.000	0.000		
30	0.000	-0.193	1.193	237.3	0.758
	0.186	-0.186	1.186		
	0.373	0.211	0.789		
	0.560	0.093	0.902		
	0.746	0.368	0.632		
	0.931	0.754	0.246		
	1.000	1.000	0.000		
31	0.000	-0.179	1.179	237.3	0.758
	0.186	-0.172	1.172		
	0.373	0.168	0.832		
	0.560	0.108	0.892		
	0.746	0.373	0.627		
	0.931	0.735	0.265		
	1.000	1.000	0.000		
32	0.000	-0.274	1.274	317.9	0.758
	0.186	-0.268	1.268		
	0.373	0.081	0.919		
	0.560	-0.006	1.006		
	0.746	0.268	0.732		
	0.931	0.710	0.290		
	1.000	1.000	0.000		
33	0.000	-0.274	1.274	317.9	0.758
	0.186	-0.268	1.268		
	0.373	0.087	0.913		
	0.560	0.010	0.990		
	0.746	0.268	0.732		
	0.931	0.710	0.290		
	1.000	1.000	0.000		
34	0.000	-0.284	1.284	360.7	0.758
	0.186	-0.278	1.278		
	0.373	0.051	0.949		
	0.560	-0.045	1.045		
	0.746	0.236	0.764		
	0.931	0.690	0.310		
	1.000	1.000	0.000		

35	0.000	-0.190	1.190	360.7	0.758
	0.186	-0.172	1.172		
	0.373	-0.190	1.190		
	0.560	0.041	0.959		
	0.746	0.276	0.724		
	0.931	0.817	0.183		
	1.000	1.000	0.000		
36	0.000	-0.302	1.302	414.5	0.758
	0.186	-0.302	1.302		
	0.373	0.0156	0.9844		
	0.560	-0.093	1.093		
	0.746	0.174	0.826		
	0.931	0.673	0.327		
	1.000	1.000	0.000		
37	0.000	-0.308	1.308	414.5	0.758
	0.186	-0.305	1.305		
	0.373	-0.022	1.022		
	0.560	-0.101	1.101		
	0.746	0.173	0.827		
	0.931	0.670	0.330		
	1.000	1.000	0.000		

Reduced Temperature Obtained for Molten Plexiglas VM 100

Test Number	Reduced Radius	Reduced Temperature$_1$	Reduced Temperature$_2$	Flow Rate	Reduced Length
	Dimensionless	Dimensionless	Dimensionless	gr/min	Dimensionless
	r/R	$\frac{T - T_1}{T_w - T_1}$	$\frac{T - T_w}{T_1 - T_w}$		z/L
1	0.000	0.650	0.350	193.5	1.000
	0.186	0.650	0.350		
	0.373	0.696	0.304		
	0.560	0.805	0.195		
	0.746	0.840	0.160		
	0.931	0.986	0.014		
	1.000	1.000	0.000		
2	0.000	0.634	0.366	193.5	1.000
	0.186	0.634	0.366		
	0.373	0.681	0.319		
	0.560	0.786	0.214		
	0.746	0.838	0.162		
	0.931	0.982	0.018		
	1.000	1.000	0.000		
3	0.000	0.664	0.336	193.5	1.000
	0.186	0.664	0.336		
	0.373	0.708	0.292		
	0.560	0.806	0.194		
	0.746	0.845	0.155		
	0.931	0.974	0.026		
	1.000	1.000	0.000		
4	0.000	0.663	0.337	193.5	1.000
	0.186	0.663	0.337		
	0.373	0.712	0.288		
	0.560	0.811	0.199		
	0.746	0.850	0.150		
	0.931	0.972	0.028		
	1.000	1.000	0.000		

5	0.000	0.568	0.432	241.9	1.000
	0.186	0.568	0.432		
	0.373	0.615	0.385		
	0.560	0.729	0.271		
	0.746	0.786	0.214		
	0.931	0.954	0.046		
	1.000	1.000	0.000		
6	0.000	0.568	0.432	241.9	1.000
	0.186	0.568	0.432		
	0.373	0.620	0.380		
	0.560	0.731	0.269		
	0.746	0.793	0.207		
	0.931	0.955	0.045		
	1.000	1.000	0.000		
7	0.000	0.575	0.425	241.9	1.000
	0.186	0.575	0.425		
	0.373	0.624	0.376		
	0.560	0.738	0.262		
	0.746	0.796	0.204		
	0.931	0.955	0.045		
	1.000	1.000	0.000		
8	0.000	0.479	0.521	316.4	1.000
	0.186	0.479	0.521		
	0.373	0.526	0.474		
	0.560	0.657	0.343		
	0.746	0.736	0.264		
	0.931	0.946	0.054		
	1.000	1.000	0.000		
9	0.000	0.479	0.521	316.4	1.000
	0.186	0.479	0.521		
	0.373	0.526	0.474		
	0.560	0.659	0.341		
	0.746	0.738	0.262		
	0.931	0.946	0.054		
	1.000	1.000	0.000		
10	0.000	0.475	0.525	316.4	1.000
	0.186	0.475	0.525		
	0.373	0.522	0.478		
	0.560	0.656	0.344		
	0.746	0.736	0.264		
	0.931	0.946	0.054		
	1.000	1.000	0.000		

11	0.000	0.387	0.613	413.4	1.000
	0.186	0.387	0.613		
	0.373	0.442	0.558		
	0.560	0.586	0.414		
	0.746	0.677	0.323		
	0.931	0.933	0.067		
	1.000	1.000	0.000		
12	0.000	0.384	0.616	413.4	1.000
	0.186	0.384	0.616		
	0.373	0.438	0.562		
	0.560	0.579	0.421		
	0.746	0.594	0.406		
	0.931	0.928	0.072		
	1.000	1.000	0.000		
13	0.000	0.363	0.637	413.4	1.000
	0.186	0.363	0.637		
	0.373	0.415	0.585		
	0.560	0.565	0.435		
	0.746	0.663	0.337		
	0.931	0.927	0.073		
	1.000	1.000	0.000		
14	0.000	0.371	0.629	477.0	1.000
	0.186	0.371	0.629		
	0.373	0.409	0.591		
	0.560	0.568	0.432		
	0.746	0.661	0.339		
	0.931	0.928	0.072		
	1.000	1.000	0.000		
15	0.000	0.377	0.623	477.0	1.000
	0.186	0.377	0.623		
	0.373	0.420	0.580		
	0.560	0.583	0.417		
	0.746	0.661	0.339		
	0.931	0.928	0.072		
	1.000	1.000	0.000		
16	0.000	0.373	0.627	477.0	1.000
	0.186	0.373	0.627		
	0.373	0.417	0.583		
	0.560	0.574	0.426		
	0.746	0.666	0.334		
	0.931	0.931	0.069		
	1.000	1.000	0.000		

17	0.000	0.728	0.272	180.9	1.000
	0.186	0.841	0.159		
	0.373	0.915	0.085		
	0.560	0.942	0.058		
	0.746	1.078	-0.078		
	0.931	1.109	-0.109		
	1.000	1.000	0.000		
18	0.000	0.658	0.342	180.9	1.000
	0.186	0.651	0.349		
	0.373	0.719	0.281		
	0.560	0.820	0.180		
	0.746	0.854	0.146		
	0.931	0.966	0.034		
	1.000	1.000	0.000		
19	0.000	0.660	0.340	180.9	1.000
	0.186	0.653	0.347		
	0.373	0.719	0.281		
	0.560	0.825	0.175		
	0.746	0.851	0.149		
	0.931	0.974	0.026		
	1.000	1.000	0.000		
20	0.000	0.463	0.537	270.4	1.000
	0.186	0.463	0.537		
	0.373	0.529	0.471		
	0.560	0.679	0.321		
	0.746	0.747	0.253		
	0.931	0.952	0.048		
	1.000	1.000	0.000		
21	0.000	0.456	0.544	270.4	1.000
	0.186	0.456	0.544		
	0.373	0.529	0.471		
	0.560	0.675	0.325		
	0.746	0.750	0.250		
	0.931	0.945	0.055		
	1.000	1.000	0.000		
22	0.000	0.456	0.544	271.5	1.000
	0.186	0.453	0.547		
	0.373	0.521	0.479		
	0.560	0.668	0.332		
	0.746	0.743	0.257		
	0.931	0.951	0.049		
	1.000	1.000	0.000		

23	0.000	0.433	0.567	382.0	1.000
	0.186	0.402	0.598		
	0.373	0.509	0.491		
	0.560	0.665	0.335		
	0.746	0.746	0.254		
	0.931	0.991	0.009		
	1.000	1.000	0.000		
24	0.000	0.389	0.611	382.0	1.000
	0.186	0.381	0.619		
	0.373	0.461	0.539		
	0.560	0.621	0.379		
	0.746	0.717	0.283		
	0.931	0.980	0.020		
	1.000	1.000	0.000		
25	0.000	-0.212	1.212	158.6	1.000
	0.186	-0.176	1.176		
	0.373	-0.129	1.129		
	0.560	-0.012	1.012		
	0.746	0.406	0.594		
	0.931	0.941	0.059		
	1.000	1.000	0.000		
26	0.000	-0.044	1.044	158.6	1.000
	0.186	-0.190	1.190		
	0.373	0.019	0.981		
	0.560	0.190	0.810		
	0.746	0.475	0.525		
	0.931	0.905	0.095		
	1.000	1.000	0.000		
27	0.000	0.068	0.932	158.6	1.000
	0.186	0.089	0.911		
	0.373	0.132	0.868		
	0.560	0.279	0.721		
	0.746	0.526	0.474		
	0.931	0.895	0.105		
	1.000	1.000	0.000		
28	0.000	0.030	0.970	197.8	1.000
	0.186	0.049	0.951		
	0.373	0.094	0.906		
	0.560	0.257	0.743		
	0.746	0.509	0.491		
	0.931	0.894	0.106		

29	0.000	0.058	0.942	197.8	1.000
	0.186	0.072	0.928		
	0.373	0.126	0.874		
	0.560	0.289	0.711		
	0.746	0.534	0.466		
	0.931	0.888	0.122		
	1.000	1.000	0.000		
30	0.000	-0.047	1.047	237.3	1.000
	0.186	-0.029	1.029		
	0.373	0.018	0.982		
	0.560	0.193	0.807		
	0.746	0.451	0.549		
	0.931	0.870	0.130		
	1.000	1.000	0.000		
31	0.000	-0.0305	1.0305	237.3	1.000
	0.186	-0.0191	1.0191		
	0.373	0.0267	0.9733		
	0.560	0.206	0.794		
	0.746	0.465	0.535		
	0.931	0.865	0.135		
	1.000	1.000	0.000		
32	0.000	-0.159	1.159	317.9	1.000
	0.186	-0.145	1.145		
	0.373	-0.142	1.142		
	0.560	0.091	0.909		
	0.746	0.338	0.662		
	0.931	0.835	0.165		
	1.000	1.000	0.000		
33	0.000	-0.169	1.169	317.9	1.000
	0.186	-0.152	1.152		
	0.373	-0.145	1.145		
	0.560	0.0845	0.9155		
	0.746	0.338	0.662		
	0.931	0.835	0.165		
	1.000	1.000	0.000		
34	0.000	-0.184	1.184	360.7	1.000
	0.186	-0.167	1.167		
	0.373	-0.191	1.191		
	0.560	0.0435	0.9565		
	0.746	0.288	0.722		
	0.931	0.820	0.180		
	1.000	1.000	0.000		

35	0.000	-0.190	1.190	360.7	1.000
	0.186	-0.172	1.172		
	0.373	-0.190	1.190		
	0.560	0.0414	0.9586		
	0.746	0.276	0.724		
	0.931	0.816	0.184		
	1.000	1.000	0.000		
36	0.000	-0.2175	1.2175	414.5	1.000
	0.186	-0.208	1.208		
	0.373	-0.250	1.250		
	0.560	-0.2175	1.2175		
	0.746	0.214	0.786		
	0.931	0.811	0.199		
	1.000	1.000	0.000		
37	0.000	-0.223	1.223	414.5	1.000
	0.186	-0.206	1.206		
	0.373	-0.265	1.265		
	0.560	-0.0229	1.0229		
	0.746	0.213	0.787		
	0.931	0.796	0.204		
	1.000	1.000	0.000		